8-2020

Cytomegalovirus Inhibition by Pluronic-Encapsulated Quercetin and Synergy with Ganciclovir

Ian Wadsworth
Utah State University

CYTOMEGALOVIRUS INHIBITION BY PLURONIC-ENCAPSULATED QUERCETIN AND SYNERGY WITH GANCICLOVIR

by

Ian Wadsworth

A thesis submitted in partial fulfillment
of the requirements for the degree

of

MASTER OF SCIENCE

in

Biological Engineering

Approved:

_____	_____
David Britt, Ph.D. Major Professor	Elizabeth Vargis, Ph.D. Committee Member
_____	_____
Brett L. Hurst, Ph.D. Committee Member	Richard Inouye, Ph.D. Vice Provost for Graduate Studies

UTAH STATE UNIVERSITY
Logan, Utah

2020

ABSTRACT

Cytomegalovirus inhibition by Pluronic-encapsulated quercetin and synergy with ganciclovir

by

Ian Wadsworth, Master of Science

Utah State University, 2020

Major Professor: Dr. David Britt
Department: Biological Engineering

Congenital cytomegalovirus (CMV) is the leading viral cause of birth defects worldwide and leads to a wide variety of debilitating neurological disorders. Despite the prevalence of this infection, there are a limited number of effective CMV inhibitors available, beyond nucleoside analogs such as ganciclovir, which is the clinical standard. Although effective, ganciclovir is expensive, requires repeated intravenous administration, and often results in severe clinical side effects such as neutropenia and thrombocytopenia, making it a high-risk treatment. Quercetin, a plant metabolite, exhibits antiviral and antioxidant activity and may provide a less toxic alternative to ganciclovir, or when co-administered, lower the effective ganciclovir dose. However, due to low water solubility and poor bioavailability, a drug delivery vehicle is needed to deliver quercetin at inhibitory concentrations. In this study, three Pluronic triblock copolymers spanning a range of hydrophilic/lipophilic ratios (P123, F127, and F68) were investigated as self-assembling quercetin drug delivery systems (DDS) for CMV inhibition.

The selected Pluronics encapsulated quercetin proportional to their lipophilic

content: P123 (92.8%), F127 (12.8%), and F68 (1.8%). Quercetin loading increased the stability of each Pluronic DDS, observed as a decrease in the critical micelle concentration. An NIH/3T3 murine embryonic fibroblast *in vitro* model was used to assess the CMV inhibition (EC50) and cytotoxicity (CC50) by the therapeutic range and selectivity index (SI = CC50/EC50) of each DDS. The SI values of maximum quercetin-loaded P123, F127, and F68 were 1.0, 3.0, and 7.4, respectively. Inherent cytotoxicity significantly lowered the SI for Pluronics P123 and F127; in contrast, Pluronic F68 exhibited low cytotoxicity and the SI was tuned by adjusting the quercetin-loading. A maximum SI of 11.4 was achieved SI of 11.4 was achieved by quercetin loaded at 75% of maximum corresponding to 0.358 – 0.012 mM quercetin and 3.567 – 0.314 mM F68.

Having identified the optimal loading and Pluronic DDS, the synergy between ganciclovir and the Pluronic F68 DDS was investigated in an attempt to reduce the effective ganciclovir concentration. Ganciclovir concentration needed to achieve 100% inhibition decreased by 3 orders of magnitude when supplemented with the maximum-loaded quercetin-F68 DDS. Synergy was defined as an increase in viral inhibition beyond addittive inhibition achieved with either ganciclovir or quercetin-F68 alone, assessed for clinically releavent ganciclovir concentrations of 0.01 – 0.07 mM. The reduction in the effective ganciclovir concentration for the tissue culture model could translate into a significant reduction in the severe clinical side effects as well as costs associated with ganciclovir used in CMV treatments.

(139 pages)

PUBLIC ABSTRACT

Cytomegalovirus inhibition by Pluronic-encapsulated quercetin and synergy with ganciclovir

Ian Wadsworth

Congenital cytomegalovirus (CMV) is the leading viral cause of birth defects worldwide and leads to a variety of complications. Ganciclovir is the most common anti-CMV drug used but often causes severe side effects. Quercetin, a plant pigment, shows anti-CMV activity that may provide a less toxic alternative to ganciclovir, or when co-administered, reduce ganciclovir treatments. However, a drug carrier is needed to deliver quercetin for CMV treatment. In this study, three Pluronic polymers (P123, F127, and F68) were investigated as a quercetin drug delivery system (DDS) for CMV treatment.

All selected Pluronics successfully encapsulated quercetin at varying degrees of efficacy. Pluronic P123 was the most efficient (92.8%), F127 was intermediate (12.8%), and F68 was the least efficient (1.8%). Anti-CMV activity and cell toxicity of each DDS were tested. Subsequent adjustment to composition and quercetin loading was performed to maximize viral inhibition and minimize toxicity. It was found that F68 loaded at 75% of maximum quercetin capacity was the optimal CMV inhibitor.

Furthermore, ganciclovir and the Pluronic F68 DDS were administered together in an attempt to reduce the ganciclovir needed to treat CMV. When administered together, 1000X less ganciclovir was needed. Supplementation of ganciclovir with Pluronic F68 DDS could reduce side effects and treatment regimen costs.

ACKNOWLEDGMENTS

Firstly, I thank my advisor Dr. David Britt for his support, guidance, and excellent mentorship throughout the project. I thank Dr. Elizabeth Vargis for all her feedback and allowing me to use her lab space and supplies. I would also like to thank Dr. Craig Day and the Utah State University virology lab technicians for providing materials and assistance for the virology assays I performed. At the University of Utah, I thank Dr. Albert Park, MD. for providing the mCMV-GFP viral stock.

I would also like to thank Taylor Eggertsen who started this work for his senior capstone project in Dr. Britt's lab. Within the Britt lab, I would especially like to thank Andrew Kjar, Mitchell Heap, and Kyle Jackson for their help in the lab, feedback on presentations, and suggestions for my research.

Ian Wadsworth

CONTENTS

Page

LIST OF TABLES

LIST OF FIGURES

LIST OF ABBREVIATIONS

AFM – Atomic force microscopy

AIDS – Acquired immunodeficiency syndrome

CTAB – Cetyltrimethylammonium bromide

CMC – Critical micelle concentration

CMV – Cytomegalovirus

CC50 – Cytotoxic concentration 50%

dGTP – Deoxyguanosine triphosphate

DNA – Deoxyribonucleic acid

DDS – Drug delivery system

DL% – Drug loading percentage

DMEM – Dulbecco's modified eagle’s medium

DPBS – Dulbecco's phosphate buffered saline

DLS – Dynamic light scattering

E – Early viral proteins

EC50 – Effective concentration 50%

EE% – Encapsulation efficiency

FBS – Fetal bovine serum

FDA – U.S. Food and Drug Administration

GFP – Green-fluorescent protein

HAD – Hexadecylamine

HEL – Human embryonic lung fibroblasts

HSV-1 – Herpes Simplex Virus-1

HLB – Hydrophilic/lipophilic balance

IE – Immediate early viral proteins

IC50 – Inhibitory concentration 50%

IV – Intravenous

kDa – Kilodalton

L – Late viral proteins

MW – Molecular weight

MWCO – Molecular weight cutoff

MDR – Multidrug resistance

MOI – Multiplicity of infection

mCMV – Murine cytomegalovirus

NR – Neutral red assay

P – Cell passage number

PFU – Plaque forming unit

PEO – Poly(ethylene oxide)

PPO – Poly(propylene oxide)

PVDF – Polyvinylidene difluoride

Q – Quercetin

ROS – Reactive oxygen species

SAR – Structure activity relationship

SEM – Scanning electron microscopy

SI – Selectivity index

SNHL – Sensorineural hearing loss

SDS – Sodium dodecyl sulfate

SAR – Structure activity relationship

TPGS – Tocopheryl polyethylene glycol succinate

CHAPTER 1

BACKGROUND AND LITERATURE REVIEW

Cytomegalovirus

Cytomegalovirus (CMV) is a widespread, opportunistic betaherpesvirus that infects 50 – 80% of Americans by the age of 40. Similar to chickenpox, CMV is not cleared from the host after primary infection, but persists throughout life in a dormant, latent phase. For immunocompetent individuals, CMV infection is generally asymptomatic and remains undetected or in the latent phase. However, immunocompromised individuals including organ transplant recipients, acquired immunodeficiency syndrome (AIDS) victims, neonates, and pregnant women are susceptible to an active CMV infection due to their weakened natural defense systems (1).

Pregnant women are at a particularly high risk because primary infection or reactivation of a latent infection can lead to CMV crossing the placental barrier and infecting the fetus, resulting in congenital CMV infection. Congenital CMV infection is the leading viral cause of birth defects worldwide with an average of 40,000 cases in the United States every year (2–4). It can lead to severe central nervous system damage and cause a wide variety of neurological sequelae including sensorineural hearing loss (SNHL), vision loss, mental disabilities, microcephaly, or cerebral palsy (2).

Standard CMV Treatment – Ganciclovir

Treatment for CMV is limited to a small class of viral inhibiting pharmaceuticals. Ganciclovir, the most common CMV inhibitor (**Figure 1A**), blocks viral DNA polymerase and the late stages of viral replication as depicted in **Figure 2** (3, 5). Upon entry into the cell, ganciclovir is phosphorylated to its active 5'-triphosphate form (6). Ganciclovir 5'-triphosphate is a nucleoside guanosine analog that competitively inhibits DNA polymerase by blocking the inclusion of deoxyguanosine triphosphate (dGTP) during viral DNA replication (7). Incorporation of ganciclovir 5'-triphosphate into replicating viral DNA suppresses chain elongation (8).

Although shown to be effective against CMV, ganciclovir is considered a high-risk treatment because there is a significant likelihood of harmful side effects, especially in pregnant women (9). Ganciclovir is mutagenic, teratogenic, and carcinogenic and often leads to neutropenia and thrombocytopenia (4). In a clinical study involving 100 neonates, 63% of the patients who received ganciclovir experienced moderate-to-severe neutropenia (9). Risk of bacterial infection is an important clinical consequence of neutropenia and is compounded further in patients who already have a compromised immune system. Other adverse effects of ganciclovir are numerous and may include seizures, hallucinations, fever, rash, abnormal liver function, changes in blood pressure, nausea, or diarrhea. It is estimated that 32% of patients receiving ganciclovir have treatments interrupted or halted due to harmful side effects (6).

Low bioavailability (6-10%) limits the oral administration of ganciclovir (10). Valganciclovir, a valine ester pro-drug of ganciclovir, was developed to increase oral

bioavailability compared to orally-administered ganciclovir. Although it demonstrated comparable CMV inhibition to ganciclovir in clinical trials involving solid organ transplant patients, the daily dose administered was 3 times higher than the average intravenous (IV) ganciclovir dose. Valganciclovir also nearly tripled neutropenia rates compared to orally administered ganciclovir (11).

The most common administration route of ganciclovir is intravenously, dosed at 5 mg/kg every 12 hours for 2 to 3 weeks (2). Results of a phase II clinical trial performed by the National Institute of Allergy and Infectious Diseases Collaborative Antiviral Study Group indicate that IV drug administration twice daily may be necessary up to a year to fully eliminate an active infection (12). Prolonged use of Ganciclovir not only increases the risk of adverse events but is also very expensive. The direct and indirect costs of treating infants with congenital CMV infection approaches $1 billion per year in the United States with the average treatment regimen costing $40,000 (12). Additionally, the emergence of ganciclovir-resistant CMV is increasingly documented by both researchers and clinicians. Mutant strains of CMV that circumvent the mechanism of action of ganciclovir have been observed both in the lab and in the clinic (6). Thus, new therapeutics that inhibit CMV through mechanisms distinct from nucleoside analogs, such as ganciclovir, with a lower long-term toxicity profile are of great interest. A combination of CMV inhibitory drugs with differing mechanisms of action can reduce the risk of antiviral-resistant mutants (13).

Potential CMV Inhibitor – Quercetin

Since the 1960's, over 5000 plant metabolites called flavonoids have been identified, many being considered potential low-cost nutraceuticals due to their combined antioxidant, anti-inflammatory, antimicrobial, and limited clinical side effects (14). In the last 20 years however, a few flavonoids with a distinct structure activity relationship (SAR) have been shown to inhibit viral replication, of which, quercetin has shown specific activity against CMV and other betaherpesviruses (15). Cotin et al. showed that quercetin effectively inhibited CMV replication with some cytotoxicity against human embryonic lung (HEL) fibroblasts (5). In another study by Evers et al., it was shown that quercetin inhibited CMV with minimal cytotoxicity against HEL fibroblasts (16). Additionally, Evers et al. proposed the unique SAR that distinguishes quercetin from other flavonoids as a potent CMV inhibitor, including the coplanar arrangement, aromatic conjugation of the benzene rings, and hydroxyl substituents on the A and B rings (**Figure 1B**) (16). The SAR unique to this flavonoid could lead to the selective CMV inhibition and relatively minimal cytotoxicity observed *in vitro*, implicating quercetin as a potential alternative to ganciclovir (5, 11).

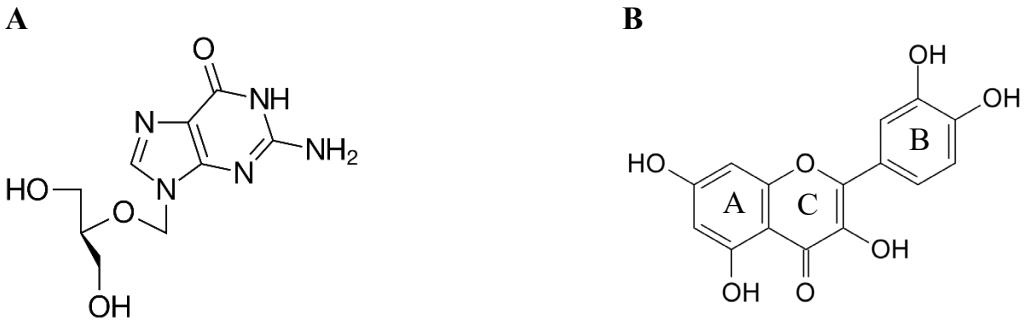

Figure 1. Chemical structure of ganciclovir **(A)**, current accepted treatment of CMV. Chemical structure of quercetin **(B)**, potential alternative to ganciclovir. The three aromatic benzene rings (A,B,C) and hydroxyl constituents result in a distinct SAR for CMV inhibition (16).

Although the exact mechanism of CMV inhibition by quercetin is not fully elucidated, several potential points of intervention in the viral replication cycle have been identified (**Figure 2**). One study used viral gene expression analysis by western blot to show that quercetin partially inhibited the production of immediate-early (IE) viral proteins and strongly blocked early (E) viral protein production in CMV-infected human embryonic lung (HEL) fibroblasts (5). Immediate-early proteins are the first viral proteins produced upon infection and are critical to subsequent viral gene expression, regulation of host cell metabolism, and host immune invasion. Early proteins are produced after IE proteins and are involved in viral DNA replication, repair enzyme production, and host immune invasion (17). Inhibition of these proteins would frustrate viral replication. In another study investigating the inhibition of human herpes simplex virus-1 (HSV-1), a virus from the same family of CMV, quercetin bound irreversibly to the virion, forming a virion-quercetin complex that blocked viral attachment to the cellular membrane and

prevented replication (15). Quercetin may also affect cell cycle progression and subsequently, viral replication, as it has been found to induce S phase arrest in breast cancer cells (18).

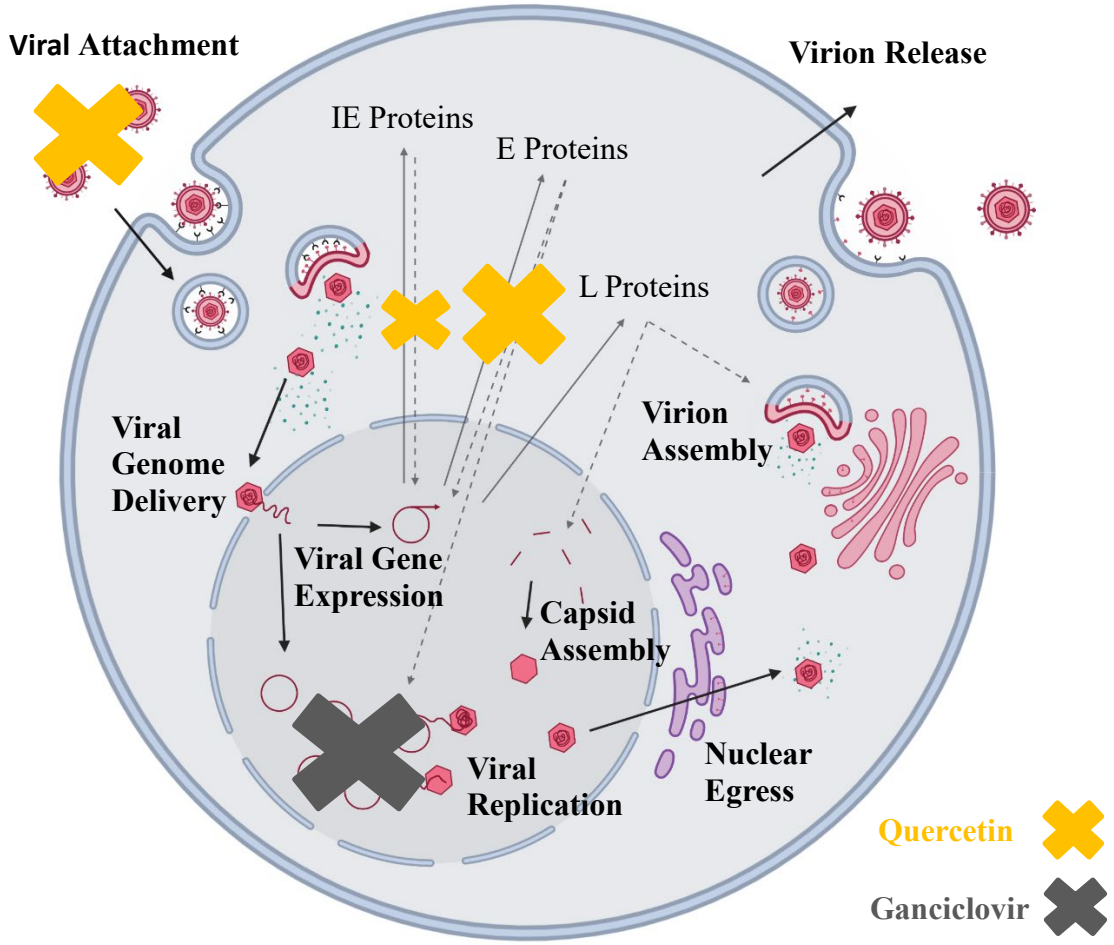

Figure 2. Steps involved in CMV replication in a fibroblast cell. The mechanism of action for ganciclovir (grey) and the potential mechanism of action of quercetin (yellow) are shown (5, 15, 18).

In addition to direct modes of action, quercetin may also benefit the host by reducing oxidative damage associated with viral infection and associated immune response. Although slightly less effective than the common antioxidant ascorbic acid

(vitamin C), the well-established antioxidant activity of quercetin could also ameliorate oxidative stress induced by CMV infection (19, 20). It has been observed that CMV in rat smooth muscle cells generated intracellular reactive oxygen species (ROS) minutes after infection. Although damaging to some cellular processes, CMV actually utilizes the generated ROS for viral gene expression and replication (21). It has been postulated that ROS generated by CMV infection in cochlear vasculature may contribute to damage of the endolymphatic potential, resulting in sensorineural hearing loss (22). Similarly, ROS generated by CMV have been implicated in diseases such as atherosclerosis and retinitis (23, 24). Because quercetin has such distinct and defined antioxidant properties, it is plausible that it could not only have antiviral action, but also mitigate the CMV infection-associated ROS and interrupt the oxidative stress pathways contributing to a variety of diseases (4, 15, 16, 18).

Although quercetin may be a promising antiviral candidate, poor water solubility (0.5 – 23 μM at 25 ºC) and rapid metabolic breakdown *in vivo* result in low bioavailability and difficulty delivering quercetin to infected cells at therapeutic doses (19). In reported *in vitro* studies, quercetin has been dissolved in DMSO or other organic solvents to increase solubility to within therapeutic range (5, 15, 16). However, the cytotoxicity and harsh nature of these solvents limit their clinical application for delivering quercetin at inhibitory doses.

Metabolic breakdown of quercetin is also a concern, as it is susceptible to the first-pass effect. Plasma breakdown occurs mainly in the liver by phase I oxidation pathways, catalyzed by P450 enzymes (25). Phase II sulfation, methylation, and glucuronidation results in sulfate, methyl, or glucuronide conjugates, respectively that

can be transported to cells, excreted to the bile and enter enterohepatic cycling, or be eliminated via urine or feces (26). Spencer et al. showed that the primary metabolites, glucuronidated and O-methylated quercetin, are significantly less protective against oxidative stress than unconjugated quercetin in human fibroblasts *in vitro* (27). Furthermore, it was observed that semiquinones, quinones, or other oxidative metabolites may be a source of cytotoxicity by mitochondrial disruption or interference with cytoplasmic enzymes as observed at high quercetin concentrations (27). In contrast, some research indicates that other quercetin metabolic products such as glutathione conjugates and small phenolic carboxylic acids also maintain high antioxidant activity (28). Fan et al. showed that quercetin-O-β-D-glucuronide, a major quercetin metabolite, exhibited *in vivo* antiviral efficacy against influenza A virus in mice (29, 30). However, the majority of antiviral research is focused on delivering native quercetin to infected cells. Therefore, shielding the chemically labile free hydroxyl of quercetin from phase I oxidative pathways could not only increase the metabolic stability in central circulation, but also represents an advancement in quercetin administration *in vivo* (26).

Due to high metabolism rates, central circulation time for quercetin is low. In a pharmacokinetics study involving 38 cancer patients, the elimination half-life of IV administered quercetin was 3.8 – 86 minutes (31). In another study involving 6 healthy volunteers, it was seen that IV administered quercetin best fit a two-compartment open model with half-lives of 8.8 ± 1.2 minutes for the α phase and 2.4 ± 0.2 h for the β phase (predominant half-life), respectively. High protein binding (98%) indicates that plasma quercetin was not available for cellular entry (32). Hence, encapsulation of quercetin within a drug delivery vehicle could potentially increase circulation time by shielding

from metabolic breakdown and extensive protein binding (26). After oral administration, no measurable quercetin concentration was detected in the plasma or urine, indicating low to no intestinal absorption (32). If effective doses of quercetin are to be administered, other modes of delivery should be considered, including IV, bolus injection, or by drug carrier that increases intestinal transmucosal uptake (26).

Chemical modification, such as glycosylation or methoxylation has been considered to increase water solubility or metabolic stability of quercetin. However, in these studies, alteration of the structure of quercetin resulted in decreased antiviral and antioxidant activity (33). These results, along with those of metabolically modified quercetin, indicate a highly specific SAR (34). A drug delivery platform is thus needed for quercetin to be a viable and clinically relevant alternative to ganciclovir by increasing its water solubility, bioavailability, and deliverability.

Drug Delivery Vehicle – Pluronic

Pluronic nanoparticles have been widely explored as carriers for cancer drug delivery and represent a well-established drug delivery system (DDS) (35–38). Pluronic is a class of commercially available, nonionic polymers that are generally regarded as safe by the U.S. Food and Drug Administration (FDA) (39, 40). They are amphiphilic triblock copolymers composed of one hydrophobic poly(propylene oxide) (PPO) block flanked by two hydrophilic poly(ethylene oxide) (PEO) blocks in the form $(PEO)_A$-$(PPO)_B$-$(PEO)_A$ (**Figure 3A**) (41). Due to the differences in hydrophobicity of the PEO and PPO blocks, the amphiphilic copolymer self-assembles into micelles when

solubilized in an aqueous solution at or above the critical micelle concentration (CMC). Pluronic micelles are thermodynamically stable nanospheres (diameters ranging from 10-100 nm) with a hydrophobic PPO core and a hydrated PEO corona (**Figure 3B**). This structure is useful for drug delivery because hydrophobic drugs can be encapsulated in the hydrophobic core while the hydrophilic surface of the micelle facilitates the suspension of the drug at concentrations much higher than free drug solubility (35, 36, 42–46).

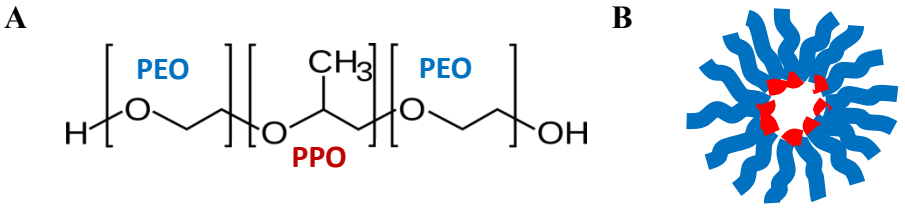

Figure 3. General Pluronic structure **(A)**. Pluronic micelle structure **(B)**. The hydrophobic PPO core (red) and hydrophilic PEO corona (blue) make it a useful platform for drug delivery.

Variation in the number of PEO/PPO repeats during production results in Pluronics with a range of physicochemical characteristics including hydrophilic/lipophilic balance (HLB), molecular weight, and CMC (47). These characteristics can have effects on drug loading efficiency and the biological response to the micelles. Selection of specific Pluronic species can allow for the tuning of a drug delivery platform optimized for a target drug and system. For example, mixed micelles of Pluronics L61 and F127 have been developed to deliver the anti-cancer drug doxorubicin to multi-drug resistant tumors. The L61/F127 Pluronic platform not only increases tumor-drug accumulation and

renal clearance evasion, but also modulates the cellular detoxification system by inhibiting drug efflux pumps (38). This anti-cancer Pluronic micelle formulation is currently in Phase III clinical trials (36, 48). Quercetin has also been encapsulated and delivered by Pluronic micelles for anticancer therapy. Patra et al. fabricated mixed micelles of Pluronics L92, P123, and P407 doped with tocopheryl polyethylene glycol succinate (TPGS) at different ratios to maximize carrying capacity, optimize micelle stability, and tune drug release (49). Quercetin encapsulated in P123/P407 (7:3) micelles and P123P407/TPGS (7:2:1) micelles showed increased *in vitro* cytotoxicity to breast (MCF-7 and MDA-MB-231), ovarian (SKOV-3), and multidrug resistant (NCI/ADR) cancer cells (49).

Pluronic micelles can effectively shield their cargo from metabolic breakdown that occurs in the liver and kidneys, thus increasing blood circulation time. In one study, the pharmacokinetics of anti-tumor paclitaxel-loaded Pluronic P123 micelles were analyzed in a rat model. It was found that encapsulation of paclitaxel in Pluronic P123 micelles increased blood circulation time and half-life, while decreasing the kidney and liver clearance compared to free paclitaxel (50). These results strongly indicate that encapsulation of a hydrophobic drug in Pluronic micelles protects it from metabolic breakdown and elimination. Although this study did not focus on the analysis of oxidative protection provided by Pluronic encapsulation, preliminary studies showed that Pluronic-encapsulated quercetin was protected against oxidative degradation (see **Appendix Figure 1 & 2**). In addition, Pluronic micellular encapsulation has also been shown to provide extended and controlled release of drug over time, further improving drug lifespan and pharmacokinetics (35, 36, 45).

Pluronic has also been used to deliver hydrophobic drugs by injection of thermo-reversible Pluronic gels. Thermo-responsive Pluronic F127 gels have been used to deliver gallic acid for the treatment of atopic dermatitis. By adjusting the percentage of F127 composing the injectable hydrogel, the mechanical properties, thermo-response, and release profile were tuned (51). Due to their permeation enhancement properties, some Pluronics have been used in drug delivery by topical gel. Pluronic F127 has been used in Pluronic lecithin organogels for the transcutaneous delivery of flurbiprofen for treatment of rat paw edema (52). Pluronic has been used to facilitate drug delivery by a variety of administration modes.

In this study, quercetin was encapsulated in Pluronic micelles to increase solubility and bioavailability. The critical micelle concentration and hydrodynamic diameters of the quercetin encapsulated micellar nano-drug delivery platforms were characterized for three different Pluronics. The CMV inhibition and cytotoxicity of each drug delivery system was assessed using an NIH/3T3 murine embryonic fibroblast cells *in vitro* with a green-fluorescent protein (GFP)-expressing murine CMV (mCMV) strain.

CHAPTER 2

DRUG DELIVERY SYSTEM CONSTRUCTION AND CHARACTERIZATION

Overview

This chapter outlines Pluronic selection for the quercetin drug delivery system (DDS). From the 30+ commercially available Pluronics, P123, F127, and F68 were chosen for investigation. Their physicochemical properties (hydrophilic/lipophilic (HLB)) span the range of available values, they are well-established in the literature, and have been widely used in drug delivery and cell culture applications. Additionally, quercetin-loaded and blank micelle construction by the thin-film hydration method is described. Characterization of the quercetin-loaded and blank micelle hydrodynamic diameter was performed by dynamic light scattering to assess the micelle size after loading. Drug loading and encapsulation efficiencies were determined by spectrophotometric methods to identify the most effective quercetin carrier. Lastly, the effect of loading on critical micelle concentration was investigated with a tensiometer to determine micelle stability for each quercetin-loaded Pluronic. A description of the techniques employed and results acquired are detailed in this section.

Pluronic Micelle Composition

Also known as poloxamers, synperonics, or kolliphor, Pluronics are a class of commercially available, nonionic triblock copolymers. There are over 30 formulations

differing in the number of hydrophobic (PPO) and hydrophilic (PEO) repeat units. Each Pluronic has unique properties including molecular weight and HLB. HLB is defined as the ratio between the number of hydrophilic (PEO) and hydrophobic (PPO) repeat units. Unique polymer properties not only dramatically affect the thermodynamics of micelle self-assembly and phase transition behavior (micelle formation), but also impact cellular interaction, and ultimately how the Pluronic species can be utilized (37).

To focus the scope of this project, only three of the 30+ Pluronics were investigated based on their physiochemical characteristics and uses described in literature. It has been shown that slight variations in HLB or molecular weight can largely impact drug carrier efficacy and cytotoxicity. For example, Pluronic F68 is commonly used as a shear reducer in suspended cell culture bioreactors, but F87 which varies only slightly in HLB and molecular weight, has shown to induce cell toxicity and should not be used in these applications (37, 53). Therefore, selecting appropriate and promising Pluronics was critical. Pluronics F68, F127, and P123 were selected using two key characteristics as a guide**:** HLB and established use with cells and biomolecules in literature.

The physiochemical parameter that guided the Pluronic selection process was the HLB. Differences in the ratio of hydrophilic/lipophilic repeats can affect Pluronic micelle thermodynamics, cell culture use, and cytotoxicity. HLB can be scaled differently depending on how the ratio is calculated, but for this work the HLB values range from 1 to 30 based on values presented in literature (37). The HLB values of the chosen Pluronics graphically represented in **Figure 4**.

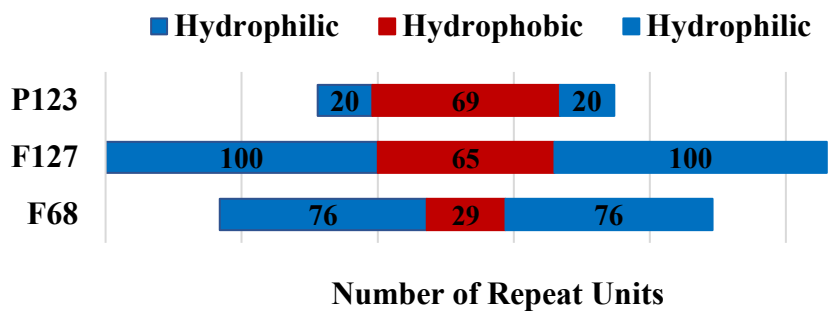

Figure 4. Visualization of the HLB for the three selected Pluronics.

The nomenclature introduced by the original Pluronic manufacturer is based on the chemical structure of the triblock copolymer. The first letter indicates the morphism of the Pluronic (liquid (L), paste (P), and flake (F)). Following is one or two numbers providing 1/300 the molar mass of the PPO block per unimer. The last digit shows 1/10 the molar mass percentage of the PEO content per unimer. For example, P103 is a paste with 300 x 10 = 3,000 g/mol PPO molecular weight, and 3 x 10% = 30% PEO content.

An HLB > 15 corresponds to a Pluronic with high PEO content and is often considered hydrophilic. Pluronic F68 is 80% PEO and 20% PPO by mass, with a PPO molecular weight of 1,800 g/mol – the resulting HLB is 29. Hydrophilic Pluronics generally have higher phase transition temperatures for a given concentration and will solubilize rapidly into an aqueous solution (37). Pluronic F127 has a 70% PEO content and 3,600 g/mol PPO molecular weight, with an intermediate HLB of 22. An HLB < 10 ranks the Pluronic as highly hydrophobic due to the high PPO relative to PEO content (54). P123 has a 30% PEO content and 3,600 g/mol PPO molecular weight, with an HLB of 8 (37). Hydrophobic Pluronic species generally have lower phase transition temperatures and can be difficult to solubilize in an aqueous solution. For Pluronics with

an extremely low HLB (1-5), it may be necessary to combine, or co-micellize, formulas with a more hydrophilic Pluronic to solubilize in an aqueous solution. The three Pluronics chosen for this research span the range of HLB values, allowing for a preliminary mapping of Pluronic HLB to quercetin encapsulation, antiviral activity, and cytotoxicity. Further tuning of the DDS could be achieved by adjusting quercetin loading, and through preparation of mixed micelles to optimize antiviral activity.

The physiochemical properties as discussed previously, greatly affect the use of Pluronics as established in literature. It was important to select Pluronics that not only spanned the HLB range, but also had been successfully used in cell culture and drug delivery applications. Selection metrics included biocompatibility, capacity for loading, and micelle stability. The three most promising Pluronics (P123, F127, and F68) were selected because they spanned the HLB range and had all been previously explored in cell culture and drug delivery applications (see **Table 1**).

Pluronic P123 has been widely explored to deliver anticancer drugs because of its high loading capacity and biological activity (35, 37). It has been observed that P123 can be used as mammalian cellular modifier due to its effect on membrane viscosity and drug efflux pumps, making it attractive for treating multidrug resistance (MDR) cancer cells (37, 38). It has been utilized in gene delivery systems to improve transfection efficacy *in vitro* and *in vivo* (55, 56). Pluronic P123 has also been used to construct a 3-dimensional electrospun scaffold for tissue engineering applications (57).

Similar to P123, Pluronic F127 has been used to deliver anticancer drugs, including paclitaxel and docetaxel (35, 37). F127 is one of two Pluronics composing the first anticancer micellar formulation to reach clinical evaluation as a doxorubicin delivery

system (58). It is commonly used as a nanoparticle stabilizer and can increase the water solubility of hydrophobic nanoparticles (37).

Pluronic F68 is commonly used as a shear reducer and antifoam agent for cell bioreactors (37). It has also been used as an encapsulating agent for anticancer DDSs and is in clinical trials for use to treat vaso-occlusive crisis in sickle cell anemia patients (37, 59). Thermoresponsive, injectable gels composed of Pluronics F68 and F127 have been produced for controlled release of anticancer drugs (60). A summary of some of the physiochemical properties and established uses of the three selected Pluronics can be seen in **Table 1**.

Table 1. Summary of the physiochemical properties and common uses for the three selected Pluronics. Listed are the molecular weight (MW), hydrophilic/lipophilic balance (HLB), critical micelle concentration (CMC) as defined in literature, and compounds encapsulated in drug delivery systems (DDSs), and other reported uses.

	MW (kDa)	**HLB**	**CMC (μM)**	**Uses in DDSs**	**Other Uses**
P123	5.75 (37)	8 (37)	4.4 (37)	Paclitaxel (35) Docetaxel (37) Gene delivery *in vitro* and *in vivo* (55, 56)	Modifier for MDR cells (37, 38) 3-D electrospun scaffolds (57)
F127	12.6 (37)	22 (37)	2.8 (37)	Paclitaxel (35) Docetaxel (37) Doxorubicin (58)	Nanoparticle stabilizer (37) Solubilization of hydrophobic compounds (37)
F68	8.4 (37)	29 (37)	480 (37)	Paclitaxel (37)	Shear reducer and antifoaming agent (37) Thermoresponsive injectable gels (60) Treatment of vaso-occlusive crisis (37)

One key parameter used to assess the Pluronic for use in this DDS was cytotoxicity. In some Pluronic micelle applications, such as anticancer drug delivery, cytotoxicity is of minimal concern once the target tumor has been reached. For this system however, the nanocarriers must demonstrate a low cytotoxicity during preliminary

in vitro testing if they are to be considered for further investigation. Although Pluronics have been used frequently in cell culture applications and commercially available products such as pharmaceuticals, cosmetics, and medical devices since the 1950's, the cell-specific *in vitro* cytotoxicity profiles of Pluronic P123, F127, and F68 have not been fully defined and vary based on assessment models (40). Literature indicates that some of these Pluronics are nontoxic and can be delivered at high concentrations, while others indicate that cytotoxicity is a concern even at lower concentrations (55, 61).

In a study investigating toxicity caused by Pluronic injections, it was found that Pluronic P123 led to significant toxicity in rabbit muscular tissue compared to other Pluronics, such as F127 (62). *In vitro* toxicity has been reported for P123 in a variety of micellular drug delivery studies. Using MCF-7 human breast cancer cells, it was seen that minimal cytotoxicity was induced within the concentration ranges tested, up to 0.01 mM (36). L929 mouse fibroblast cells showed some toxicity to P123 at concentrations of 0.02 mM (63). Another study reported minimal toxicity on human cancer cell lines HepG2, A549, and B16 up to concentrations of 0.03 mM (64). In general, toxicity is induced at relatively low Pluronic P123 concentrations. But whether or not a cytotoxic concentration of P123 is necessary for this particular system will be addressed in chapter 3.

Literature addressing the toxicity of Pluronic F127 is more varied. Butt et al. (65) and Arranja et al. (61), showed minimal toxicity below concentrations of 0.08 mM against Chinese hamster lung fibroblasts and 0.4 mM against NIH/3T3 mouse fibroblasts, respectively. Agata el al. reported no toxicity for F127 concentrations up to 0.8 mM against rat colorectal cancer DHD/K12/TRb cells, but toxicity at higher concentrations (66). Whereas minimal cytotoxicity was observed in HepG2 at F127 concentrations

below 8 mM, but above which, cell death was significant (67). It appears that toxicity of F127 is not only dependent on the cell line, but the method used to quantify it, making it difficult to apply these reported toxicity profiles to this work.

Pluronic F68 has shown minimal toxicity *in vitro* and *in vivo* (53). It has been used to promote cell membrane healing and increase 3T3/NIH mouse fibroblast viability after chemical permeabilization (67, 68). Approved by the FDA for use in humans, F68 has been successfully been used as a cleanser and antibiotic-delivery gel for open wounds (69, 70). It has shown only slight cytotoxicity when injected into mouse breast cancer tumors (71). Based on results found in literature, F68 is the least cytotoxic out of the 3 chosen Pluronics.

Other common amphiphilic surface-acting agents used in DDS synthesis and biological analysis applications, such as sodium dodecyl sulfate (SDS), cetyltrimethylammonium bromide (CTAB), or hexadecylamine (HAD), are highly cytotoxic. These surface-active agents are thought to interference with cell membrane activity and lead to reactive oxygen species (ROS) generation, causing cell death (72). In contrast to Pluronics, these are ionic surfactants with molecular weights several orders of magnitude lower than Pluronics. Therefore, comparing mechanisms of cytotoxicity between the classes of detergents is difficult even though both are highly surface-active compounds commonly used in nanoparticle synthesis applications.

Non-ionic surfactants that have widely been used in hydrophobic drug delivery applications, such as Kolliphor HS 15, Kolliphor EL, or polysorbate 80, exhibit a more mild cytotoxicity compared to ionic surfactants (73). Kolliphor HS 15 has been extensively studied as a solubilizer, emulsifier, stabilizer, and excipient for a wide variety

of DDS due to its amphiphilic nature, biological activity, and low toxicity *in vitro* and *in vivo* (73). It is FDA approved in a host of injectable and ophthalmic drugs (73). Compared to Pluronic P123, F127, and F68, Kolliphor HS 15 has a molecular weight about 2 orders of magnitude lower but spontaneously forms micelles that are comparable in diameter (~10 nm)(73). The hydrophobic drug carrying capacity is similar to Pluronic F127 and some oxidative protection properties have been observed (74). Similar to Pluronics, Kolliphor HS 15 inhibits P-glycoprotein efflux pumps and may exhibit some neuroprotective activity (73, 75). Even though Kolliphor HS 15 and Pluronics have many similarities, to the best of the author's knowledge no literature exists that specifically compares and contrasts the mechanisms of toxicity between the two classes of surfactants.

The exact causes of Pluronic cytotoxicity are not elucidated, however the interactions between Pluronic and cellular processes and components have been investigated. The strong surface activity of some Pluronics can have a significant effect on the mammalian cell membrane. Kabanov et al. reported that some Pluronics are incorporated into lipid rafts within the cell membrane, altering the lipid bilayer viscosity and leading to changes in membrane activity. These alterations may include transmembrane transport mechanisms, cell-cell interactions, and cell adhesive properties (38). Pluronic-induced permeabilization has been shown to induce neural cell apoptosis (76).

Pluronic within the cell is trafficked to the endoplasmic reticulum and mitochondria. Incorporation of some Pluronics within the membrane of the mitochondria is accompanied by inhibition of cellular respiration and a decrease in ATP production

(38). Additional metabolic pathways are also affected by Pluronic within cell cytoplasm. Both cytochrome c and ROS levels are increased when cells are exposed to certain Pluronics, suggesting the induction of proapoptotic pathways (38). Inhibition of the glutathione/glutathione-S-transferase detoxification pathway and drug efflux pumps by some Pluronics have promoted apoptosis (38). The degree of cytotoxicity and cellular interference is dependent of the physicochemical properties of the Pluronic formula.

Different Pluronic species induce mixed cytotoxic responses. Despite having the same chemistry of PEO and PPO repeats, differences in block molecular weights impart a distinct HLB which influences self-assembly and interfacial activity. In one study investigating the polymer property leading to cytotoxicity, it was seen that adjustments in Pluronic HLB led to differing cytotoxic profiles (53). When MCF-7 human cancer cells were exposed to a Pluronic with a high HLB (high PEO content), there was little to no resultant cytotoxicity. Conversely, when exposed to a Pluronic with a low HLB (high PPO content), the cells exhibited signs of moderate to high cytotoxicity, suggesting that toxicity is influenced by the net hydrophilicity or hydrophobicity of the polymer as well as the HLB. It is possible that HLB affects how readily the Pluronic is incorporated into the cell membrane or cytoplasm and in turn, how influential it is on cellular mechanisms. For some Pluronics, integration into the cellular membrane can repair membrane integrity and function rather than damage it. Chen H. et al. showed that adding Pluronic F68, which has a high HLB, to chemically permeabilized 3T3 fibroblasts resulted in membrane stabilization and healing (68). Pluronic F68 has also been shown to be neuroprotective. Shelat et al. showed that Pluronic F68 rescued rat hippocampal neurons from apoptosis after oxygen–glucose deprivation (77). Additionally, it has been seen that

F68 reduces mitochondrial dysfunction and mitochondria-dependent death pathways in neural injury models, and may act directly on mitochondria to inhibit mitochondrial outer membrane permeabilization (78). It is clear that the physicochemical properties, such as HLB, have a large bearing on how each Pluronic formula will affect cellular function and toxicity however, it is not the only factor.

Cytotoxicity literature indicates that surfactant toxicity profiles are cell specific (72). If different cell types respond differently to Pluronic exposure, an exhaustive analysis of each Pluronic species' cytotoxicity profile would be difficult to tabulate. Therefore, it is necessary to closely monitor the cytotoxicity of the selected Pluronics in this specific cell culture model. Assessment was performed throughout the development of the system to steer how the composition was modulated. These results will be addressed further in Chapter 3.

Pluronics, P123, F127, and F68 were chosen for investigation as delivery vehicles for quercetin encapsulation and delivery into cells. Their physicochemical properties (HLB) span the range of available values, they are well-established in the literature, and have been widely used in drug delivery and cell culture applications. Quercetin-loaded and blank micelles from each Pluronic species were constructed and compared to identify the carrier that exhibits the highest quercetin loading, preserves micellular structure, and remains stable when loaded.

Micelle Construction – Thin-film Hydration Method

Quercetin-loaded and blank Pluronic micelles were constructed by the thin-film hydration method. This well-defined and straightforward protocol is used frequently for fabricating and loading polymeric, self-assembling nanocarriers (41). Although one of several common methods, thin-film hydration is advantageous because it does not utilize heating, sonication, or harsh solvents that can degrade Pluronic structure, resulting in toxic byproducts (79). Also, the quercetin structure is maintained and protected against pre-oxidation, preserving the structure activity relationship (80, 81). Disruption of quercetin structure has shown to reduce antiviral and antioxidant activity (33). No lengthy solubilization steps are needed, making it a relatively rapid and scalable process. Additionally, this method has shown to yield high loading efficiencies compared to other drug loading methods, making it promising for constructing quercetin-loaded Pluronic micelles (41).

In general, this method employs co-solubilization of the hydrophobic compound (quercetin) and self-assembling carrier (Pluronic) in acetone to facilitate mixing and close association of compound and carrier. The acetone is then removed, leaving behind a thin compound/carrier film that is resuspended in an aqueous solution. Hydrophobic interactions drive the self-assembly of the Pluronic micelle, sequestering the compound into the hydrophobic core and thus, encapsulating it in the carrier. See **Figure 5** for a schematic of the steps involved in this method.

A detailed description of the steps involved follows. First, a 24 mM stock solution of quercetin in acetone was prepared. For thin-film preparations, quercetin stock volumes

and Pluronic P123, F127, and F68 masses were added to corresponding conical tubes according to **Table 2**. A consistent quercetin/Pluronic ratio of 8% w/w was used for each preparation, resulting in a quercetin-saturated solution. Additional acetone was added to P123 and F68 preparations to bring the total volume to 15 mL. All preparations were vortexed until thoroughly mixed, but not sonicated to avoid Pluronic breakdown.

Table 2. Maximum quercetin-loaded Pluronic preparations for thin-film hydration method.

	Mass Pluronic Added (mg)	**Volume of 24 mM Quercetin Stock (mL)**	**Quercetin/ Pluronic (w/w)**
P123	572	5.7	8%
F127	1260	12.4	8%
F68	830	8.2	8%

The preparations were then transferred to 25 mL round bottom flasks. The acetone was evaporated by rotoevaporation for 20-30 min at 100 rpm in a 40 °C water bath, leaving behind a thin film in the flask. The flasks were transferred to a laminar flow hood and dried overnight, after which, 10 mL of sterile Dulbecco's phosphate buffered saline (DPBS) was added to each round bottom flask and vigorously swirled. The flasks were stored in the refrigerator at 4 ^{0}C until the Pluronic thin film was fully resuspended.

Since each preparation was quercetin-saturated for maximum loading, excess free quercetin remained within the suspension. To remove it, each sample was passed through a 0.2 µm pore size, polyvinylidene difluoride (PVDF) syringe filter. The free quercetin

adsorbed to the hydrophobic filter surface, while the encapsulated quercetin passed through. Blank micelles were formed following these same procedures, except for the addition of quercetin to the acetone preparation.

Pluronic micelle solutions were diluted into cell culture media for assessment with the cell culture model. Dilutions were maintained above the CMC. Concentrations of DPBS and media were the same for all dilutions of Pluronic micelles.

As it is thermodynamically favorable for the hydrophobic quercetin to associate with the hydrophobic PPO polymer block, the majority of the compound probably resides within the core of the Pluronic micelle. However, the exact location of quercetin within the micelle is unknown. It is possible that some of the quercetin is trapped within the hydrated PEO blocks of the micellular corona, or even adherent to the exposed surface of the micelle.

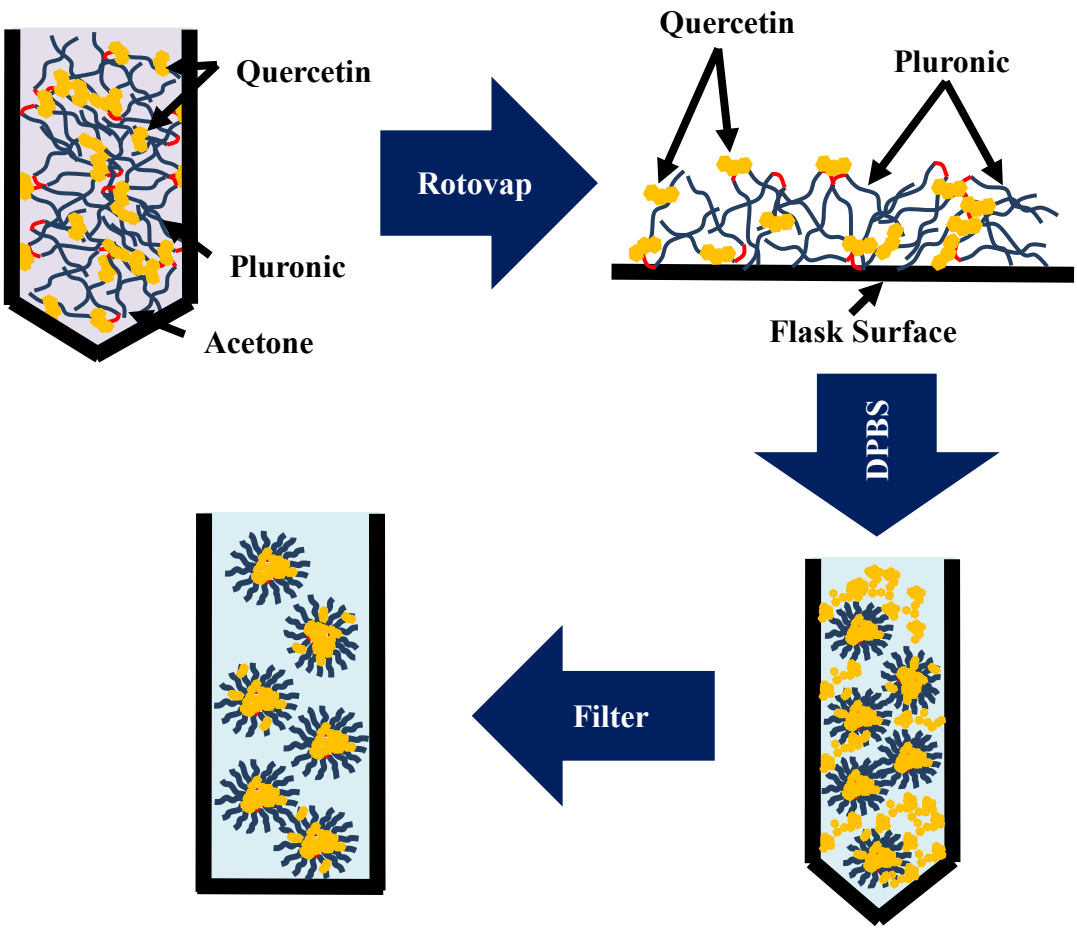

Figure 5. Schematic of the steps involved in the thin-film hydration method for loaded-micelle fabrication.

Using the thin-film hydration method, blank and quercetin-loaded Pluronic micelles were fabricated. In order to quantify micelle diameter and quantitatively ensure proper nanocarrier formation, the hydrodynamic diameters of the particles were assessed.

Micelle Hydrodynamic Diameter – Dynamic Light Scattering

Characterization of the Pluronic micelle hydrodynamic diameter was performed

to confirm nanocarrier formation, asses the size of both blank and quercetin-loaded micelles, and investigate micelle size distribution. They hydrodynamic diameters were measured using dynamic light scattering (DLS).

DLS measures the random Brownian motion of a particle in solution by capturing the time-dependent fluctuations of scattered light passing through the sample. The light fluctuations are directly related to the diffusion coefficient of the solute or particles using an auto-correlation function (82). From the coefficient of diffusion, the hydrodynamic diameter of the particle is calculated using the Stokes-Einstein equation, which relates solute diffusion coefficient with solvent viscosity, temperature, and solute diameter. DLS also provides information about the size distribution of the particles. Particles with a narrow size distribution are considered monodisperse with a discrete particle diameter. Conversely, a wide size distribution is indicative of polydisperse particles that do not have a uniform hydrodynamic diameter. In this way, DLS provides information about particle hydrodynamic diameter and size distribution that can be helpful in drawing conclusions about the morphology of the nano-sized Pluronic micelles.

Both blank and quercetin-loaded P123, F127, and F68 Pluronic micelles were analyzed. Measurements were performed at 25°C with DPBS as the solvent. Results are presented in **Table 3**.

Table 3. Hydrodynamic diameter and polydispersity percentage. n = 7 mean ± std. dev.

	Blank Micelles		**Maximum Quercetin-Loaded Micelles**	
	Diameter (nm)	**Polydispersity (%)**	**Diameter (nm)**	**Polydispersity (%)**
P123	17.4 ± 0.3	20.0 ± 3.4	19.3 ± 3.3	20.3 ± 3.8
F127	28.8 ± 2.4	20.7 ± 7.0	29.1 ± 4.1	21.1 ± 4.6
F68	4.4 ± 0.1	14.0 ± 3.6	Non-discrete*	Polydisperse

*Discrete diameters were observed for F68 micelles when quercetin loading was reduced from maximum, as briefly discussed in Chapter 3 and seen in **Appendix Figure 3.**

The DLS results confirmed successful polymer nanoparticle formation for all three Pluronics, with no distinct differences in both blank and quercetin-loaded micelle size except for F68.

There is no exact polydispersity threshold when assessing the size distribution of a particle, but in general, it is considered monodisperse when the polydispersity percentage is around or below 20% and polydisperse when it is greater (83). All blank Pluronic micelles were monodisperse with the F127 having the greatest polydispersity of 20.7%. Discrete hydrodynamic diameters ranged from 4.4 to 28.8 nm.

Similar to blank, quercetin-loaded Pluronic P123 and F127 micelles could also be considered monodisperse based on the observed polydispersity values. Statistical analysis by a two-sample t-test between blank and quercetin-loaded micelle diameters revealed that there was no significant difference, indicating that there was no quercetin-loading induced changes in micelle diameter. However, quercetin loading of F68 micelles resulted in non-discrete diameter formation (see **Appendix Figure 4**). It is possible that

quercetin loading facilitated the inter-micelle adhesion and led to micelle agglomeration, formation of lamellar sheets, or other self-assembled structures.

To better understand and visualize the morphology of the quercetin-loaded F68 micelles, atomic force microscopy (AFM) imaging was performed in tapping mode on a sample dried on a glass slide. Results were inconsistent and no viable AFM images were captured. For more detailed analysis, scanning electron microscopy (SEM) imaging could be performed.

DLS confirmed particle formation and characterized the morphology of the Pluronic micelles. Analysis of quercetin loading within the micelles was then performed.

Assessment of Quercetin Encapsulation

Visual observation was used first to qualitatively asses encapsulation and evaluate resultant quercetin solubility increases. The strong yellow hue produced by quercetin when in solution was used to detect and compare free quercetin to micelle-encapsulated quercetin. Free quercetin was solubilized in a DPBS solution at concentrations comparable to those of the micelle-encapsulated solutions. Even after vigorous mixing with a vortexer, the turbidity of the free quercetin solution was far greater than the encapsulated quercetin. Indicating that not only was quercetin encapsulated within the Pluronic micelles and successfully suspended in a DPBS solution, but that the quercetin solubility concentration was greatly increased compared to free.

To investigate how stable the suspension of encapsulated quercetin was compared

to free quercetin, scintillation vials were filled with samples of each solution (free quercetin, quercetin-loaded P123, F127, and F68) and allowed to sit for 12 hours undisturbed at room temperature (**Figure 6**). DPBS was used as the solvent for each sample. At the end of 12 hours, a film of precipitated quercetin had formed at the bottom of the free quercetin vial, while the solution above appeared to have little to no yellow hue. No films were observed in any of the three quercetin-loaded Pluronic micelle solutions and the solutions maintained a deep clear yellow due over the 12 hours. Thus, it can be concluded that micellular encapsulation in Pluronics P123, F127, and F68 increased the quercetin solubility and stability in a DPBS solution over time. Similar results were seen by Patra et al. when quercetin was encapsulated in Pluronic P123/P407 (7:3) micelles and P123P407/tocopheryl polyethylene glycol succinate (TPGS) (7:2:1) micelles (49).

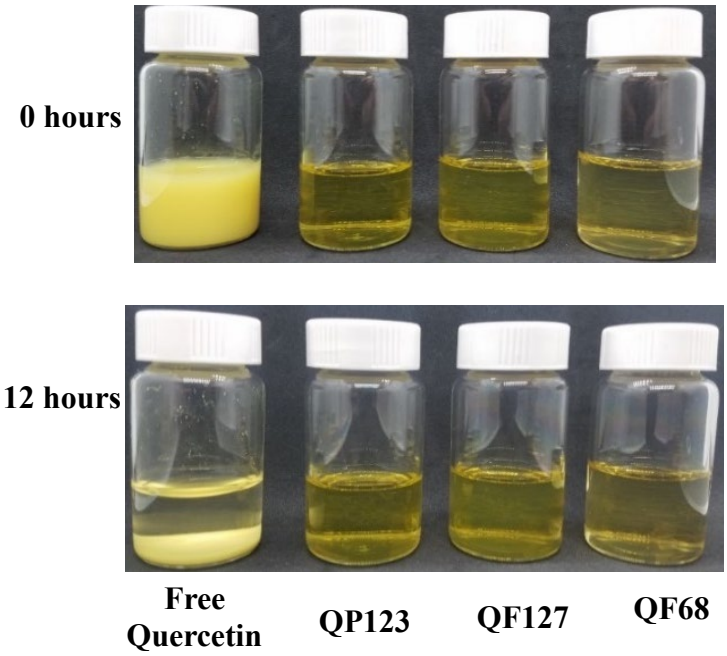

Figure 6. Encapsulation of quercetin in Pluronic micelles successfully increased water solubility compared to free quercetin. "Q" = quercetin-loaded at maximum carrying capacity.

To quantitatively ensure that quercetin was successfully loaded within the micelles, the UV-vis spectra of free quercetin in DPBS and Pluronic micelle-encapsulated quercetin were compared (**Figure 7**). There are two characteristic absorbance peaks of the quercetin spectrum, corresponding to the ring structures comprising the compound. The peak at 268 nm is caused by rings A and B and is known as absorbance Band I. The peak at 373 nm is caused by the cinnamoyl group of rings B and C and is known as absorbance Band II (84).

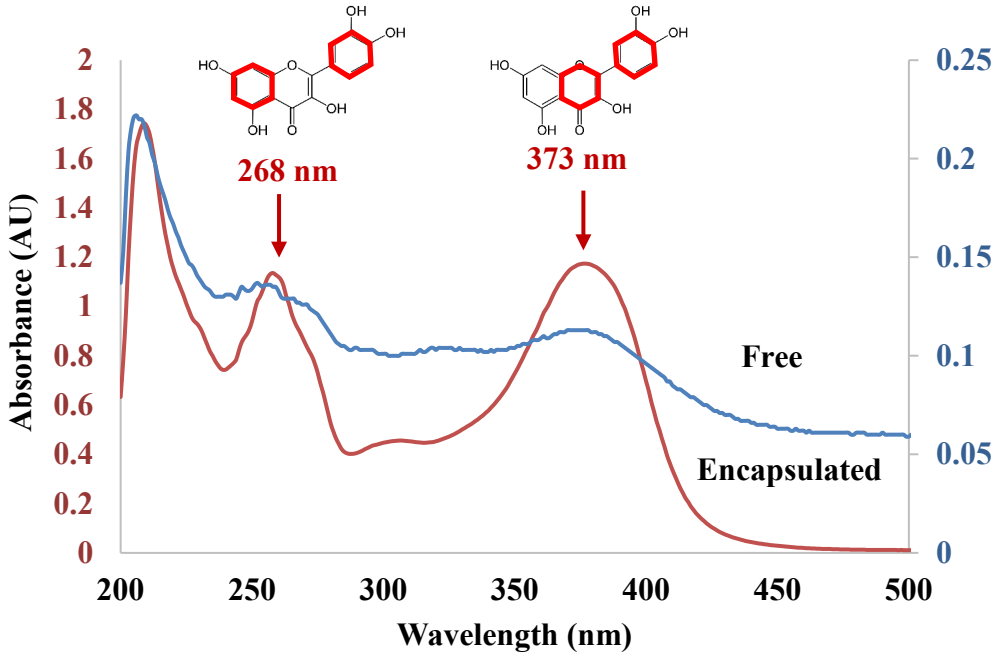

Figure 7. From the UV-vis spectra of free and Pluronic micelle-encapsulated quercetin, it can be seen that encapsulation was successful. Characteristic quercetin absorbance peaks were observed.

Comparison of the free quercetin and encapsulated spectra showed that characteristic peaks were observed in both, confirming that quercetin was present in the Pluronic micelle system and was successfully encapsulated.

Drug Loading and Encapsulation Efficiencies

From the visual observation of color intensity differences, it was apparent that each micelle species resulted in distinct quercetin carrying capacities. Because each Pluronic micelle species was loaded with quercetin at the same carrier-to-quercetin ratio,

discrepancies were likely a result of unique Pluronic characteristics. When designing a drug delivery system (DDS), carrying capacity is a critical parameter to assess and consider for two reasons: loading efficiency and flexibility.

From an engineering perspective, any DDS should be as efficient as possible to reduce cost and impact, while still maintaining efficacy. The carrier concentration should be kept to a minimum to avoid any potentially negative physiological impacts. Therefore, the quercetin carrying capacity or drug encapsulation efficiency of the micelle system should be maximized.

The flexibility offered with a high carrying capacity allows the drug to be loaded into the system at a wider concentration range for any given carrier concentration. This adjustability is highly desirable when tuning the drug concentration to within therapeutic ranges. The ability to modify drug loading concentrations without changing the carrier itself makes the iterative design process quicker and more straightforward.

Two efficiency parameters describe the carrying capacity of a delivery vehicle: drug loading percentage (DL%) and encapsulation efficiency (EE%). DL% describes the percentage of drug mass encapsulated with respect to the drug mass added and the carrier mass, see **Equation 1**. It is a useful because the encapsulated drug mass is normalized to carrier mass. However, EE% is slightly more commonly reported than DL% and describes the percentage of drug mass encapsulated to drug mass added, see **Equation 2**.

(1) $$DL\% = \frac{Mass\ of\ encapsulated\ drug}{Mass\ of\ drug\ added + Mass\ of\ Pluronic\ added} \times 100\%$$

(2) $$EE\% = \frac{Mass\ of\ encapsulated\ drug}{Mass\ of\ drug\ added} \times 100\%$$

Because EE% is the mass of encapsulated drug relative to the mass of drug added, this value can be manipulated by adjusting the mass drug added to inflate efficiency. But because quercetin was loaded in excess at the same quercetin/Pluronic (w/w) ratios for all maximum loading micelles (see **Table 3**), the EE% values can be compared between the 3 assessed Pluronics. The DL% values are also reported to allow for more translational comparison across carrier systems assessed in other studies.

The DL% and EE% for Pluronics P123, F127, and F68 were assessed using the following procedures. Samples from each of the three quercetin-loaded Pluronics were diluted 1:100 in 200 proof ethanol to disrupt the micelles and release the quercetin into solution. Quercetin is highly soluble in ethanol, and unlike acetone, the ethanol solvent is compatible with polystyrene well plates. Using a BioTek Synergy/HTX multi-mode plate reader and a Corning UV-transparent polystyrene 96-well plate, the absorbance at 373 nm was measured and compared to a quercetin-ethanol standard curve (see **Appendix Figure 5**), from which the quercetin concentrations and total mass encapsulated were calculated. Because all maximum quercetin-loaded micelles were fabricated at saturation and required filtration to remove free quercetin as the last step in the fabrication process (see previous section for micelle construction details), it was assumed that the free quercetin concentration was negligible (1.7 μM was the measured solubility in DPBS at room temperature) and all quercetin measured was from encapsulation. Then using equations (1) and (2), DL% and EE% were calculated and presented in **Table 4**.

Table 4. Drug Loading (%) and Encapsulation Efficiency (%) for Pluronic P123, F127, and F68. Mean ± Std. Deviation, n = 7.

	DL%	**EE%**
P123	6.9 ± 1.3	92.8 ± 17.5
F127	0.9 ± 0.2	12.8 ± 8.6
F68	0.1 ± 0.02	1.8 ± 0.3

Pluronic P123 had an EE% of 92.8%, notably higher than F127 (12.8%) and F68 (1.8%). DL% followed a similar trend where P123 was significantly higher at 6.9% compared to F127 (0.9%) and F68 (0.1%). This pronounced trend is inversely correlated with the HLB, namely as HLB decreases the encapsulation efficiency increases. This is not surprising as a lower HLB corresponds to a higher percentage of hydrophobic PPO repeats, which are the presumptive quercetin binding sites in the Pluronic micelle. Therefore, it can be inferred that quercetin is predominately located within the hydrophobic PPO core rather than the hydrophilic PEO corona or surface of the micelle. For more efficient Pluronics (P123 and F127), the hydrophobic core occupies more of the total micelle volume. Interestingly, it seems that the hydrodynamic diameter itself did not correlate with the encapsulation efficiency. Although F127 had a larger hydrodynamic diameter, P123 was more efficient, indicating that the ratio of the hydrophobic core/hydrophilic corona volume, not total micelle volume affects encapsulation efficiency (**Figure 8**).

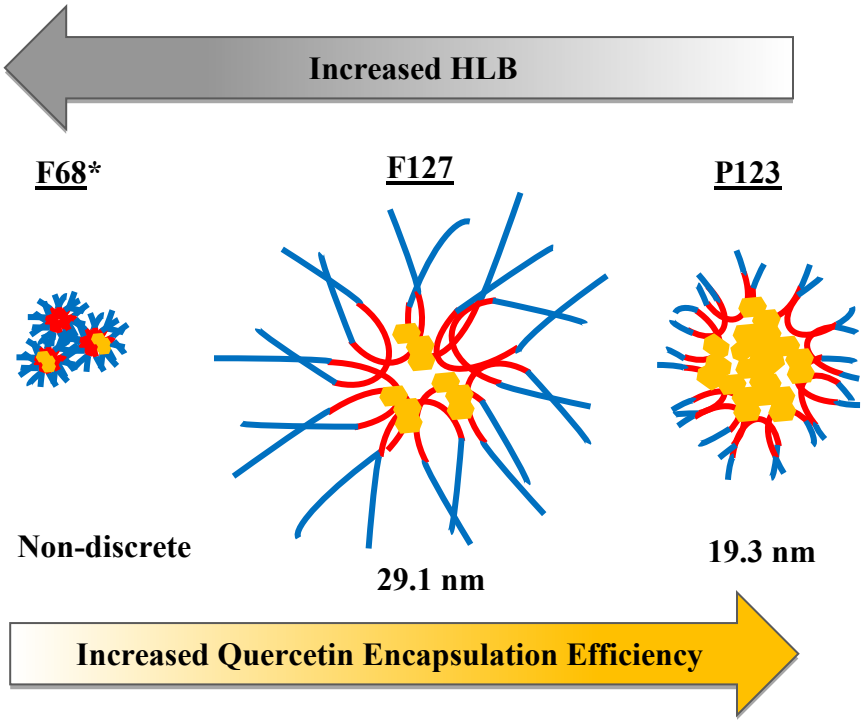

Figure 8. Schematic visualizing the relationship between micelle hydrodynamic diameter and encapsulation efficiency. There was no correlation between hydrodynamic diameter and encapsulation efficiency. Rather, encapsulation efficiency inversely correlated with HLB. *F68 resulted in non-discrete diameters when maximum loaded (see previous section for discussion).

From these results, it can be concluded that if a higher loading efficiency is needed for a given DDS, a Pluronic with a lower HLB should be used. However, it is important to note that Pluronics with low HLB values have been shown to exhibit higher cell toxicity (53). Thus, finding the Pluronic that appropriately balances quercetin loading efficiency with low toxicity is crucial for viral inhibition.

Micelle Stability – Critical Micelle Concentration

Critical micelle concentration (CMC) is the minimum surfactant concentration necessary to induce micelle formation. At Pluronic concentrations below CMC, the polymer exists in its "unimer" form with no micelle formation. As the concentration is increased up to the CMC, Pluronic unimers begin to aggregate as micelles. If the concentration is increased further up to the sol/gel concentration, the micelles aggregate, forming arrangements of close-packed spheres. At this stage, the Pluronic is classified as a gel (47). Measuring the CMC of each Pluronic species for both blank and quercetin-loaded micelles, can help predict micelle stability upon dilution. More stable micelles will exhibit a lower CMC while less stable micelles will begin to disassemble at higher concentrations, resulting in a higher CMC.

Because the target method of this DDS is IV administration, dilution will occur as the drug is delivered throughout central circulation. Although it is desirable for the micelles to eventually disassemble or merge with a cellular membrane, releasing the quercetin payload into the blood stream or into cell cytoplasm, robust micelles that are capable of remaining stable upon dilution could prolonged drug release, which is advantageous for most DDSs. The stability of Pluronic micelles in biologically relevant media has been explored *in vitro* and *in vivo*. Results from the *in vitro* evaluation of F127/L121 mixed Pluronic micelle stability in PBS containing fetal bovine serum albumin indicate that micelles remain stable even upon dilution to near CMC concentrations (85). Hsiao et al. showed that Pluronic F68 micelles were stable for at least 4 hours of incubation on a freshly excised mouse cornea at concentrations above

CMC (86). *In vivo*-administered F68 micelle eye drops remained stable for at least 1 hour in mice before corneal excision and analysis (86).

In vitro quantification of the CMC can be used to define the lower Pluronic concentration threshold necessary to successfully encapsulate quercetin in the micelle carrier. Therefore, Pluronics cannot be diluted below CMC, even to prevent cytotoxicity, as this would promote carrier disassembly. *In vitro* results could also be used to predict micelle stability upon *in vivo* administration.

In order to determine the CMC, the interfacial activity of each of the investigated Pluronics was characterized using a wire probe tensiometer (Kibron MicrotroughS, with tungsten wire probe and PTFE coated 12-well plate). Pluronic unimers in solution organize at all surfaces and fluid-air interfaces, causing a reduction in the fluid surface tension. Below CMC, increasing Pluronic concentration results in more unimer aggregation at the interface, causing a concentration-dependent surface tension decrease. At or above CMC however, the interface is saturated with Pluronic unimers. Therefore, an increase in Pluronic concentration above the CMC has no further effect on the surface tension. The Pluronic concentration at the surface tension inflection point corresponds to the CMC. Taken from the Kruss-Scientific website, **Figure 9** is a schematic of the relationship between CMC and surface tension (87).

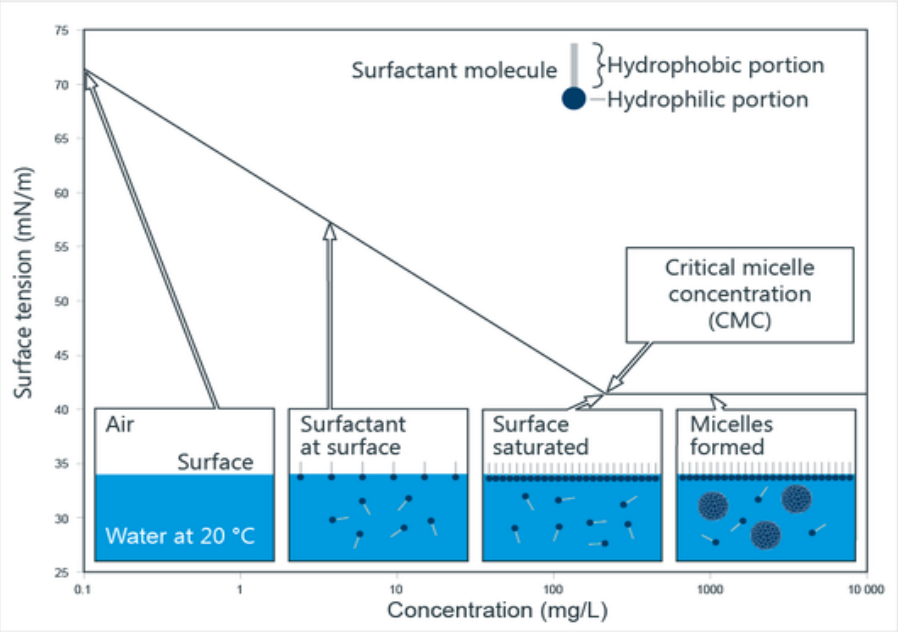

Figure 9. Schematic depicting how the CMC is characterized by changes in surface tension. The Pluronic concentration at the surface tension inflection point is the CMC. Taken from the Kruss-Scientific website (87).

Stock solutions of blank and maximum quercetin-loaded Pluronic P123, F127, and F68 micelles were prepared and serially diluted into DPBS to concentrations ranging from 1 – 5.08×10^{-5} mM. The surface tension of each dilution series was tested at 25 °C. Three acquisitions were made at each concentration with the probe being washed in double distilled H_2O between each one. The inflection point was estimated graphically using Excel (data samples presented in **Appendix Figure 6**). Each Pluronic was tested in triplicate and statistical analysis was performed between blank and quercetin-loaded values using a two-sample t-test. See **Figure 10** for results.

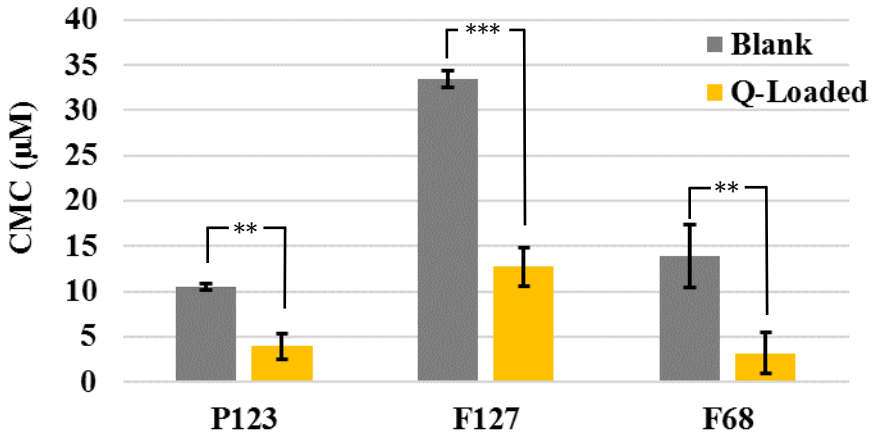

Figure 10. Maximum encapsulation of quercetin in micelles lowers the CMC for all Pluronics. Pluronics in DPBS at 25°C. Error bars = Std. Deviation, n = 3. **P<0.01 *** P<0.001

For each Pluronic formula, quercetin loading significantly lowered the CMC, making the micelle more stable at lower concentrations compared to blank micelles. It is possible that quercetin loaded within the micelle exhibits a stabilizing effect on the hydrophobic core, making micellization more thermodynamically favorable at lower concentrations (44). This stabilizing effect shows promise for the IV administration of the quercetin-loaded micelles, and potential development of a sustained release system. To more fully understand and contextualize how CMC would affect quercetin concentrations in central circulation over time, the pharmacokinetics of the system should be analyzed *in vivo.* But due to the complexity and cost of such studies, that is beyond the scope of this *in vitro* work, which has been designed to provide a preliminary analysis to assess quercetin-loaded Pluronic micelle DDS properties and test antiviral and cell cytotoxicity using a tissue culture model.

Conclusions

Pluronics P123, F127, and F68 were chosen for this work based on HLB values and established uses in drug delivery and cell culture applications. From the literature, the HLB values were 8, 22, and 29 for P123, F127, and F68, respectively. Quercetin-loaded and blank micelles were successfully constructed by the thin-film hydration method. Pluronic and quercetin integrity was maintained throughout the process.

Quercetin-loaded and blank micelle hydrodynamic diameters were characterized by dynamic light scattering. P123, F127, and F68 Pluronics formed micelles with discrete sizes when blank. However, Pluronic F68 formed micelles with non-discrete diameters when maximum quercetin-loaded, possibly caused by micelle agglomeration, formation of lamellar sheets, or other self-assembled structures. Maximum quercetin-loading in P123 and F127 Pluronics resulted in discrete micelles with diameters not statistically different from blank.

Using spectrophotometric methods, the most efficient quercetin carrier was determined to be Pluronic P123 with an encapsulation and drug loading efficiency of 92.8 ± 17.5 and 6.9 ± 1.3%, respectively. Pluronic F68 was the most inefficient carrier with an encapsulation and drug loading efficiency of 1.8 ± 0.3 and 0.1 ± 0.02%, respectively. Pluronic F127 exhibited intermediate carrying capacity.

The stability of quercetin-loaded micelles was also investigated. Quercetin loading decreased the critical micelle concentration for all investigated Pluronics. Quercetin-loading results in a micelle more stable at lower Pluronic concentrations.

CHAPTER 3

ASSESSMENT AND ADJUSTMENT OF THE PLURONIC MICELLE-BASED QUERCETIN DELIVERY SYSTEM

Overview

This chapter outlines the metrics, model, and methods used to assess the quercetin drug delivery system (DDS) *in vitro*. Cytotoxicity and viral inhibition were selected as the upper and lower criteria, respectively, to define the therapeutic antiviral range of quercetin carried by three difference Pluronic DDSs. As demonstrated in Chapter 2, the threes Pluronics, F123, F127, and F68 exhibited quercetin loading efficiencies correlation to their hydrophilic/lipophilic balance (HLB) values. In this chapter, quercetin and the Pluronic carriers were evaluated for anti-cytomegalovirus activity using an NIH/3T3 mouse fibroblast 96-well plate tissue culture model. This high throughput assay permitted a range of quercetin concentrations to be evaluated for each Pluronic DDS. From these assays the drug selectivity index (SI) was calculated as the ratio of Pluronic concentration leading to 50% cell death over the concentration leading to 50% viral inhibition. The outcomes guided the composition of the DDS and quercetin loading to maximize the therapeutic range.

Of the three Pluronics at maximum quercetin loading, F68 exhibited the lowest cytotoxicity with significant viral inhibition, resulting in an SI of 7.4. Reduction of F68 loading to 75% of maximum lowered toxicity and increased the SI to 11.4, higher than any other quercetin/Pluronic combination tested. The F68 DDS was further evaluated for synergy with the anti-CMV pharmaceutical ganciclovir. When supplemented with

maximum-loaded F68 DDS, ganciclovir concentrations needed to achieve 100% inhibition were dropped by 3 orders of magnitude without any added toxicity. Addition of blank F68 to the ganciclovir treatment increased the SI an estimated 22-fold compared to ganciclovir alone. With quercetin-loaded F68 DDS, the estimated SI was upwards of 500-fold greater.

Assessment Metrics

The drug delivery system (DDS) was assessed by therapeutic range comparison, which provides insight into efficacy compared to toxicity. Calculated from the therapeutic range, the selectivity index (SI) is the ratio of toxicity to efficacy and is commonly used to differentiate selective viral inhibition from cytotoxicity. For this study, the therapeutic ranges and corresponding SIs of Pluronic P123, F127, and F68 DDSs were tabulated and compared. Pluronic DDSs with a narrow therapeutic range and low SI were considered cytotoxic and non-selective. Differences in the toxicity of maximum quercetin-loaded and non-loaded (blank) DDSs determined the tunability of the system. When maximum quercetin loading was too cytotoxic, but blank was minimally toxic, loading was reduced to increase the therapeutic range and SI. The DDS was optimized when the Pluronic formula and quercetin loading resulted in a maximum SI.

There are two values that define the limits of the therapeutic range. The upper limit is conventionally defined by the cytotoxic concentration 50% (CC50), which is the antiviral concentration (mM) resulting in a 50% reduction in cell viability compared to a

non-treated and non-infected cell control. Concentrations above CC50 are regarded too toxic for consideration. Ideally, a treatment has little to no cell toxicity and produces a high CC50. Although 50% toxicity is an arbitrary value and does not represent a regulatory threshold, it is a well-established comparison metric.

The lower limit is the effective concentration 50% (EC50), sometimes referred to as the inhibitory concentration 50% (IC50). The EC50 is defined as the antiviral concentration (mM) that results in 50% viral inhibition compared to a non-treated virally infected control, referred to as the viral control. Below the EC50, the antiviral activity is minimal and is not considered effective. A low EC50 is characteristic of an antiviral that exhibits high inhibitory activity. Similar to CC50, 50% viral inhibition is an arbitrary value but is commonly considered a valid metric for comparison.

With the CC50 defining the maximum toxicity threshold and EC50 defining the antiviral activity threshold, the therapeutic range is established. A wide therapeutic range, where CC50 is greater than EC50, is representative of an antiviral that has distinct and effective inhibitory activity. A narrow therapeutic range, where CC50 is equal to EC50, is usually indicative of an antiviral that exhibits inhibitory activity caused by toxicity. It is critical to assess EC50 in conjunction with CC50 to ensure that viral inhibition is not a result of host cell death. The ratio of CC50 to EC50 is known as the selectivity index (SI), see **Equation 3**. The SI is a unitless value used to describe the width of the therapeutic index and is a standard benchmark for comparing antiviral efficacy across systems.

(3) $$SI = \frac{CC50\ (mM)}{EC50\ (mM)}$$

Quantification of CC50 and EC50 for therapeutic range establishment and SI calculation was performed *in vitro* using a cell culture model, as described below.

Cell Culture Model

An *in vitro* model was developed to perform the antiviral screening assay used to establish the therapeutic range. Although there are distinct limitations with using an *in vitro* model to represent a complicated and dynamic process, it is a relatively rapid assay that is a prerequisite to further studies of antivirals in animal models. The low cost, controlled, and straightforward nature of this model allows for high throughput screening of potential antiviral compounds over a range of concentrations.

For this research, NIH/3T3 murine embryonic fibroblasts were employed because they are well-defined, commonly used, and susceptible to infection from murine CMV (mCMV) (88, 89). Cells below passage #15 (P<15) were used. CMV infection was performed using GFP-expressing recombinant mCMV obtained from Dr. Albert Park at the University of Utah. GFP expression occurs if viral genes are also being expressed, with the magnitude of expression being directly related. Although this is not considered a direct viral infection characterization method, this secondary indicator allows for rapid visualization (see **Figure 11**) and relative quantification of viral load in the culture (90).

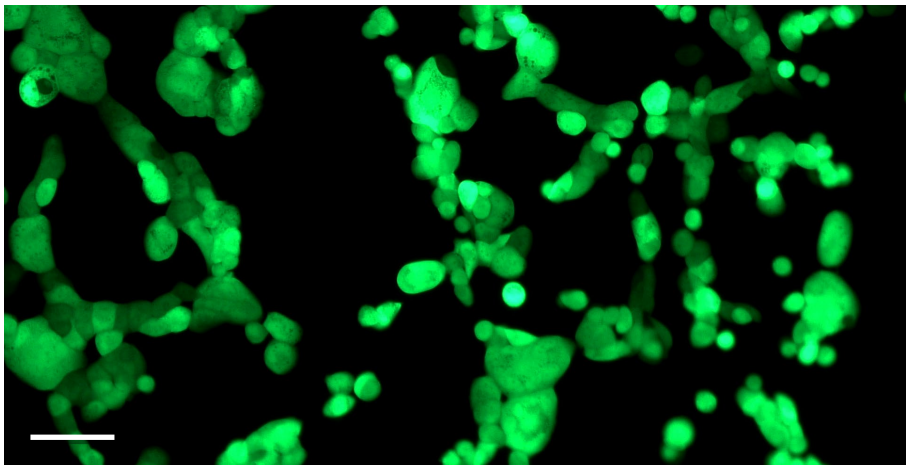

Figure 11. Fluorescent image (10X) of the GFP expression seen in the viral control. mCMV is freely replicating, causing infected 3T3 fibroblasts to brightly fluoresce. GFP can be used as a secondary indictor for relative viral load quantification. Scale bar = 100 µm.

The model was developed in a standard plasma-treated polystyrene 96-well plate to perform both the toxicity (CC50) and viral inhibition (EC50) analysis simultaneously. Cytotoxicity characterization was performed on non-virally infected cells exposed to a concentration range of the DDS, adjusted to produce a range of cytotoxicity from approximately 0 – 100%. Similarly, antiviral activity characterization was performed on mCMV-infected cells exposed to a concentration range of the DDS adjusted to provide a range from approximately 0 – 100% antiviral activity. In one 96-well plate, both quercetin-loaded and blank micelles were tested to isolate the effect of quercetin from the Pluronic carrier. Cells exposed just to quercetin were also evaluated within the solubility limit of quercetin in water (DPBS). To achieve statistical triplicates, each experiment was repeated three times in separate plates.

Also incorporated into the 96-well plate model are the appropriate controls. The

cell control includes non-virally infected 3T3 fibroblasts, with an appropriate volume of DPBS added instead of the tested DDS and is used to monitor normal cell health, representing 0% cytotoxicity. The viral control includes mCMV-infected 3T3 fibroblasts with an appropriate volume of DPBS added instead of the tested DDS, and is used to monitor unrestrained viral replication, representing 0% viral inhibition. Also included are blank wells without cells, used for background subtraction during analysis. As adapted by Taylor Eggertsen and Dr. Craig Day for mCMV, a schematic of the 96-well plate cell culture model layout can be seen in **Figure 12.**

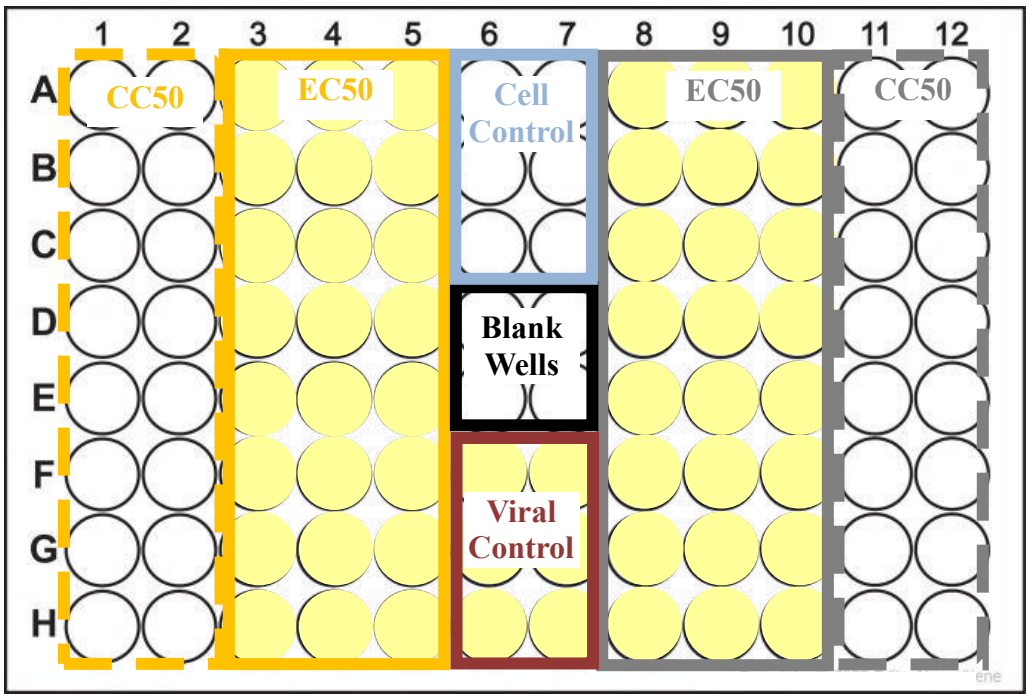

Figure 12. EC50/CC50 assay 96-well plate layout. Yellow wells are infected with mCMV at a multiplicity of infection (MOI) of 0.3. CC50 was be observed in wells in the "dashed boxes" and EC50 was observed in wells in the "solid boxes."

CC50/EC50 Assay Procedure

With the development of the cell culture model, it was necessary to optimize the CC50/EC50 assay procedure for this treatment regimen. A former undergraduate researcher in our lab, Taylor Eggertsen, had performed this assay previously with 3T3 fibroblasts and mCMV; however, changes were made in the cell seeding density, assay duration, viral attachment time, and media removal/refreshment to avoid cell monolayer detachment that was observed in early iterations (**Figure 13)**. A description of the iterations performed in protocol development can be seen in **Appendix Protocol 1**.

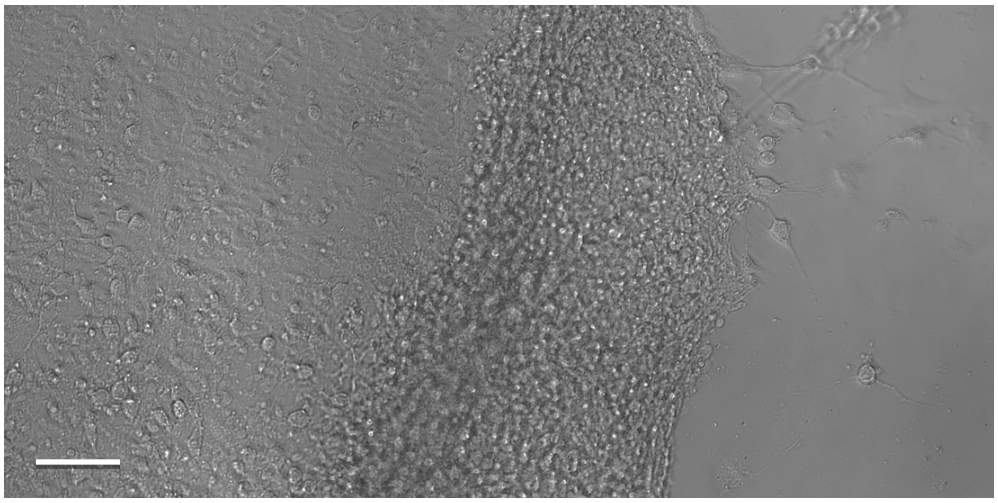

Figure 13. Brightfield image (10X) of a 3T3 fibroblast monolayer 2 days post-seeding. The monolayer detached and folded onto itself in many of the wells, irrespective of Pluronic treatment. It was apparent that the cells were not killed by the treatment because they began growing out of the cell mass within 24 hours after sheet detachment. Optimization of assay protocol was necessary. Scale bar = 100 μm.

The optimized assay procedure used for this work follows. First, a VWR® Standard plasma-treated polystyrene 96-well plate was seeded with NIH/3T3 fibroblasts (P<15) at a density of $3x10^4$ cell/cm^2, about 45-50% confluence as observed with brightfield microscopy. Culture media used throughout the experiment was Dulbecco's modified eagle's medium (DMEM) F12 supplemented with 10% fetal bovine serum (FBS). All wells were seeded except blank wells, see **Figure 12** for layout. Cells were allowed to adhere for 4 hours at standard mammalian cell culture conditions (37 °C, 5% CO_2). After which, all media was removed and 100 µL of warm viral inoculum media, that was prepared previously (see **Appendix Protocol 2**), was added to all EC50 and viral control wells. Inoculation density was $3x10^3$ plaque forming units (pfu)/well or at a multiplicity of infection (MOI) of 0.3. Multiplicity of infection is the ratio of virions to cells. Also, 100 µL of warm normal DMEM media was added to all CC50 and cell control wells. The plate was then incubated for 10 minutes for viral attachment. CMV entry is a rapid process occurs within 5 minutes for some epithelial and endothelial cells (91). A concentration range of DDS was prepared previously (see **Appendix Protocol 3**) with each row of wells receiving a distinct DDS dilution. After viral attachment, 100 µL of the DDS dilution was pipetted into corresponding wells, bringing total well volume to 200 µL. The treatment layout can be seen in **Figure 12**. A multichannel pipette was used when possible. The plate was then incubated at 37 °C, 5% CO_2 for 3 days. No media/treatment replacement or refreshment was performed. Lastly, CC50 and EC50 analysis was performed for therapeutic range quantification.

Using this protocol, no cell monolayer detachment was observed, the cell controls appeared healthy, and the virus was successfully proliferating in the viral controls (see

Figure 14).

A.

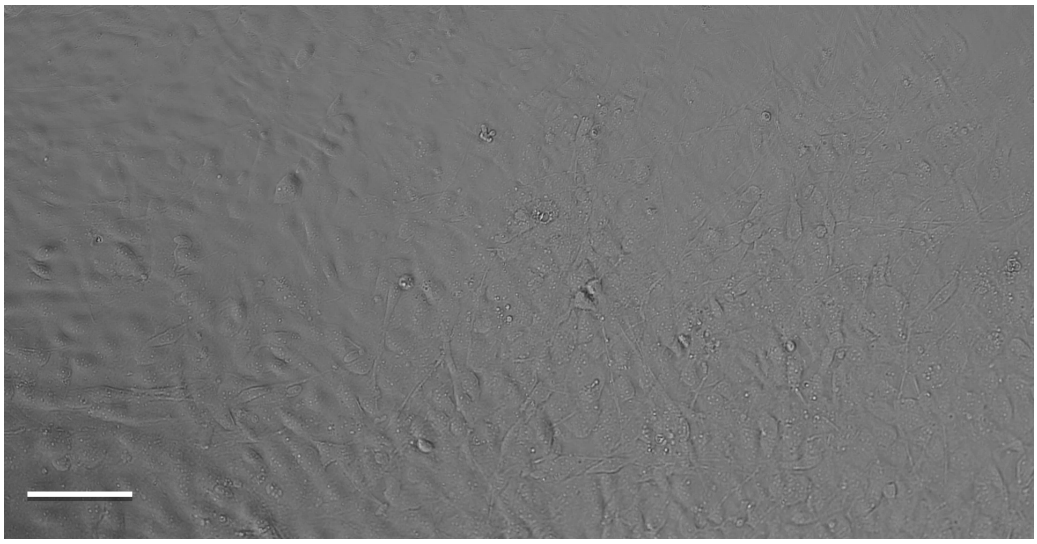

B.

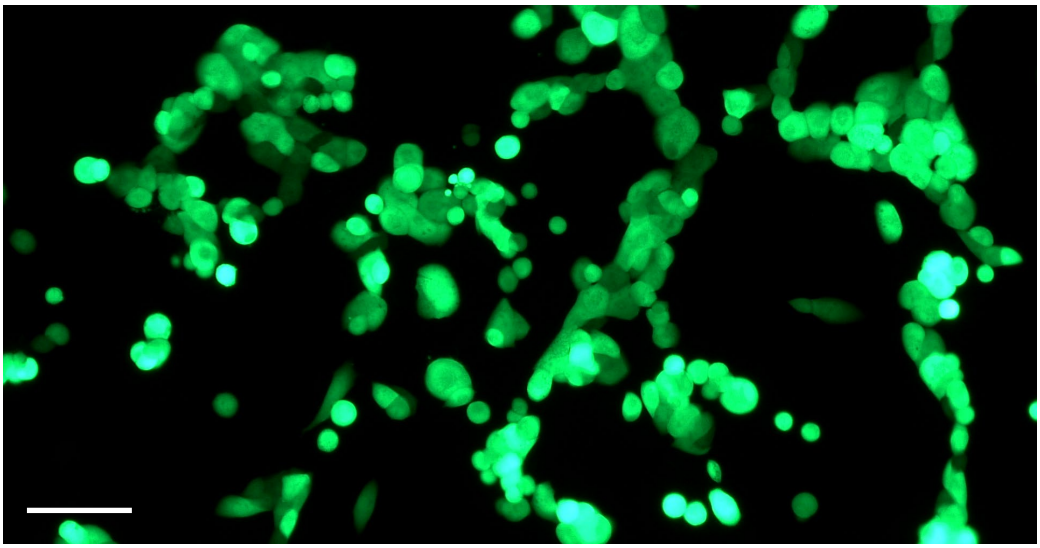

Figure 14. Brightfield image (10X) of cell control **(A)**. After 3 days, the cell control forms a healthy 3T3 fibroblast monolayer. No detachment was observed. Fluorescent image (10X) of viral control **(B).** Viral proliferation can be characterized by GFP expression. After 3 days, GFP expression was strong in the viral controls. Scale bar = 100 µm.

Assessment Techniques

It was necessary to employ a straightforward, streamlined, and repeatable CC50 and EC50 analysis methods to quickly quantify the therapeutic range for DDS tuning. Initially, CC50 and EC50 quantification techniques were long and labor intensive that yielded highly variable results. However, adjustments were made to successfully increase the speed and accuracy of these methods (see **Appendix Protocol 4**). The following is a description of the optimized approaches used in this work.

EC50 Analysis: Antiviral activity was assessed by measuring the viral load in CMV-infected (EC50) wells compared to viral control well, which represented 100% viral load or 0% inhibition. Relative GFP expression, which is directly correlated to viral gene expression, was used to indicate the CMV load. Acting as a secondary indicator, high GFP expression denoted low inhibition, while low GFP expression represented high mCMV inhibition. From varying degrees of inhibition, the EC50 was calculated.

EC50 analysis was performed before CC50 after the 3-day incubation. First, spent media was aspirated from all wells and replaced with warm 200 µL of DPBS (including blank wells). Removal of quercetin eliminated background fluorescence that overlapped with GFP (~509 nm).

A BioTek Synergy/HTX multi-mode plate reader was used to measure GFP fluorescence using an area scan programed in the GEN5 3.04 software. The filter wheel was set to 488/520 nm. Using the 5 mm diameter bottom probe and a gain of 50, the scan averaged 25 area acquisitions (398 µm horizontally and 398 µm vertically) evenly spaced throughout each 6.6 µm diameter well. Acquisitions were averaged to produce a single

mean fluorescence value. The plate was incubated at 37°C for the duration of the scan. All CC50, EC50, viral control wells, and blank wells were analyzed. See **Figure 15** for a representation of the raw data that is produced from the scanning fluorescence program.

	1	2	3	4	5	6	7	8	9	10	11	12
A	122	80	186	157	222			1822	2426	1824	23	25
B	54	46	94	90	100			2474	2522	1709	13	8
C	15	3	111	148	154			3538	3510	2195	4	5
D	37	19	1126	1135	1136	-5	-1	8829	8519	9283	21	39
E	44	46	1478	1430	1260	-7	13	7926	8756	8741	39	62
F	13	22	4491	5003	4679	7786	7966	8914	9361	9242	35	59
G	10	17	8418	9912	9411	6880	7677	8938	8307	9481	47	49
H	36	16	7879	8628	9476	8283	8267	7553	8321	6519	96	140

Figure 15. Raw data produced from the scanning fluorescence program of a Pluronic F127 plate. The left half of the plate is quercetin-loaded F127 and the right half is blank F127. Center columns are the viral control and blank wells. Values represent the mean fluorescent value generated from each well. The heat map is generated based on relative fluorescent intensities. All values are blanked against the 4 center “blank” wells. These values are used to calculate the EC50.

Any remaining background fluorescence was subtracted using the non-virally infected (CC50) and blank wells. The relative fluorescent value was then compared to the viral control and the percent viral inhibition was calculated. In each plate, three wells were exposed to the same DDS concentration. They were averaged and used as one replicate.

Viral inhibition was visualized by graphing percent inhibition vs. treatment concentration. The EC50 was determined by graphing percent inhibition vs. log(treatment concentration). The DDS concentration resulting in 50% inhibition was then calculated by linear interpolation.

Direct quantification of CMV load could be perform with a viral titer of spent media. For this reason, 50 µL samples from all CC50 and viral control wells were collected before replacing with DPBS. Samples were stored at -80 °C. A viral titer is an involved assay lasting 5-10 days and requires an additional 3-5 fully seeded 96-well plates to analyze the samples from one replicate of the CC50/EC50 assay. Hence, analysis by GFP expression was considered appropriate for this work.

CC50 Analysis: Cytotoxicity was assessed by measuring cell viability in non-CMV-infected (CC50) wells compared to cell control wells, which represented 100% viability or 0% toxicity. Viability assessment was performed by the Neutral Red (NR) assay, which is straightforward, sensitive, and commonly used in cytotoxicity analysis (92). The NR assay utilizes a vital red dye that is taken into cells through active transport mechanisms and incorporated into lysosomes. Non-viable cells will not uptake the dye (93).

The NR assay was performed after EC50 analysis by adding 100 µL of NR dye to all CC50, cell control, and blank wells. The DPBS was not removed before the addition of dye. After incubating at 37 °C and 5% CO_2 for 2 hours, the dye and DPBS were completely aspirated. Then, 200 µL of an extraction buffer composed of 50% Sorensen buffer and 50% ethanol was added to each well. The plate was incubated at room temperature protected from light and then gently agitated. The absorbance at 540 nm was

then measured using a BioTek Synergy/HTX multi-mode plate reader. In each plate, two CC50 wells were exposed to the exact same DDS concentration. They were averaged and used as one replicate. Absorbance of the test wells was compared to the control wells and the percent cytotoxicity was calculated. See **Figure 16** for a representation of the raw data that is produced from the scanning fluorescence program.

	1	2	3	4	5	6	7	8	9	10	11	12
A	0.08	0.03				0.33	0.36				0.10	0.13
B	0.10	0.10				0.34	0.31				0.29	0.22
C	0.12	0.14				0.34	0.28				0.30	0.24
D	0.18	0.23				0.00	-0.01				0.38	0.16
E	0.28	0.32				-0.01	0.01				0.30	0.23
F	0.33	0.37									0.30	0.28
G	0.30	0.32									0.29	0.23
H	0.25	0.26									0.23	0.15

Figure 16. Raw neutral red (NR) absorbance data produced from a Pluronic F68 plate. The left half of the plate is quercetin-loaded F68 and the right half is blank F68. Center columns are the cell control and blank wells. Values represent the absorbance (540 nm) from each CC50 test well and controls. The heat map is generated based on relative absorbance intensities. All values are blanked against the 4 center blank wells. These values are used to calculate the CC50.

Similar to EC50, the cytotoxicity was visualized by graphing percent cytotoxicity vs. treatment concentration. The CC50 was determined by graphing percent cytotoxicity vs. log(treatment concentration). The DDS concentration resulting in 50% cytotoxicity was then calculated by linear interpolation.

Because the cells are not initially seeded at 100% confluence before the test antiviral is added, it is possible that results from the NR assay indicate proliferation

inhibition rather than cytotoxicity. However, these assay results still provide valuable insight into the toxicity profile of the test compound. Further metabolic or gene expression analysis could be performed to determine if perceived toxicity is caused by slowed metabolism or suppressed cell division rather than cell death directly.

Adjustment of Micelle Composition and Quercetin Loading

The therapeutic range and SI, as determined by the CC50/EC50 assay, were used to guide the optimization of the quercetin DDS in an iterative process. The DDS was optimized when the Pluronic formula and quercetin loading resulted in a maximum SI.

The antiviral activity and cytotoxicity of free quercetin was tested first. Then, differences in the toxicity of maximum quercetin-loaded and non-loaded (blank) P123, F127, and F68 DDSs were utilized to determine the quercetin-loading tunability. Loading within the DDS was considered tunable if the blank exhibited relatively low toxicity compared to maximum loaded. The quercetin loading in F127 and F68 DDSs was reduced to minimize toxicity and increase the therapeutic range. To compare against the clinical standard CMV treatment, pure ganciclovir was also tested. Additionally, the synergy between ganciclovir and F127 or F68 DDSs was investigated. Results from those experiments follow.

Free Quercetin – CC50/EC50

The maximum solubility of free quercetin in DPBS at room temperature was determined using spectrophometric methods to be approximately 1.7 μM, which is within the range described in literature (0.5 -23 μM) (19). At maximum solubility, the toxicity and viral inhibition of free quercetin was characterized. However, due to low solubiliy however, concentrations resulting in either toxicity or viral inhibition were not achieved. No cellular or viral effects were observed. This result was not suprising, as previous experiments described in the literature use a solvent to increase quercetin solubility to antiviral or cytotoxic levels, usually DMSO (15, 16, 18, 46). However, this preliminary investigation did reaffirm that some quercetin carrier was necessary to delivery quercetin at effective concentrations.

Maximum Loaded and Blank P123 – CC50/EC50

Pluronic P123 was tested first. Pluronic micelle carriers or the quertin payload could contribute to either cytotoxicity or antiviral activity. In order to identify if the carrier or the payload is the cause of any viral or cellular effects, both blank and quercetin-loaded micelles were tested.

The CC50/EC50 assay was perfromed as described in a previous section. The raw data can be presented in the line charts seen in **Figure 17**.

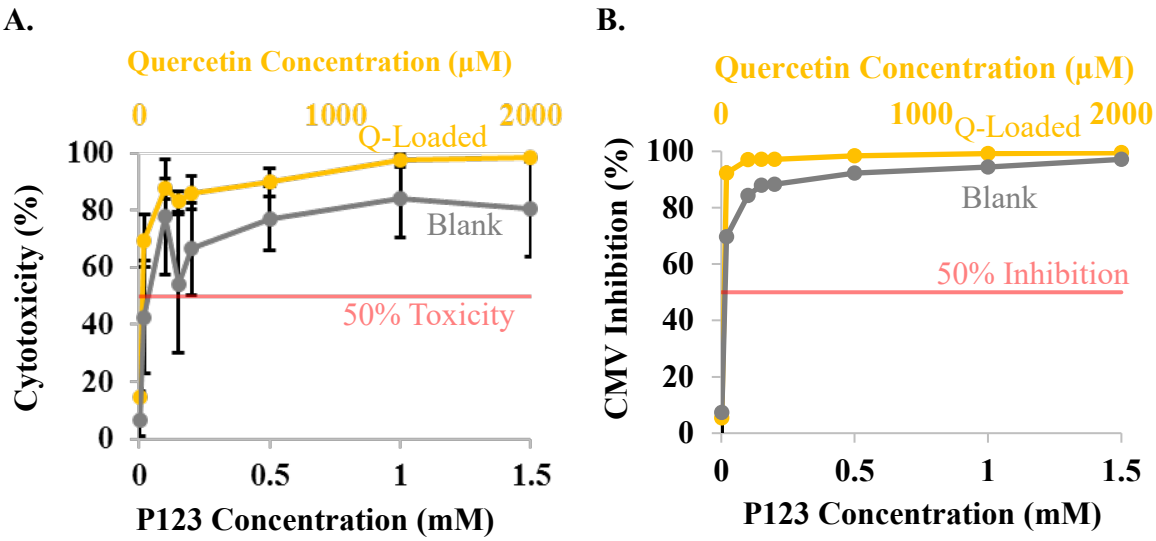

Figure 17. Cytotoxicity profile of blank (grey) maximum quercetin (Q)-loaded (yellow) Pluronic P123 micelles **(A)**. Quercetin did not add significant cytotoxicity to Pluronic P123 micelles. Viral inhibition profile of blank (grey) maximum quercetin-loaded (yellow) Pluronic P123 micelles **(B)**. Both blank and Q-loaded micelles were highly inhibitory. Error bars = Std. Deviation, n = 3.

Using linear interpolation, the CC50 and EC50 values were calculated from the data seen above. For maximum quercetin-loaded P123, the CC50 and EC50 values were 0.01 ± 0.006 and 0.006 ± 0.001 mM, respectively. For blank P123, the CC50 and EC50 values were 0.02 ± 0.007 and 0.01 ± 0.005 mM, respectively. With these values the therapeutic range of the system was determined, see **Figure 18**.

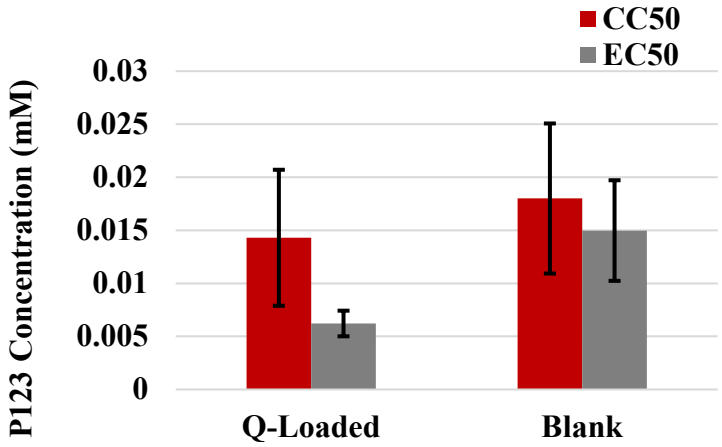

Figure 18. Therapeutic range of maximum quercetin (Q)-loaded and blank Pluronic P123. There was no statistical difference between CC50 and EC50 for Q-loaded or blank micelles. Error bars = Std. Deviation, n = 3.

The CC50 of maximum quercetin-loaded and blank P123 micelles were not significantly different, indicating that the toxicity from quercetin loading is either minimal or is masked by the toxicity of the delivery system itself. Although the difference between EC50 of quercetin-loaded and blank P123 micelles was not statistically significant, there seemed to be a slight antiviral effect added by quercetin loading, which could be an artifact of added toxicity. The SI was determined to be 1.0.

Because there was no difference between the CC50 and EC50 of blank P123 micelles, it can be concluded that the viral inhibition observed was a result of cytotoxicity. The SI was calculated to be 1.4. Despite the high encapsulation efficiency of pure P123 Pluronic micelles, the cytotoxic observed was too high for it to be a viable option for the DDS.

Maximum Loaded and Blank F127 – CC50/EC50

In hopes of reducing cytotoxicity, the CC50/EC50 of maximum quercetin-loaded and blank F127 micelles was investigated. The raw data from the CC50/EC50 assay can be seen in **Figure 19**.

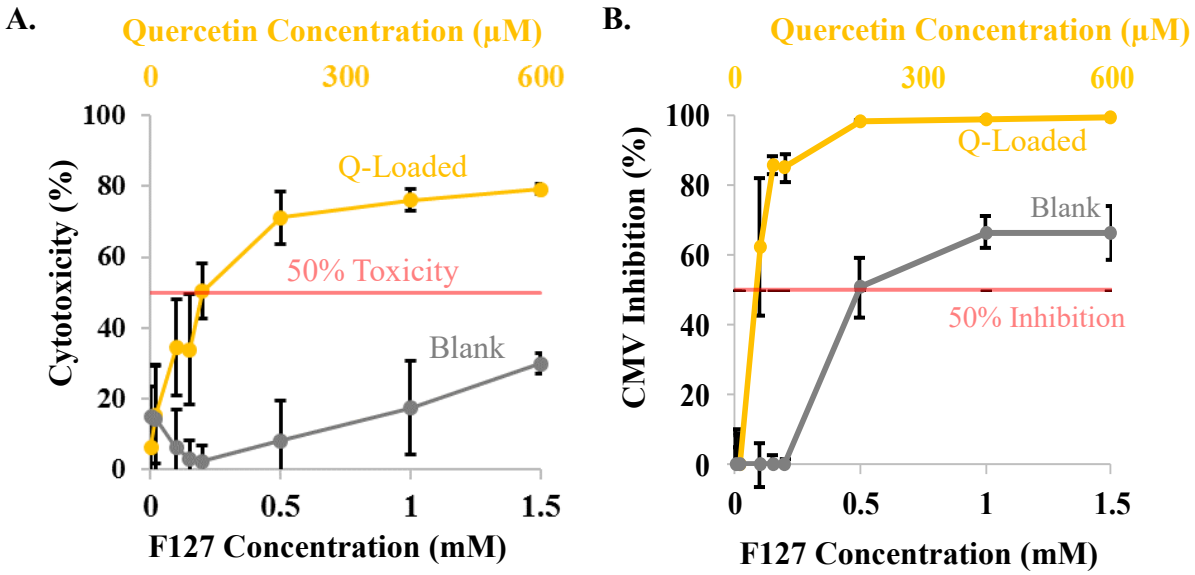

Figure 19. Cytotoxicity profile of blank (grey) maximum quercetin (Q)-loaded (yellow) Pluronic F127 micelles **(A)**. Blank F127 micelles had lower cytotoxicity than Q-loaded. Viral inhibition profile of blank (grey) maximum quercetin-loaded (yellow) Pluronic F127 micelles **(B)**. Q-loaded micelles were more inhibitory than blank. Error bars = Std. Deviation, n = 3.

Using linear interpolation, the CC50 and EC50 values were calculated from the data seen above. For maximum quercetin-loaded F127, the CC50 and EC50 values were 0.2 ± 0.1 and 0.07 ± 0.01 mM, respectively. For blank P123, the CC50 and EC50 values were 3.7 ± 0.3 and 0.6 ± 0.1 mM, respectively. The therapeutic range of pure Pluronic

F127 can be visualized in **Figure 20**.

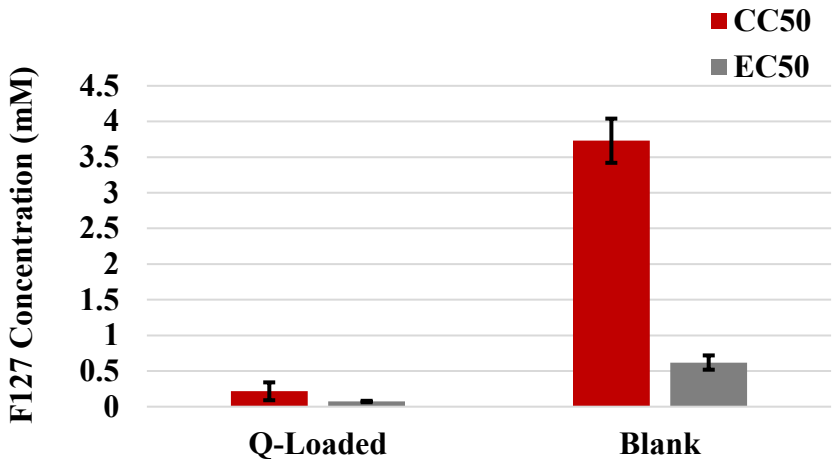

Figure 20. Blank F127 micelles inhibited CMV with lower cytotoxicity than P123. Quercetin loaded F127 had strong CMV inhibition, a narrow therapeutic window due to associated cytotoxicity. Error bars = Std. Deviation, n = 3.

The CC50 of blank F127 micelles was nearly 200X greater than blank P123, indicating F127 Pluronic was much less cytotoxic than P123. The statistically significant difference between the CC50 and EC50 of blank F127 suggests that the F127 carrier itself has some CMV inhibitory effect. This inhibition could be due to changes in membrane viscosity arising from Pluronic/membrane interactions, possibly disrupting virion attachment or release(38). Pluronic may interact with the virion, affecting attachment and entry. It is also possible that F127 Pluronic may slow 3T3 fibroblast metabolism and subsequently, viral replication rates (38).

Quercetin-loading resulted in nearly a 20X decrease of the CC50 compared to blank F127, indicating that maximum quercetin loading contributed to cytotoxicity. Additionally, the difference between blank and loaded CC50 values suggested that

reducing quercetin loading of pure F127 micelles may reduce cytotoxicity and widen the therapeutic range.

Reduced Loading F127 – CC50/EC50

While it is generally the goal to achieve maximum loading in a drug delivery vehicle such as a Pluronic micelle, for quercetin it was necessary to reduce the loading to minimize cytotoxicity and increase the therapeutic range. Thus the quercetin loading of Pluronic F127 was reduced to 80% and 50% of maximum. A summary of the CC50/EC50 assay results can be seen in **Figure 21**.

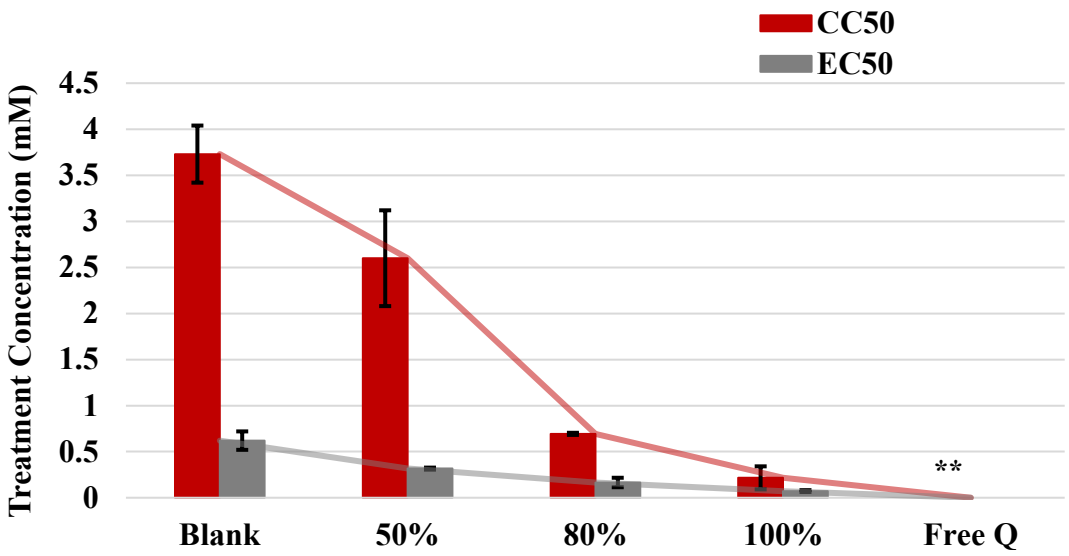

Figure 21. Quercetin loading percentages were reduced from maximum to increase therapeutic range. QF127 50% of max loading resulted in widest therapeutic range. Percentages (%) are referring to percent of maximum loading capacity. Error bars = Std. Deviation, n = 3. **Free quercetin solubility was below EC50 and CC50.

Reduction of the quercetin loading resulted in a decrease in the toxicity of the system, as reflected in a higher CC50 value. However, the reduced loading also decreased the antiviral activity as seen with higher EC50 values. It appears that 50% maximum quercetin loaded Pluronic F127 micelles exhibited the widest therapeutic range with CC50 and EC50 Pluronic concentrations of 2.6 ± 0.5 and 0.3 ± 0.01 mM, respectively. To more conveniently identify which of these loading variations resulted in the widest therapeutic range, the SI values were calculated and compared, see **Figure 22**.

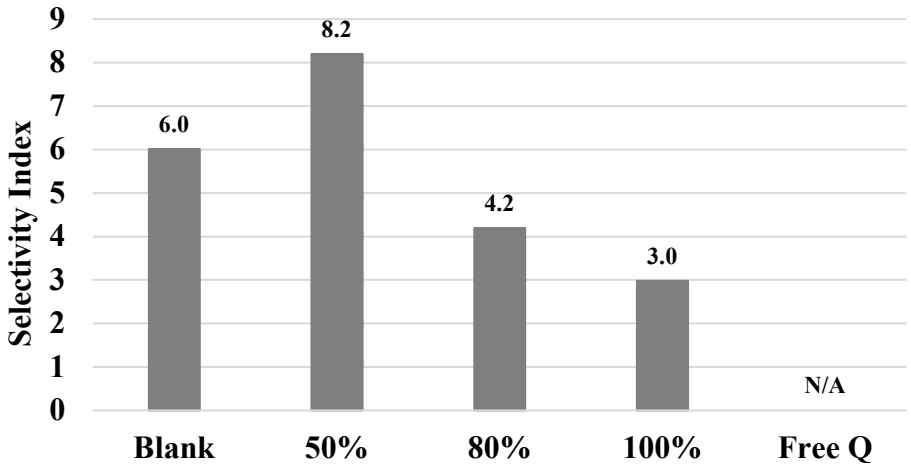

Figure 22. Using the SI, different potential antiviral can be compared. 50% maximum quercetin loaded Pluronic F127 micelles exhibited the widest therapeutic range. Percentages (%) are referring to percent of maximum loading capacity.

From these results, it can be seen that 50% maximum quercetin loaded Pluronic F127 micelles exhibited the widest therapeutic range with an SI of 8.2. The added cytotoxicity resulting from the quercetin loaded into the micelles was compensated by increased antiviral activity. Blank Pluronic F127 micelles showed the second widest therapeutic range, probably due to lower cytotoxicity from an absence of quercetin. These results show that quercetin delivered to mCMV infected 3T3 fibroblasts via Pluronic F127 micelles can inhibit viral replication. Additionally, by reducing the quercetin loading, the therapeutic range was successfully widened, making 50% maximum loaded the most attractive Pluronic F127 mCMV inhibitor.

Although 50% loaded F127 exhibited the widest therapeutic range, an SI of 8.2 is

representative of only moderate antiviral activity with mostly toxicity. An antiviral that demonstrates distinct inhibitory activity without cytotoxicity would have an SI approximately 30 or greater. Although the FDA does not have a designated threshold for SI, few antivirals exhibiting an SI less than 15 *in vitro* are considered for further investigation (94). The limitation observed with the 50% quercetin-loaded F127 system is most likely due to the toxicity of the Pluronic carrier. Although reducing the quercetin loading decreased toxicity, the inherent toxicity from the F127 carrier could be masking the antiviral activity of the quercetin payload. Further exploration of Pluronic micelle composition was necessary to reduce toxicity, increase the therapeutic range and SI, and deliver quercetin at inhibitory but non-toxic concentrations.

Maximum Loaded and Blank F68 – CC50/EC50

F68 was investigated to reduce the toxicity of the Pluronic micelle carrier. Initially, Pluronic F68 was not considered a viable option for this system because it exhibited a poor carrying capacity compared to the other two Pluronics, but results from Pluronics P123 and F127 indicated that high quercetin loading contributed to toxicity. A reduction of quercetin was necessary to increase the therapeutic range of the F127 carrier, therefore F68 was reconsidered despite the lower loading. Additionally, literature indicates that F68 exhibits the mildest toxicity of the three selected Pluronics.

Maximum quercetin-loaded and blank Pluronic F68 micelles were tested using the CC50/EC50 assay. The raw data can be seen in **Figure 23**.

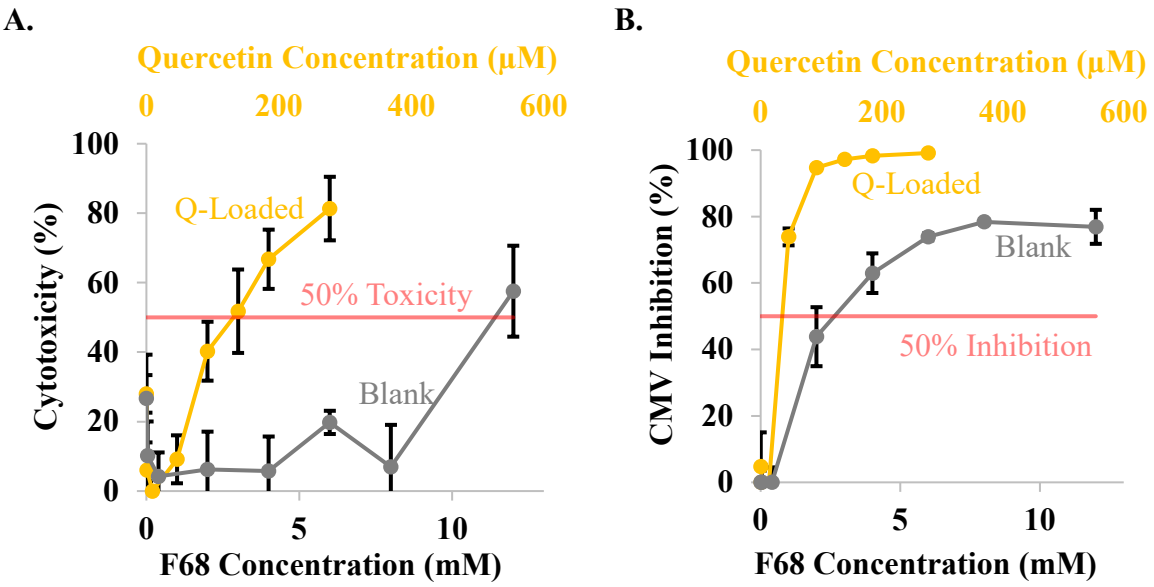

Figure 23. Cytotoxicity profile of blank (grey) maximum quercetin (Q)-loaded (yellow) Pluronic F68 micelles **(A)**. Blank F68 micelles had a significantly lower cytotoxicity than Q-loaded. Viral inhibition profile of blank (grey) maximum quercetin-loaded (yellow) Pluronic F68 micelles **(B)**. Q-loaded micelles were more inhibitory than blank. Error bars = Std. Deviation, n = 3.

Using linear interpolation, the CC50 and EC50 values for the tested formulations were calculated from the data seen above. For maximum quercetin-loaded F68, the CC50 and EC50 values were 3.0 ± 0.4 and 0.4 ± 0.1 mM, respectively. For blank F68, the CC50 and EC50 values were 11.0 ± 1.0 and 2.1 ± 0.7 mM, respectively. The therapeutic range of Pluronic F68 can be visualized in **Figure 24**.

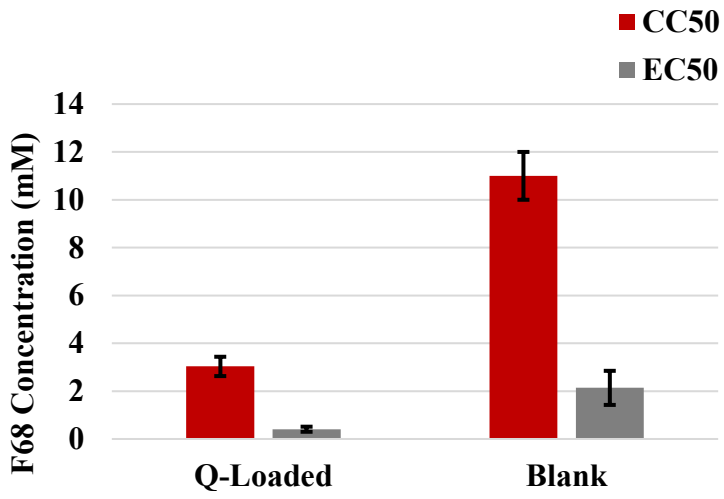

Figure 24. Blank F68 micelles had the highest CC50 value of all Pluronics tested, yet still showed some antiviral activity. Quercetin-loaded F68 had a much lower CC50 than blank F68, but also resulted in increased viral inhibition.

The CC50 of blank F68 is much greater than Pluronics P123 and F127, meaning that F68 is far less cytotoxic. This finding was not surprising, as F68 is commonly used in a wide variety of mammalian cell culture applications with little to no cytotoxicity (53). In fact, some studies have shown that Pluronic F68 acts as a membrane annealer. Chen H. et al. showed that adding Pluronic F68 to chemically permeabilized 3T3 fibroblasts resulted in membrane stabilization and healing (68). It was also shown by Maskarinec S. A. et al. that F68 incorporation into damaged membranes increases membrane surface pressure up to healthy levels. Upon the restoration of normal pressure levels, the Pluronic is excised or “squeezed out” of the healthy membrane and functionality is restored (95). In this way, Pluronic F68 may in fact improve 3T3 fibroblast health to a certain degree, rather than result in toxicity. The low toxicity of F68 is highly desirable for this system.

Similar to blank F127, the EC50 value of blank F68 suggests that there was some viral inhibition from the Pluronic carrier alone. To the author's knowledge, this is the first time the antiviral activity of Pluronic F68 or F127 has been reported. Thus, the exact mechanism of this activity has not been addressed in the literature. There are several points of the viral replication cycle that may be disrupted by Pluronic F127 or F68. The surface activity of the Pluronics may dismantle the virion itself, preventing attachment. These Pluronics may also interfere with viral attachment or egress by changing cellular membrane viscosity or altering receptor activity (38, 55, 95). It is also possible that the antiviral activity is a secondary response caused by effects on normal cell function or metabolism. Some Pluronics have shown to reduce ATP production and slow metabolism (38). Therefore, the F127 or F68 may be slowing viral replication rather than inhibiting it. However, to fully elucidate the antiviral activity of Pluronic F127 and F68 alone, experimentation addressing virion/Pluronic interaction, viral attachment and release, and viral gene expression in the presence of these Pluronics should be performed. Such experimentation is beyond the scope of this work. But from the experimentation performed, it has been observed that Pluronic F127 and F68 micelles are not just inert carriers, but also appear to exhibit intrinsic antiviral activity themselves.

The maximum quercetin-loaded F68 micelles were significantly more cytotoxic than blank micelles, indicating that the degree of loading that was achieved with F68 exceeded subtoxic levels. Although too much quercetin was delivered to the cells at maximum loading, resulting in higher level of toxicity, it was demonstrated that the relatively low carrying capacity of F68 (EE% of 1.8%, and DL% of 0.1%) was sufficient to deliver a quercetin cargo at inhibitory levels.

Exhibiting both relatively low toxicity and sufficient quercetin-carrying capacity, it was determined that the Pluronic F68 DDS was the most appropriate for delivering quercetin for CMV inhibition. Adjustment of the quercetin loading was necessary to optimize the toxicity and inhibition of the F68 DDS.

Reduced Loading F68 – CC50/EC50

The quercetin loading within Pluronic F68 micelles was reduced to 75%, 50%, and 25% of maximum to reduce toxicity in an effort to increase the therapeutic range (see **Appendix Protocol 5**). In order for the therapeutic range to increase by reduced loading, the rate of CC50 increase should be greater than EC50. Optimization occurs at the point where the difference of CC50 and EC50 is greatest. If the rates of change are equal, the DDS is not tunable. A summary of the CC50/EC50 assay results can be seen in **Figure 25**.

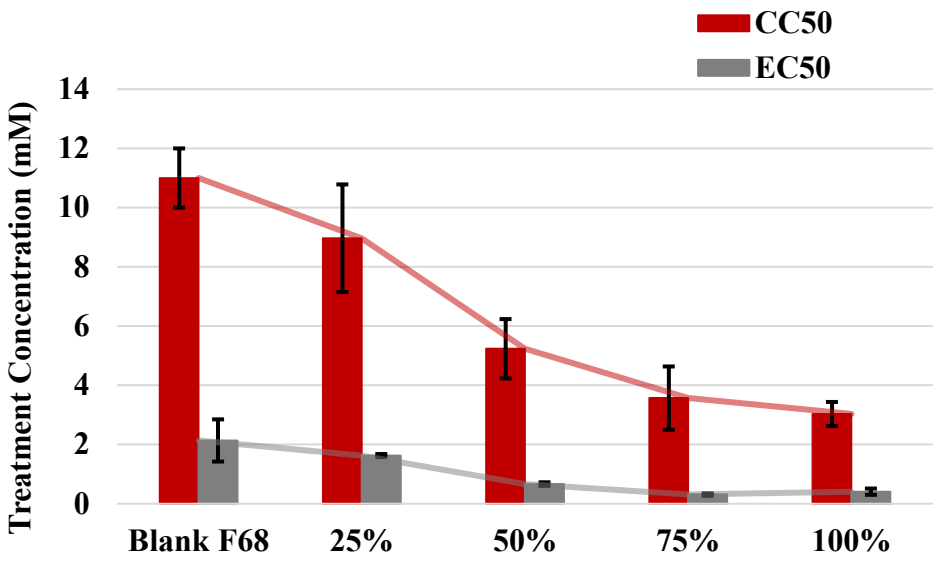

Figure 25. Quercetin loading percentages were reduced from maximum to increase therapeutic range. Percentages (%) are referring to percent of maximum loading capacity. Error bars = Std. Deviation, n = 3.

To more conveniently identify which of these Pluronic micelle variations resulted in the widest therapeutic range, the SI values were calculated and compared, see **Figure 26**.

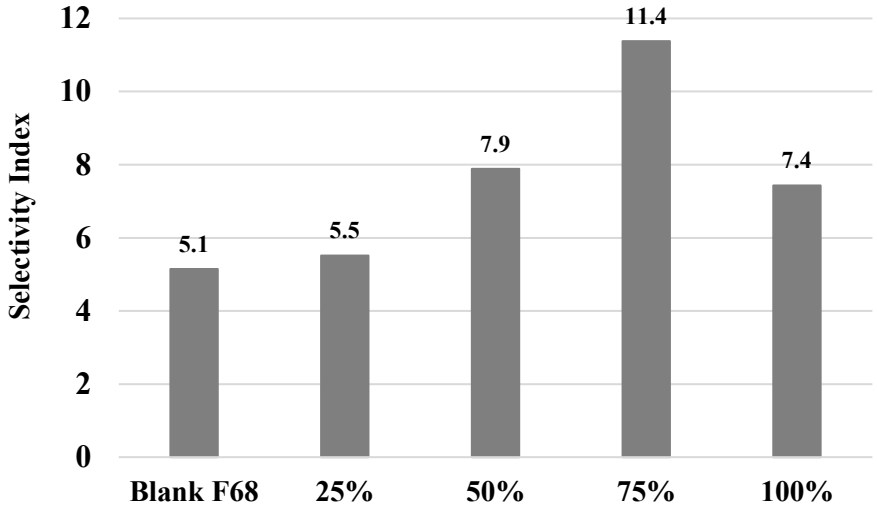

Figure 26. Using the SI, the therapeutic ranges of different quercetin loading were compared. 75% maximum quercetin loaded Pluronic F68 micelles exhibited the widest therapeutic range. Percentages (%) are referring to percent of maximum loading capacity.

The 75% quercetin-loaded F68 DDS exhibited the widest therapeutic range with an SI of 11.4 and thus had the optimal quercetin loading. The increased toxicity from the quercetin loading was compensated by the increased viral inhibition, making the inhibitor more effective. Compared to all other variations of quercetin-loaded Pluronic carriers tested in this work, 75% quercetin-loaded F68 DDS was the most effective at inhibiting mCMV in this *in vitro* model.

It is interesting to note the change in micelle size and aggregation due to a reduction in quercetin loading. At maximum loading, F68 micelles did not form discrete particle diameters (see **Table 3**). When the loading was reduced to 75%, 50%, and 25%

of maximum capacity, micelles with discrete diameters ranging from 5.4 – 5.8 nm were observed (see **Appendix Figure 3**). Measurements were taken with the same conditions as described in Chapter 2.

To contextualize the SI of 75% quercetin-loaded F68 DDS, the therapeutic range of the commonly used CMV antiviral drug, ganciclovir, was assessed using the same model and procedures.

Ganciclovir – CC50/EC50

As a positive control for the model and to compare against Pluronic/quercetin results, the CC50 and EC50 of ganciclovir was investigated using this same cell culture model and methods. Results can be seen in **Figure 27.**

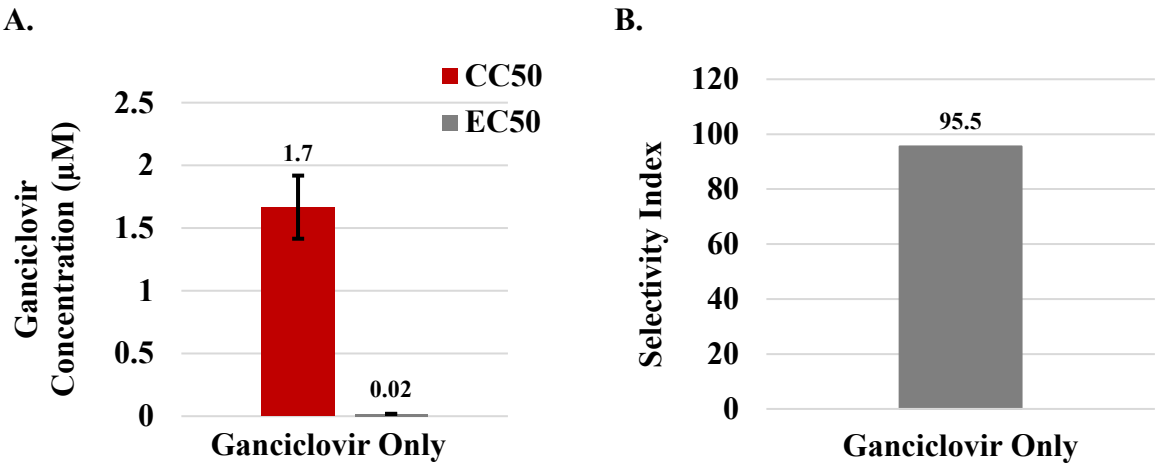

Figure 27. Summary of the therapeutic range of ganciclovir only **(A)**. SI as defined by the CC50 and EC50 **(B)**. Error bars = Std. Deviation, n = 3.

The CC50 and EC50 values for ganciclovir were determined to be 1.7 ± 0.3 and 0.02 ± 0.002 mM, respectively. With these values, the SI was calculated to be 95.5. These results show that ganciclovir is highly active and causes minimal toxicity in this cell culture model. These results are not surprising as ganciclovir is engineered specifically to inhibit CMV, making it the current clinical standard (6). As a positive control, these results show that the assay is in fact sensitive enough to detect antiviral activity and cytotoxicity, validating the results from this *in vitro* model. Conversely, this model does not properly recapitulate the damaging side effects well documented in clinical use of ganciclovir.

When comparing the ganciclovir SI (95.5) with the 75% quercetin-loaded F68 SI (11.4), it is apparent that the therapeutic range of this system needs to be improved to replace ganciclovir. The cytotoxicity of the Pluronic/quercetin system needs to be greatly decreased or the efficacy of viral inhibition more targeted. Currently, the viral inhibition observed with the tested system may be a result of toxicity. However, this system does demonstrate promise. But because this *in vitro* model is limited in how well it can reflect the clinical efficacy of an antiviral, further *in vivo* experimentation is warranted. It is possible that this system demonstrates high viral inhibition without the clinical side effects produced by ganciclovir.

Ganciclovir and F68 Synergy – CC50/EC50

The use of quercetin-loaded Pluronic micelles as an alternative to ganciclovir may

be limited due to cytotoxicity at concentrations required to achieve significant viral inhibition. However, the possibly of using this system in concert with ganciclovir rather than a replacement may also be beneficial. Any reduction in the ganciclovir dose necessary to achieve viral inhibition may reduce harmful clinical side effects, such as neutropenia, thrombocytopenia, seizures, or abnormal liver function (6).

With this goal in mind, the combination of maximum quercetin-loaded Pluronic F127 DDS + ganciclovir was explored. Despite the intermediate carrying capacity of F127 DDS (EE% of 12.8% and DL% of 0.9%), moderate antiviral activity (SI of 8.2), and micelle stability, the results did not show synergy (see **Appendix Figure 7**). The cytotoxicity of the F127 DDS probably masked any promising effect that may have existed.

Synergy between ganciclovir and the least cytotoxic, Pluronic F68 DDS was investigated. The CC50/EC50 assay was performed as described previous, but adjustments were made to treatment preparation. A constant 1 mM F68 DDS was co-administered with a ganciclovir concentration range. The 1 mM F68 concentration was chosen because it was within the therapeutic range (SIs of 5.1 to 11.4), minimally cytotoxic, and above the critical micelle concentration (CMC) as seen in Chapter 2. Quercetin loading was tuned to 100%, 50%, and 25% of maximum for testing (see **Appendix Protocol 5**). Results from 75% quercetin loading were nearly identical to the 100% quercetin loading and can be seen in **Appendix Figure 8**. By varying the ganciclovir concentration but maintaining constant 1 mM F68 DDS concentration, it was possible to observe the effect F68 on the ganciclovir CC50 and EC50 only. Furthermore, it was possible to see how the Pluronic F68 influenced the cellular and viral effect of the

ganciclovir. Cytotoxicity results from this assay can be seen in **Figure 28.**

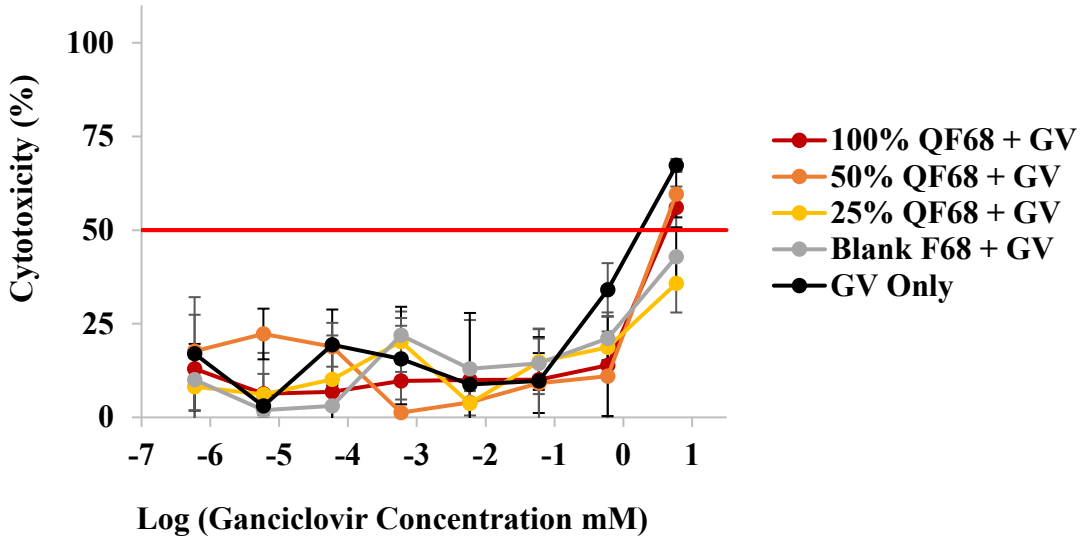

Figure 28. A constant 1 mM F68 DDS was added to all ganciclovir concentrations. Toxicity from the addition of quercetin-loaded F68 to the ganciclovir was comparable to ganciclovir only. Variations in cytotoxicity results are probably due to inherent fluctuations in the NR assay used to acquire these data. Error bars = Std. Deviation, n = 3. Percentages (%) in key are referring to the percentage of maximum quercetin loading.

The CC50 values of blank and 25% quercetin-loaded F68 + ganciclovir were not achieved within the ganciclovir concentrations tested. It can be seen from results that the addition of quercetin-loaded or blank F68 Pluronic did not increase the toxicity compared to ganciclovir only. Meaning that any additional antiviral activity is not a result of increased toxicity. Viral inhibition results can be seen in **Figure 29.**

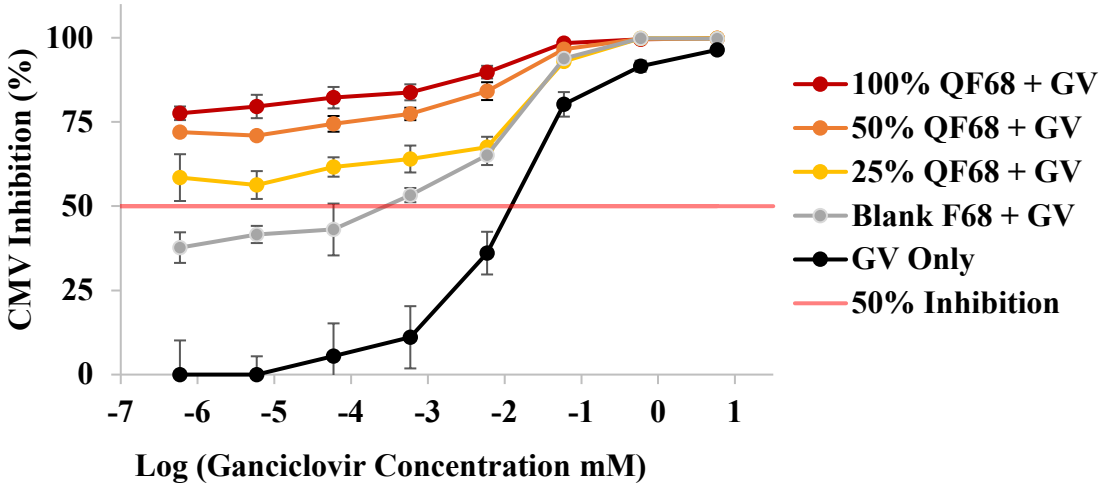

Figure 29. A constant 1 mM F68 DDS was added to all ganciclovir concentrations. Supplementation of maximum quercetin-loaded and blank F68 improved the viral inhibition of ganciclovir. The EC50 of ganciclovir only (0.022 mM) was decreased to about 0.003 mM with the addition of blank F68 DDS. Inhibition was too great for other F68 DDS loadings to calculate EC50s. Error bars = Std. Deviation, n = 3. Percentages (%) in key are referring to the percentage of maximum quercetin loading.

It was seen previously in this chapter that 1 mM F68 alone, at the selected quercetin-loadings (excpet 25%), exhibited antiviral activity above 50% inhibition. Even at low ganciclovir concentrations, CMV inhibtion was too great to calcluate EC50 values. However, there is a distinct increase in antiviral activity resulting from the addition of 1 mM F68 to the ganciclovir treatment regimen. Based on the F68 toxicity results (**Figure 28**), this activity increase is not a result of increased toxicity but rather true viral inhibition.

Ganciclovir alone was approximately 100% inhibitory at 10 mM but also nearly

75% cytotoxic. At 1 mM, 75% inhibition and 35% cytotoxicity were observed. When the ganciclovir concentration was lowered to more clinically relavent concentrations around 0.01 mM, inhibition and cytotoxicity decreased to 35% and 10%, respectively (6). However, when 0.01 mM ganciclovir was coadministered with 1 mM maximum quercetin-loaded QF68, CMV inhibition was increased to nearly 100%, while cytotoxicity still remained at 10%. Thus, ganciclovir concentrations needed to achieve 100% inhibition were dropped by 3 orders of magnitude when supplemented with maximum quercetin-loaded F68 DDS. During the average ganciclovir treatment regimen, plasma ganciclvoir concentrations are maintained at 0.01 – 0.07 mM (6). In this model, ganciclovir only at these concentrations results in 35% - 75% inhibition. But when administered with 1 mM maximum quercetin-loaded F68 DDS, inhibition at that concentration range is 80% - 100%.

These results would have direct clinical relavence if 1 mM quercetin-loaded F68 + 0.01 mM ganciclovir is less likely to cause neutropenia, thrombocytopenia, or other side effects that may be observed from 0.1 mM ganciclovir alone. Additional trials with animal models would be necessary to confirm this. However, a 3-order of magnitude reduction in the effective ganciclovir concentration would certainly reduce treatment regimen costs.

It was also observed from the results that the supplementation efficacy is dependant on the extent of ganciclovir loading within the F68 micelles, where maximum-loaded increased inhibition drastically and blank F68 micelles increased inhibition intermediately. Blank Pluronic F68 micelles were also inhibitory, indicating that the micelles are not inert carries but have direct or indirect antiviral activity as discussed in

previous sections. Future studies involving addition of Pluronic F68 prior to viral infection may provide insight into how membrane-altering activity contributes to antiviral activity (68). Studies involving quantification of gene expression of cells exposed to F68 could also help elluciate how this Pluronic affects metablosim and/or gene expression leading to observed antiviral activity. Quercetin also plays an important role in the antiviral system, as it increases CMV inhibition in a concentration-dependant manner.

It is important to note that the exact SI values from this assay could not be determined because not all the CC50 and EC50 values could be tabulated, however the SI values could be estimated based on extrapolated values. Addition of blank F68 to the ganciclovir treatment increased the SI an estimated 22-fold compared to ganciclovir alone. With quercetin-loaded F68 DDS, the estimated SI was upwards of 500-fold greater.

The combined antiviral activity of the quercetin-loaded F68 Pluronic micelle system and ganciclovir produced an antiviral cocktail that not only exhibited low toxicity but strong high viral inhibition *in vitro.* There may be a variety of potential anti-CMV mechanisms at work, resulting in a more effective inhibitor. Ganciclovir blocks viral DNA replication by competitively inhibiting DNA polymerase. Quercetin has been shown to interfere with viral entry, viral protein production, and may disrupt viral gene expression (5, 81, 96). Pluronic may compromise virion integrity, disrupt virion attachment or release, or slow cell metabolism and viral replication rates. An antiviral cocktail is more effective with multiple points of disruption in the viral replication cycle.

This observed synergy could have direct clinical implications, as a reduction in ganciclovir dosage could drastically reduce the serious side effects so commonly

observed in human subjects. Further *in vivo* testing should be performed to confirm the effect that was observed with this cell culture model.

Conclusions

An *in vitro* model using NIH/3T3 mouse fibroblast cells was developed and a viral load reduction and cytotoxicity assay was optimized for testing the quercetin delivery system. The CMV inhibition and cytotoxicity were quantified by the EC50 and CC50 to establish the therapeutic ranges and SI values for Pluronic P123, F127, and F68. At maximum quercetin-loading the SI values for Pluronic P123, F127, and F68 were 1.0, 3.0, and 7.4 respectively. By comparing the SI values of maximum-loaded and blank DDSs, Pluronic F68 was identified as the least cytotoxic and most tunable, making it the most appropriate for this application.

Both blank and maximum quercetin-loaded Pluronic P123 were cytotoxic and not suitable for this system, despite having a high carrying capacity (EE% of 92.8% and DL% of 6.9%). Maximum quercetin-loaded Pluronic F127 was cytotoxic (SI of 3.0), but blank F127 exhibited only moderate toxicity (6.0). Therefore, the quercetin loading within the F127 was reduced to 80% and 50% and SI values were compared. Pluronic F127 at 50% loading resulted in the widest therapeutic range (SI of 8.2). Due to quercetin toxicity at higher concentrations, maximum loaded had the narrowest therapeutic range (SI of 3.0).

To reduce toxicity further, Pluronic F68 was investigated. Blank Pluronic F68

exhibited minimal toxicity (SI of 5.1). Various quercetin loadings (100%, 75%, 50%, and 25% of maximum carrying capacity) were tested in the F68 DDS. It was found that 75% quercetin-loaded resulted in the widest therapeutic range (SI of 11.4), representing a 33% increase from 50% loaded F127. Although this was the widest therapeutic range achieved with the Pluronic quercetin DDS, there still exists some toxicity and lack of targeted CMV inhibition. Moreover, the SI of ganciclovir is 95.5, as established with this model. However, this model does not recapitulate the *in vivo* side effects widely observed, such as neutropenia, thrombocytopenia, seizures, or abnormal liver function, making the low cytotoxicity observed misleading (6). Therefore, the synergy between ganciclovir and the Pluronic F68 DDS was investigated in an attempt to reduce the effective ganciclovir concentration.

Strong synergy between ganciclovir and 1 mM maximum-loaded F68 DDS was achieved. Coadministeration dropped the 100% effective ganciclovir dose 3 orders of magnitude without increasing toxicity. CMV inhibition was increased from 35% - 75% to 80% - 100% over the target ganciclvoir concentration range (0.01 – 0.07 mM) without added toxicity (6). A reduction in the effective ganciclovir concentration could avoid severe clinical side effects and reduce treatment regimen costs.

CHAPTER 4

ENGINEERING SIGNIFICANCE AND FUTURE WORK

Overview

In this chapter, the basic engineering principles that were utilized in this work are discussed. The thermodynamics governing Pluronic micelle formation and quercetin-loading by the thin-film hydration method is explained. Quercetin stability and drug release modeling are discussed. Future directions include assessment of drug delivery through micelle/membrane interaction and development of more advanced cell-culture and animal models.

Pluronic Micelle Thermodynamics – Thin-film Hydration

The thermodynamic principles of the thin-film hydration drive efficient quercetin loading, facilitate rapid micelle formation, and allow for low cost and straightforward fabrication. The efficient loading of the Pluronic micelles is achieved by the first step of the method, where the quercetin and Pluronic are both dissolved in a mutual solvent, allowing for the close interaction of carrier and cargo. Upon evaporation of the acetone and formation of the dried film, the hydrophobic regions of the Pluronic are already quercetin-saturated. Thus, when resuspension in an aqueous solution occurs, the quercetin is rapidly and efficiently sequestered within the hydrophobic core of the micelles as they form. In contrast, direct solubilization methods that rely solely on the

hydrophobic effect and associated entropic penalty of hydrated drug to drive quercetin into formed micelles, are less efficient and require longer loading times (41). They are limited by the diffusion of quercetin in solution and the random incorporation of quercetin into the micelles, rather than a controlled and engineered process.

The rapid resuspension of Pluronic and subsequent micelle formation is achieved in the last step of the method by lowering the solution temperature to 4 °C. Because temperature affects the entropic penalty resulting from the hydration of the Pluronic PPO block, changes can directly influence the micellization driving force (47). Gibbs free energy equation can be used to describe the effect of temperature on the driving force:

(3) $$\Delta G = \Delta H - T\Delta S$$

where ΔG describes change in Gibbs free energy, ΔH is change in enthalpy, T is temperature, and ΔS is change in entropy. A favorable reaction is represented by a negative ΔG, where the smaller the ΔG the more favorable the reaction. At lower temperatures, the change in entropy can be larger (large entropic penalty) and still result in a favorable reaction. Thus, by lowering the temperature, the entropic penalty is minimized, and micelles form more readily.

Although changes in temperature also affect the carrying capacity of the micelles, the loading at 4 °C was sufficient for this system. Resuspension was performed at 37 °C to investigate efficiency differences. The carrying capacity nearly doubled for F68 micelles (see **Appendix Figure 9**).

Compared to other drug loading techniques, the thin-film hydration method is low cost and requires straightforward procedure. The only reagent used in this method is

acetone and the total process is completed in a few steps. The only equipment needed is a rotoevaporator, so it can be performed in most laboratories. In other procedures, such as the supercritical antisolvent process, a variety of solvents are needed for numerous involved steps (97). The equipment necessary is expensive and niche. Although other techniques such as temperature-induced emulsification or direct solubilization, do not require expensive equipment, the preparation time can be significant and the procedure may not be Pluronic- or quercetin-compatible (41).

Quercetin Stability

Although the stability of the Pluronic micelle carriers was addressed in chapter 2 with CMC quantification, the stability of the quercetin payload was not addressed. To maintain an active form, it is necessary to prevent metabolism and oxidative degradation of quercetin (19). Therefore, addressing the stability of quercetin encapsulated within the micelles could provide useful insight into system shelf-life and oxidative protection.

Stability of encapsulated quercetin was analyzed by an assay performed by Andrew Kjar and Mitch Heap. The goal of the assay was to determine which Pluronic species would provide the most efficient oxidative protection. Micelle-encapsulated quercetin was exposed to various levels of oxidative stress by a range of H_2O_2 concentrations. The rate of degradation was quantified by observing the production of quercetin degradation products by UV-vis spectroscopy. It was found that Pluronic F127 provided the best protection against oxidative degradation.

Drug Release

An important aspect of any drug delivery system (DDS) is the mechanism and kinetics of release. This system is not targeted and cannot be considered a method of controlled release, but rather a systemic release of quercetin as the micelles are diluted and disassemble. However, due to the surface activity of the Pluronic carrier and its ability to integrate into a mammalian cell membrane or induce endocytosis, it is possible that the carrier actively participates in quercetin uptake by the cells (38). Evidence of this mechanism was observed *in vitro.* It was observed with brightfield microscopy that P123 induced significant vesicle formation in 3T3 fibroblasts (see **Figure 30**).

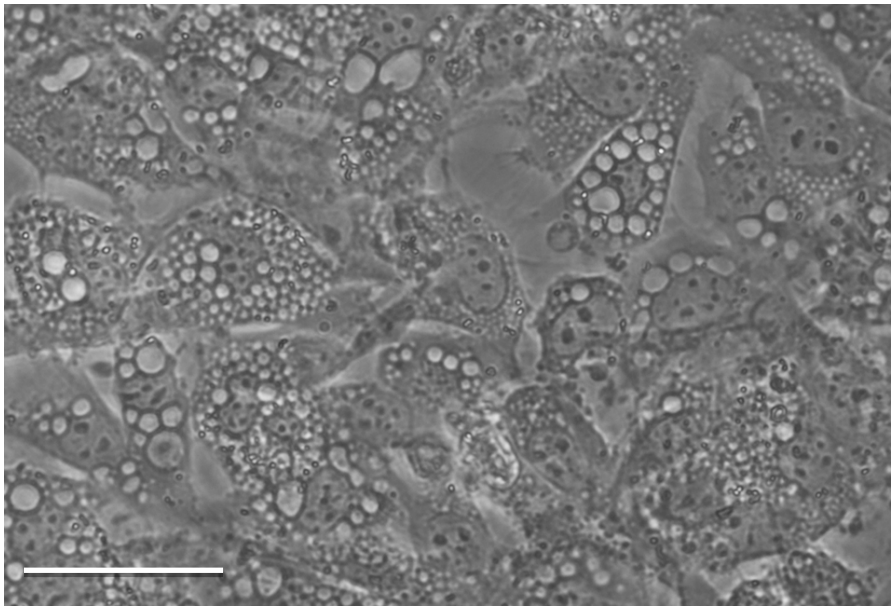

Figure 30. Brightfield image (40X) of 3T3 fibroblasts exposed to P123. P123 induced extreme vesicle formation. Scale bar = 50 μm.

When exposed to quercetin-loaded P123, the vesicles contained high concentrations of quercetin (see **Figure 31**), as observed by imaging the intrinsic

fluorescence of quercetin with a fluorescent microscope.

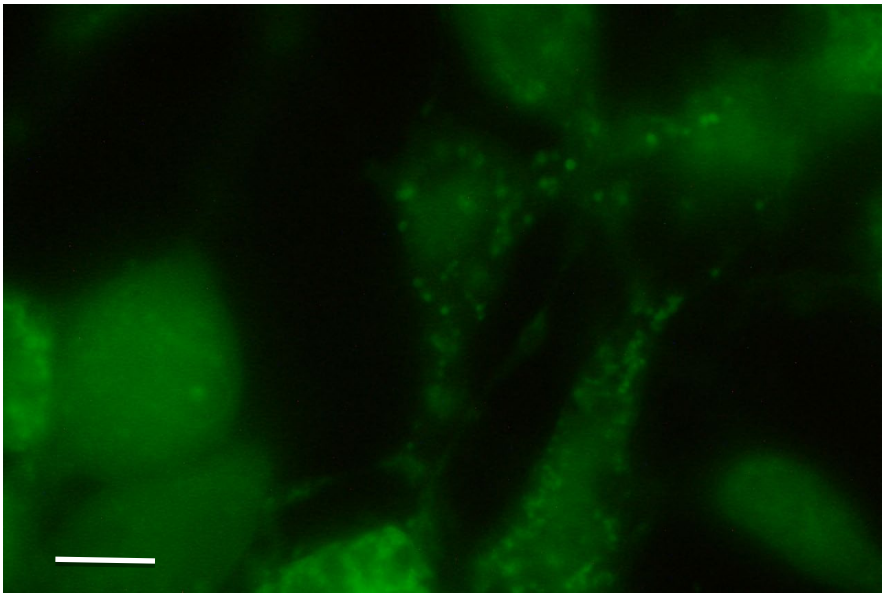

Figure 31. Fluorescent image (100X) of 3T3 fibroblasts exposed to quercetin-loaded P123. Quercetin-loaded vesicle formation was induced. Scale bar = 10 μm.

This extreme vesicle formation was only observed in cells exposed to Pluronic P123. However, it is possible that F127 or F68 also deliver quercetin into the cell through similar mechanisms. To investigate further, fluorescent images of F68 and F127 treated cells should be captured and analyzed. If small quercetin-loaded vesicles are also observed, it can be concluded that they also actively participate in quercetin uptake. Although this mode of delivery cannot be considered a form of controlled drug release or cell targeting, it is important to note that the carrier is not a static carrier but a dynamic participant in the release mechanism.

A model and test protocol was developed to quantify the release mechanism kinetics. A Slide-A-Lyzer molecular weight cutoff (MWCO) membrane of 3,500 Daltons

was loaded with quercetin-loaded Pluronic micelles and placed in a 50 mL centrifuge tube. The MWCO membrane prevented the passing of any micelles but allowed quercetin to pass. The centrifuge tube was filled with a dialysate buffer of 20% ethanol and DPBS to create a sufficient sink condition. The tube was then placed in a shaker incubator at 37 °C and 100 rpm. Dialysate samples (100 µL) were taken out every 8 hours for 48 hours and replaced with fresh buffer. Quercetin concentration in the samples was determined using a spectrophotometer.

Analysis of maximum quercetin-loaded F127 and F68 was performed but due to variation in results and human error, this analysis was inconclusive (see **Appendix Figure 10**). For future work, this procedure and model will be useful for the quantification of quercetin release kinetics from the Pluronic micelle system.

Future Work

Future directions for this work include additional *in vitro* testing on a more specific and relevant cell line for further cytotoxicity and viral inhibitory analysis. The goal of these future directions is to assess the clinical relevance of the developed system using more representative models. Results from better *in vitro* models may lead to *in vivo* testing using an animal model.

The 3T3 fibroblast model used to perform initial analysis of the system was effective at identifying basic toxicity and viral inhibition. However, it would be insightful to assess the system *in vitro* using a human cell line that is highly affected by a clinical

CMV infection, rather than a robust mouse cell line. One cell type that is of particular interest is stria vascularis. Located in the outer wall of the cochlea, these cells are implicated in CMV-caused sensorineural hearing loss (SNHL), and have been shown to be sites of high CMV replication in an infected patient (22, 98). A stria vascularis *in vitro* model could provide valuable insight into any cell-specific cytotoxicity or CMV inhibition. The translation of results from this model to the clinic are more relevant, and could provide useful information on how the system would perform in treating a CMV infection in a human patient with CMV-related SNHL.

When inhibition and toxicity results are from a 2D cell culture model are promising, it is appropriate to develop a 3D *in vitro* model that more accurately represents a target treatment tissue. For this system, a 3D model of the cochlear vasculature could be used to investigate quercetin delivery kinetics by Pluronic micelles. Using a Transwell permeable support well-plate insert, a coculture of cochlear endothelial cells and stria vascularis cells could be performed. By loading the quercetin delivery system on the endothelial cell side of the Transwell membrane, but measuring quercetin concentrations on the stria vascularis side, the kinetics of quercetin transport can be modeled. Assessment of cytotoxicity and viral inhibition could also be performed to understand the efficacy of the delivery system in the model. Results from such a model could help understand how well the micelle system would deliver quercetin to CMV infected stria vascularis cells if administered via the blood stream. Understanding how the system interacts with the tissue is key to moving to more advanced models.

Although necessary for preliminary screening, there are inherent limitations with testing a drug delivery system with any *in vitro* model. It is difficult to isolate viral

inhibition or toxicity model artifacts that may affect system analysis. Therefore, *in vivo* testing is necessary to further assess the DDS. Not only would testing the quercetin delivery system in an animal model help eliminate any potential artifactual results, it would provide conclusions that are more translational to the clinical treatment of CMV. A mouse or guinea pig model have both been used for CMV studies and would be appropriate for testing this system (22, 98). Results from this preliminary screening *in vitro* work were promising, warranting further modeling and analysis of the system.

REFRENCES

1. van Zuylen WJ, Hamilton ST, Naing Z, Hall B, Shand A, Rawlinson WD. 2014. Congenital cytomegalovirus infection: Clinical presentation, epidemiology, diagnosis and prevention. Obstet Med 7:140–146.

2. Burny W, Liesnard C, Donner C, Marchant A. 2004. Epidemiology, pathogenesis and prevention of congenital cytomegalovirus infection. Expert Rev Anti Infect Ther 2:881–894.

3. Schleiss MR. 2008. Cytomegalovirus Vaccine Development. Curr Top Microbiol Immunol 325:361–382.

4. Cheeran MC-J, Lokensgard JR, Schleiss MR. 2009. Neuropathogenesis of Congenital Cytomegalovirus Infection: Disease Mechanisms and Prospects for Intervention. Clin Microbiol Rev 22:99–126.

5. Cotin S, Calliste C-A, Mazeron M-C, Hantz S, Duroux J-L, Rawlinson WD, Ploy M-C, Alain S. 2012. Eight flavonoids and their potential as inhibitors of human cytomegalovirus replication. Antiviral Res 96:181–186.

6. Faulds D, Heel RC. 1990. Ganciclovir. A review of its antiviral activity, pharmacokinetic properties and therapeutic efficacy in cytomegalovirus infections. Drugs 39:597–638.

7. McGavin JK, Goa KL. 2001. Ganciclovir: an update of its use in the prevention of cytomegalovirus infection and disease in transplant recipients. Drugs 61:1153–1183.

8. Matthews T, Boehme R. 1988. Antiviral activity and mechanism of action of ganciclovir. Rev Infect Dis 10 Suppl 3:S490-494.

9. Nassetta L, Kimberlin D, Whitley R. 2009. Treatment of congenital cytomegalovirus infection: implications for future therapeutic strategies. J Antimicrob Chemother 63:862–867.

10. Pescovitz MD, Rabkin J, Merion RM, Paya CV, Pirsch J, Freeman RB, O'Grady J, Robinson C, To Z, Wren K, Banken L, Buhles W, Brown F. 2000. Valganciclovir results in improved oral absorption of ganciclovir in liver transplant recipients. Antimicrob Agents Chemother 44:2811–2815.

11. Paya C, Humar A, Dominguez E, Washburn K, Blumberg E, Alexander B, Freeman R, Heaton N, Pescovitz MD. 2004. Efficacy and Safety of Valganciclovir vs. Oral Ganciclovir for Prevention of Cytomegalovirus Disease in Solid Organ Transplant Recipients. Am J Transplant 4:611–620.

12. Whitley RJ, Cloud G, Gruber W, Storch GA, Demmler GJ, Jacobs RF, Dankner W, Spector SA, Starr S, Pass RF, Stagno S, Britt WJ, Alford C, Soong S, Zhou XJ, Sherrill L, FitzGerald JM, Sommadossi JP. 1997. Ganciclovir treatment of symptomatic congenital cytomegalovirus infection: results of a phase II study. National Institute of Allergy and Infectious Diseases Collaborative Antiviral Study Group. J Infect Dis 175:1080–1086.

13. Antiretroviral Drug Discovery and Development | NIH: National Institute of Allergy and Infectious Diseases.

14. Anand David AV, Arulmoli R, Parasuraman S. 2016. Overviews of Biological Importance of Quercetin: A Bioactive Flavonoid. Pharmacogn Rev 10:84–89.

15. Kaul TN, Middleton E, Ogra PL. 1985. Antiviral effect of flavonoids on human viruses. J Med Virol 15:71–79.

16. Evers DL, Chao C-F, Wang X, Zhang Z, Huong S-M, Huang E-S. 2005. Human cytomegalovirus-inhibitory flavonoids: studies on antiviral activity and mechanism of action. Antiviral Res 68:124–134.

17. Landolfo S, Gariglio M, Gribaudo G, Lembo D. 2003. The human cytomegalovirus. Pharmacol Ther 98:269–297.

18. Srivastava S, Somasagara RR, Hegde M, Nishana M, Tadi SK, Srivastava M, Choudhary B, Raghavan SC. 2016. Quercetin, a Natural Flavonoid Interacts with DNA, Arrests Cell Cycle and Causes Tumor Regression by Activating Mitochondrial Pathway of Apoptosis. Sci Rep 6:24049.

19. Cai X, Fang Z, Dou J, Yu A, Zhai G. 2013. Bioavailability of quercetin: problems and promises. Curr Med Chem 20:2572–2582.

20. Ambadath V, Venu RG, Madambath I. 2010. Comparative Study of the Efficacy of Ascorbic Acid, Quercetin, and Thiamine for Reversing Ethanol-Induced Toxicity. J Med Food 13:1485–1489.

21. Speir E, Shibutani T, Yu Z-X, Ferrans V, Epstein SE. 1996. Role of reactive oxygen intermediates in cytomegalovirus gene expression and in the response of human smooth muscle cells to viral infection. Circ Res 79:1143–1152.

22. Carraro M, Almishaal A, Hillas E, Firpo M, Park A, Harrison RV. 2017. Cytomegalovirus (CMV) Infection Causes Degeneration of Cochlear Vasculature and Hearing Loss in a Mouse Model. J Assoc Res Otolaryngol 18:263–273.

23. Speir E. 2006. Cytomegalovirus Gene Regulation by Reactive Oxygen Species: Agents in Atherosclerosis. Ann N Y Acad Sci 899:363–374.

24. Oh JJ, Carter JJ, Nemeno JGE, Dix RD. 2019. Parthanatos-associated proteins are stimulated intraocularly during development of experimental murine cytomegalovirus retinitis in mice with retrovirus-induced immunosuppression. J Med Virol 92:394–398.

25. Rastogi H, Jana S. 2014. Evaluation of Inhibitory Effects of Caffeic acid and Quercetin on Human Liver Cytochrome P450 Activities. Phytother Res 28:1873–1878.

26. Thilakarathna SH, Rupasinghe HPV. 2013. Flavonoid Bioavailability and Attempts for Bioavailability Enhancement. Nutrients 5:3367–3387.

27. Spencer JPE, Kuhnle GGC, Williams RJ, Rice-Evans C. 2003. Intracellular metabolism and bioactivity of quercetin and its in vivo metabolites. Biochem J 372:173–181.

28. Walle T, Walle UK, Halushka PV. 2001. Carbon Dioxide Is the Major Metabolite of Quercetin in Humans. J Nutr 131:2648–2652.

29. Fan D, Zhou X, Zhao C, Chen H, Zhao Y, Gong X. 2011. Anti-inflammatory, antiviral and quantitative study of quercetin-3-O-β-D-glucuronide in Polygonum perfoliatum L. Fitoterapia 82:805–810.

30. Yang L-L, Xiao N, Li X-W, Fan Y, Alolga RN, Sun X-Y, Wang S-L, Li P, Qi L-W. 2016. Pharmacokinetic comparison between quercetin and quercetin 3- O - β -glucuronide in rats by UHPLC-MS/MS. 1. Sci Rep 6:1–9.

31. Ferry DR, Smith A, Malkhandi J, Fyfe DW, deTakats PG, Anderson D, Baker J, Kerr DJ. 1996. Phase I clinical trial of the flavonoid quercetin: pharmacokinetics and evidence for in vivo tyrosine kinase inhibition. Clin Cancer Res 2:659–668.

32. Gugler R, Leschik M, Dengler HJ. 1975. Disposition of quercetin in man after single oral and intravenous doses. Eur J Clin Pharmacol 9:229–234.

33. Dymarska M, Janeczko T, Kostrzewa-Susłow E. 2018. Glycosylation of 3-Hydroxyflavone, 3-Methoxyflavone, Quercetin and Baicalein in Fungal Cultures of the Genus Isaria. Mol J Synth Chem Nat Prod Chem 23.

34. Wang T, Li Q, Bi K. 2018. Bioactive flavonoids in medicinal plants: Structure, activity and biological fate. Asian J Pharm Sci 13:12–23.

35. Wei Z, Hao J, Yuan S, Li Y, Juan W, Sha X, Fang X. 2009. Paclitaxel-loaded Pluronic P123/F127 mixed polymeric micelles: formulation, optimization and in vitro characterization. Int J Pharm 376:176–185.

36. Zhao L, Shi Y, Zou S, Sun M, Lil L, Zhail G. 2011. Formulation and in vitro evaluation of quercetin loaded polymeric micelles composed of pluronic P123 and D-a-tocopheryl polyethylene glycol succinate. J Biomed Nanotechnol 7:358–365.

37. Pitto-Barry A, Barry NPE. 2014. Pluronic® block-copolymers in medicine: from chemical and biological versatility to rationalisation and clinical advances. Polym Chem 5:3291–3297.

38. Batrakova EV, Kabanov AV. 2008. Pluronic block copolymers: evolution of drug delivery concept from inert nanocarriers to biological response modifiers. J Control Release Off J Control Release Soc 130:98–106.

39. GRAS Notices.

40. Yang M, Lai SK, Wang Y-Y, Zhong W, Happe C, Zhang M, Fu J, Hanes J. 2011.

Biodegradable nanoparticles composed entirely of safe materials that rapidly penetrate human mucus. Angew Chem Int Ed Engl 50:2597–2600.

41. Bodratti AM, Alexandridis P. 2018. Formulation of Poloxamers for Drug Delivery. J Funct Biomater 9.

42. Zhai Y, Guo S, Liu C, Yang C, Dou J, Li L, Zhai G. 2013. Preparation and in vitro evaluation of apigenin-loaded polymeric micelles. Colloids Surf Physicochem Eng Asp 429:24–30.

43. Sahu A, Kasoju N, Goswami P, Bora U. 2011. Encapsulation of curcumin in Pluronic block copolymer micelles for drug delivery applications. J Biomater Appl 25:619–639.

44. Parmar A, Singh K, Bahadur A, Marangoni G, Bahadur P. 2011. Interaction and solubilization of some phenolic antioxidants in Pluronic® micelles. Colloids Surf B Biointerfaces 86:319–326.

45. Zhao L, Du J, Duan Y, Zang Y, Zhang H, Yang C, Cao F, Zhai G. 2012. Curcumin loaded mixed micelles composed of Pluronic P123 and F68: preparation, optimization and in vitro characterization. Colloids Surf B Biointerfaces 97:101–108.

46. Zhang Y, Yang Y, Tang K, Hu X, Zou G. 2008. Physicochemical characterization and antioxidant activity of quercetin-loaded chitosan nanoparticles. J Appl Polym Sci 107:891–897.

47. Alexandridis P, Holzwarth JF, Hatton TA. 1994. Micellization of Poly(ethylene oxide)-Poly(propylene oxide)-Poly(ethylene oxide) Triblock Copolymers in Aqueous Solutions: Thermodynamics of Copolymer Association. Macromolecules 27:2414–2425.

48. SP1049C.

49. Patra A, Satpathy S, Shenoy AK, Bush JA, Kazi M, Hussain MD. 2018. Formulation and evaluation of mixed polymeric micelles of quercetin for treatment of breast, ovarian, and multidrug resistant cancers. Int J Nanomedicine 13:2869–2881.

50. Han L-M, Guo J, Zhang L-J, Wang Q-S, Fang X-L. 2006. Pharmacokinetics and biodistribution of polymeric micelles of paclitaxel with Pluronic P123. Acta Pharmacol Sin 27:747–753.

51. Chatterjee S, Hui PC, Kan C, Wang W. 2019. Dual-responsive (pH/temperature) Pluronic F-127 hydrogel drug delivery system for textile-based transdermal therapy. Sci Rep 9:11658.

52. Pandey M, Belgamwar V, Gattani S, Surana S, Tekade A. 2009. Pluronic lecithin organogel as a topical drug delivery system. Drug Deliv 17:38–47.

53. Budkina OA, Demina TV, Dorodnykh TYu, Melik-Nubarov NS, Grozdova ID. 2012. Cytotoxicity of nonionic amphiphilic copolymers. Polym Sci Ser A 54:707–717.

54. William C. Griffin. 1949. Classification of Surface-Active Agents by “HLB”". J Cosmet Chem 1.

55. Kabanov AV, Lemieux P, Vinogradov S, Alakhov V. 2002. Pluronic® block copolymers: novel functional molecules for gene therapy. Adv Drug Deliv Rev 54:223–233.

56. Ochietti B, Lemieux P, Kabanov AV, Vinogradov S, St-Pierre Y, Alakhov V. 2002. Inducing neutrophil recruitment in the liver of ICAM-1-deficient mice using polyethyleneimine grafted with Pluronic P123 as an organ-specific carrier for

transgenic ICAM-1. Gene Ther 9:939–945.

57. Mirhosseini MM, Haddadi-Asl V, Zargarian SSh. 2016. Fabrication and characterization of hydrophilic poly(ε-caprolactone)/pluronic P123 electrospun fibers. J Appl Polym Sci 133.

58. Valle JW, Lawrance J, Brewer J, Clayton A, Corrie P, Alakhov V, Ranson M. 2004. A phase II, window study of SP1049C as first-line therapy in inoperable metastatic adenocarcinoma of the oesophagus. J Clin Oncol 22:4195–4195.

59. Pluronic F68 - US.

60. Rarokar NR, Saoji SD, Raut NA, Taksande JB, Khedekar PB, Dave VS. 2016. Nanostructured Cubosomes in a Thermoresponsive Depot System: An Alternative Approach for the Controlled Delivery of Docetaxel. AAPS PharmSciTech 17:436–445.

61. Arranja A, Schroder AP, Schmutz M, Waton G, Schosseler F, Mendes E. 2014. Cytotoxicity and internalization of Pluronic micelles stabilized by core cross-linking. J Controlled Release 196:87–95.

62. Johnston TP, Miller SC. 1985. Toxicological Evaluation of Poloxamer Vehicles for Intramuscular Use. PDA J Pharm Sci Technol 39:83–89.

63. Wojtoniszak M, Chen X, Kalenczuk RJ, Wajda A, Łapczuk J, Kurzewski M, Drozdzik M, Chu PK, Borowiak-Palen E. 2012. Synthesis, dispersion, and cytocompatibility of graphene oxide and reduced graphene oxide. Colloids Surf B Biointerfaces 89:79–85.

64. Liu Z, Liu D, Wang L, Zhang J, Zhang N. 2011. Docetaxel-Loaded Pluronic P123 Polymeric Micelles: in Vitro and in Vivo Evaluation. 3. Int J Mol Sci 12:1684–1696.

65. Butt AM, Amin MCIM, Katas H, Sarisuta N, Witoonsaridsilp W, Benjakul R. 2012. In Vitro Characterization of Pluronic F127 and D- -Tocopheryl Polyethylene Glycol 1000 Succinate Mixed Micelles as Nanocarriers for Targeted Anticancer-Drug Delivery. J Nanomater 2012:e916573.

66. Mendonça DVC, Lage LMR, Lage DP, Chávez-Fumagalli MA, Ludolf F, Roatt BM, Menezes-Souza D, Faraco AAG, Castilho RO, Tavares CAP, Barichello JM, Duarte MC, Coelho EAF. 2016. Poloxamer 407 (Pluronic® F127)-based polymeric micelles for amphotericin B: In vitro biological activity, toxicity and in vivo therapeutic efficacy against murine tegumentary leishmaniasis. Exp Parasitol 169:34–42.

67. Khattak SF, Bhatia SR, Roberts SC. 2005. Pluronic F127 as a Cell Encapsulation Material: Utilization of Membrane-Stabilizing Agents. Tissue Eng 11:974–983.

68. Chen H, McFaul C, Titushkin I, Cho M, Lee R. 2018. Surfactant Copolymer Annealing of Chemically Permeabilized Cell Membranes. Regen Eng Transl Med 4:1–10.

69. Rodeheaver GT, Kurtz L, Kircher BJ, Edlich RF. 1980. Pluronic F-68: A promising new skin wound cleanser. Ann Emerg Med 9:572–576.

70. Faulkner DM, Sutton ST, Hesford JD, Faulkner BC, Major DA, Hellewell TB, Laughon MM, Rodeheaver GT, Edlich RF. 1997. A new stable pluronic® F68 gel carrier for antibiotics in contaminated wound treatment. Am J Emerg Med 15:20–24.

71. Bonhomme-Faivre L, Mathieu MC, Depraetere P, Grossiord JL, Seiller M. 1997. Formulation of a charcoal suspension for intratumoral injection: influence of the pluronic F68® concentration. Int J Pharm 152:251–255.

72. Zhang Y, Newton B, Lewis E, Fu PP, Kafoury R, Ray PC, Yu H. 2015. Cytotoxicity of

Organic Surface Coating Agents Used for Nanoparticles Synthesis and Stability. Toxicol Vitro Int J Publ Assoc BIBRA 29:762–768.

73. Ali S, Kolter K. 2019. Kolliphor® HS 15 - An Enabler for Parenteral and Oral Formulations. Am Pharm Rev.

74. Hou Y, Zhang F, Lan J, Sun F, Li J, Li M, Song K, Wu X. 2019. Ultra-small micelles based on polyoxyl 15 hydroxystearate for ocular delivery of myricetin: optimization, in vitro, and in vivo evaluation. Drug Deliv 26:158–167.

75. Lin HW, Saul I, Gresia VL, Neumann JT, Dave KR, Perez-Pinzon MA. 2014. Fatty acid methyl esters and Solutol HS 15 confer neuroprotection after focal and global cerebral ischemia. Transl Stroke Res 5:109–117.

76. Bardi G, Tognini P, Ciofani G, Raffa V, Costa M, Pizzorusso T. 2009. Pluronic-coated carbon nanotubes do not induce degeneration of cortical neurons in vivo and in vitro. Nanomedicine Nanotechnol Biol Med 5:96–104.

77. Shelat PB, Plant LD, Wang JC, Lee E, Marks JD. 2013. The Membrane-Active Tri-Block Copolymer Pluronic F-68 Profoundly Rescues Rat Hippocampal Neurons from Oxygen–Glucose Deprivation-Induced Death through Early Inhibition of Apoptosis. J Neurosci 33:12287–12299.

78. Wang JC, Bindokas VP, Skinner M, Emrick T, Marks JD. 2017. Mitochondrial mechanisms of neuronal rescue by F-68, a hydrophilic Pluronic block co-polymer, following acute substrate deprivation. Neurochem Int 109:126–140.

79. Wang R, Hughes T, Beck S, Vakil S, Li S, Pantano P, Draper RK. 2013. Generation of toxic degradation products by sonication of Pluronic® dispersants: implications for

nanotoxicity testing. Nanotoxicology 7:1272–1281.

80. Zhou A, Kikandi S, Sadik OA. 2007. Electrochemical degradation of quercetin: Isolation and structural elucidation of the degradation products. Electrochem Commun 9:2246–2255.

81. Zakaryan H, Arabyan E, Oo A, Zandi K. 2017. Flavonoids: promising natural compounds against viral infections. Arch Virol 162:2539–2551.

82. Understanding Dynamic Light Scattering Theory. Wyatt Technol.

83. Khurshid S, Saridakis E, Govada L, Chayen NE. 2014. Porous nucleating agents for protein crystallization. Nat Protoc 9:1621–1633.

84. Sengupta B, Sengupta PK. 2002. The interaction of quercetin with human serum albumin: a fluorescence spectroscopic study. Biochem Biophys Res Commun 299:400–403.

85. Pepić I, Lovrić J, Hafner A, Filipović-Grčić J. 2014. Powder form and stability of Pluronic mixed micelle dispersions for drug delivery applications. Drug Dev Ind Pharm 40:944–951.

86. Hsiao F, Huang P-Y, Aoyagi T, Chang S-F, Liaw J. 2018. In vitro and in vivo assessment of delivery of hydrophobic molecules and plasmid DNAs with PEO–PPO–PEO polymeric micelles on cornea. J Food Drug Anal 26:869–878.

87. 2018. Critical micelle concentration (CMC) and surfactant concentration - KRÜSS.

88. Muller MT, Hudson JB. 1977. Cell cycle dependency of murine cytomegalovirus replication in synchronized 3T3 cells. J Virol 22:267–272.

89. Muller MT, Hudson JB. 1977. Thymidine kinase activity in mouse 3T3 cells infected by murine cytomegalovirus (MCV). Virology 80:430–433.

90. Haller TJ, Price MS, Lindsay SR, Hillas E, Seipp M, Firpo MA, Park AH. 2020. Effects of ganciclovir treatment in a murine model of cytomegalovirus-induced hearing loss. The Laryngoscope 130:1064–1069.

91. Bodaghi B, Slobbe–vanDrunen MEP, Topilko A, Perret E, Vossen RCRM, Dam–Mieras MCE van, Zipeto D, Virelizier J-L, LeHoang P, Bruggeman CA, Michelson S. 1999. Entry of Human Cytomegalovirus into Retinal Pigment Epithelial and Endothelial Cells by Endocytosis. Invest Ophthalmol Vis Sci 40:2598–2607.

92. Repetto G, del Peso A, Zurita JL. 2008. Neutral red uptake assay for the estimation of cell viability/cytotoxicity. Nat Protoc 3:1125–1131.

93. Neutral Red Assay Kit (ab234039) | Abcam.

94. Research C for DE and. 2019. Antiviral Product Development--Conducting and Submitting Virology Studies to the Agency. US Food Drug Adm.

95. Maskarinec SA, Wu G, Lee KYC. 2006. Membrane Sealing by Polymers. Ann N Y Acad Sci 1066:310–320.

96. Wu W, Li R, Li X, He J, Jiang S, Liu S, Yang J. 2015. Quercetin as an Antiviral Agent Inhibits Influenza A Virus (IAV) Entry. Viruses 8.

97. Fraile M, Buratto R, Gómez B, Martín Á, Cocero MJ. 2014. Enhanced Delivery of Quercetin by Encapsulation in Poloxamers by Supercritical Antisolvent Process. Ind Eng Chem Res 53:4318–4327.

98. Strauss M. 1990. Human cytomegalovirus labyrinthitis. Am J Otolaryngol 11:292–298.

APPENDIX – PROTOCOLS

Appendix Protocol 1: A description of iterations performed to optimize CC50/EC50 assay procedure.

The first iteration was a 10-day assay. The plate was seeded with 3T3 fibroblasts at $3.2x10^4$ cell/$cm^{2,}$ which were allowed to proliferate for 48 hours until about 95% confluence, as determined using brightfield microscopy. The viral control and EC50 wells were virally infected at a multiplicity of infection (MOI) of about 0.3. MOI is the ratio of virions to cells. Two hours were allowed for viral attachment, after which the viral media was removed and 200 µL of the test antiviral/Pluronic solution was added to the appropriate wells. Non-viral media was used for non-infected wells, but the addition and removal of media was performed the same. The antiviral and media were refreshed after every 3 days. CC50 and EC50 analysis was to be performed after 10 days.

The analysis was not performed however, because there was significant cell monolayer detachment after the 2nd antiviral and media change, 6 days after the assay was started. It appeared that the shear force associated with removing and replacing all of the media was detaching the cell sheet. In order to alleviate this issue, the media and treatment refreshment procedure was altered for the next iteration.

For the 2nd iteration, the cell seeding and viral infection procedures were not changed. However, after the viral media was removed, 250 µL of the test treatment was added instead of 200 µL. Every day, 50 µL of the spent media or treatment was removed and carefully replaced. The assay was to last for 10 days with daily refreshment, but after monolayer detachment was observed, the assay was stopped after 5 days.

Because there was no correlation between treatment type and which wells were

affected, monolayer detachment was probably a result of procedure rather than treatment. Thus, the entirety of the protocol was reassessed with four goals in mind 1. Decrease potential shear stress on cells by eliminating media changes and treatment refreshment 2. Reduce the duration of the assay 3. Avoid chances of monolayer detachment by reducing time for cell proliferation before infection 4. Streamline the procedure to minimize chance of human error.

The following assay was performed as the 3rd iteration. 3T3 fibroblasts were seeded on the plate at $1x10^5$ cell/cm^2 (about 95% confluence) and allowed to attach for 4 hours. Viral infection was performed at an MOI of 0.2 by adding 100 µL of viral media into the appropriate wells and incubating for 10 min. Fresh media was added to non-infected wells. Then 100 µL of treatment was carefully added to the corresponding wells, bringing total well volume to 200 µL, and the plate was incubated for 3 days. No media changes or refreshment was performed. CC50 and EC50 analysis was to performed after 3 days.

With this new procedure, monolayer detachment was greatly reduced but still occurred randomly throughout the plate. To eliminate any detachment, the same assay procedure was used but cell seeding density was reduced to $5.25x10^4$ cell/cm^2 and then $3.75x10^4$ cell/cm^2. At these densities, detachment decreased but still occurred in one or two wells per plate. After reducing further to $3x10^4$ cell/cm^2, no monolayer detachment was observed.

<u>Appendix Protocol 2:</u> A protocol for viral inoculation media preparation used in CC50/EC50 assay.

Viral inoculation media prepared at $3.0x10^4$ pfu/mL for $3.0x10^3$ pfu/well. All procedures were performed aseptically.

1. Thawed CMV stock ($2.8x10^6$ pfu/mL) stored in liquid nitrogen
2. Added 150 µL CMV stock to 13.85 mL DMEM + 10% FBS
3. Vortexed thoroughly
4. Returned CMV stock to liquid nitrogen
5. Aliquoted 12 mL of DMEM for non-infected wells
6. Warmed non-infectious media and CMV media before adding to wells

<u>Appendix Protocol 3:</u> A protocol for DDS dilution preparation used in CC50/EC50 assay.

Dilutions were prepared for the completion of the CC50/EC50 assay. Quercetin-loaded or blank DDSs were fabricated using the thin-film hydration method and filtered by PVDF syringe filter before dilution preparation. All procedures were performed aseptically.

1. First, concentrations were determined, appropriate dilutions were calculated, and volumes were organized in a table. See following example:

QF68 + DPBS Volumes for Dilutions (600 uL Total)

Final Volume (uL)	Final Concentration (mM)	Volume of QF68 (uL)	Volume of DPBS (uL)	Volume of DMEM (uL) – Bring Volume to 600 uL
600	3	**360**	**0**	**240**
	2	**240**	**120**	**240**
	1.5	**180**	**180**	**240**
	1	**120**	**240**	**240**
	0.5	**60**	**300**	**240**
	0.1	**12**	**348**	**240**
	0.01	**1.2**	**358.8**	**240**
	0.001	**0.12**	**359.88**	**240**

2. Using a multichannel pipette, DMEM volumes were added to a VWR® 1.2 mL 96-well strip rack
3. Using a multichannel pipette, DPBS volumes were added to appropriate rows
4. Volume of DDS was added to appropriate wells
5. Viral and cell controls were prepared by adding equivalent volumes of DPBS and DMEM
6. Preparations were warmed and thoroughly mixed before being added to the CC50/EC50 assay plate

Appendix Protocol 4: A description of initial CC50 and EC50 quantification techniques used in the CC50/EC50 assay.

EC50 Analysis: Initially, the GFP expression within each test well was quantified using fluorescent microscopy. First, each mCMV infected well was stained with a NucBlu live nuclear stain and each well was using a Laxco LMI-6000 inverted fluorescent microscope. A blue DAPI filter was used to observe the nuclei and a green filter was used to identify the GFP. There was significant interference from the

background fluorescence of quercetin within the solution, which has an intrinsic fluorescence at about the same wavelength of GFP (~509 nm). Therefore, the spent media and treatment solutions were gently aspirated and replaced with DPBS.

ImageJ was used to count the number of GFP-expressing and total cells in the selected images. The ratio of GFP-expressing cells to total cells was used to determine the percent viral inhibition for each well. The average was calculated across the triplicate wells and standard deviation was calculated. High variation was observed between like samples.

This procedure was far too slow, time consuming, and not consistent enough to be used to efficiently assess viral load for all the iterations performed in this work. A quicker and less involved process for GFP quantification was needed.

CC50 Analysis: Initially, cell viability was quantified using a Trypan blue exclusion assay by trypsinizing each cytotoxicity well of the 96-well plate and transferring the cells to a corresponding microfuge tube. The viability in each tube was determined using a Vi-Cell cell counter.

This procedure was not only extremely time consuming, but the low number of cells in each well made the counting with the Vi-Cell inconsistent. It was apparent that a quicker, more sensitive, and streamlined assay was need to assess cell viability.

Appendix Protocol 5: Protocol used to fabricate reduced loading (75, 50, and 25% of maximum) F68 micelles.

Reduced quercetin-loaded F68 micelles (QF68) were prepared at final Pluronic concentrations of 40 mM in DPBS.

1. Measure 3320 mg of Pluronic F68 into a 50 mL conical tube for each sample
2. Prepare quercetin in acetone to a concentration of 24 mM
3. Add quercetin / acetone solution to each 50 mL conical tube, based on the following table. 100% loaded is based on the encapsulation efficiency found in previous experiments (0.35 mM quercetin encapsulated in 10mM F68).

Desired Loading	25%	50%	75%	100%
Volume Added	144.25 µL	288.50 µL	432.75 µL	577.00 µL

4. Add pure acetone as necessary to fully dissolve quercetin and Pluronics (~20 mL)
5. Vortex until Pluronic is completely dissolved in acetone and optically clear
6. Transfer Pluronic / quercetin / acetone solution to autoclaved round - bottom flasks (in hood)
7. Seal round - bottom flasks with parafilm before removing from hood
8. Evaporate samples in a rotary evaporator for 30 minutes. Samples will be still slightly wet but should have significantly less volume.
9. Set cooling tube to 4 C; water bath to 40 C; watch carefully to ensure the solution does not boil over
10. Seal samples with parafilm
11. Transfer samples to hood, loosely cover with aluminum foil
12. Let samples sit in running blower overnight to dry any remaining acetone
13. Resuspend in 10mL sterile DPBS
14. Refrigerate to speed dissolution; agitate every few hours to ensure all material is resuspended

15. Once solution is homogeneously resuspended, sterile filter using a 0.22 um syringe filter
16. Sterile filter twice more; store at room temperature

APPENDIX – FIGURES

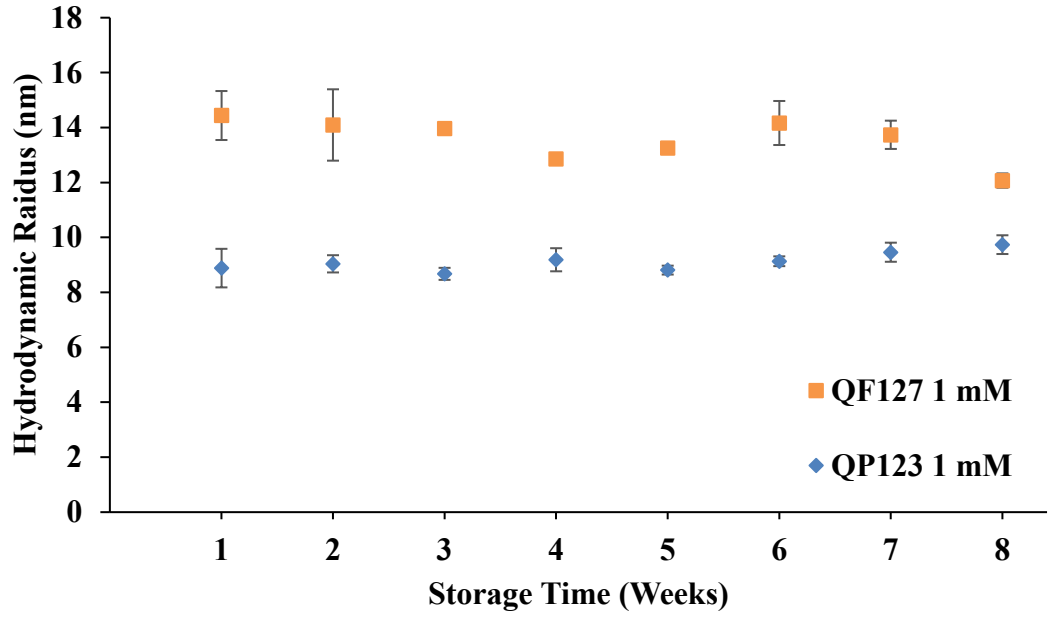

Appendix Figure 1. Particle characterization of quercetin-Pluronic formulations reveals that QF127 and QP123 nanoparticles are stable over the course of two months. Average radii are 13.57 and 9.12 nm for QF127 and QP123, respectively.

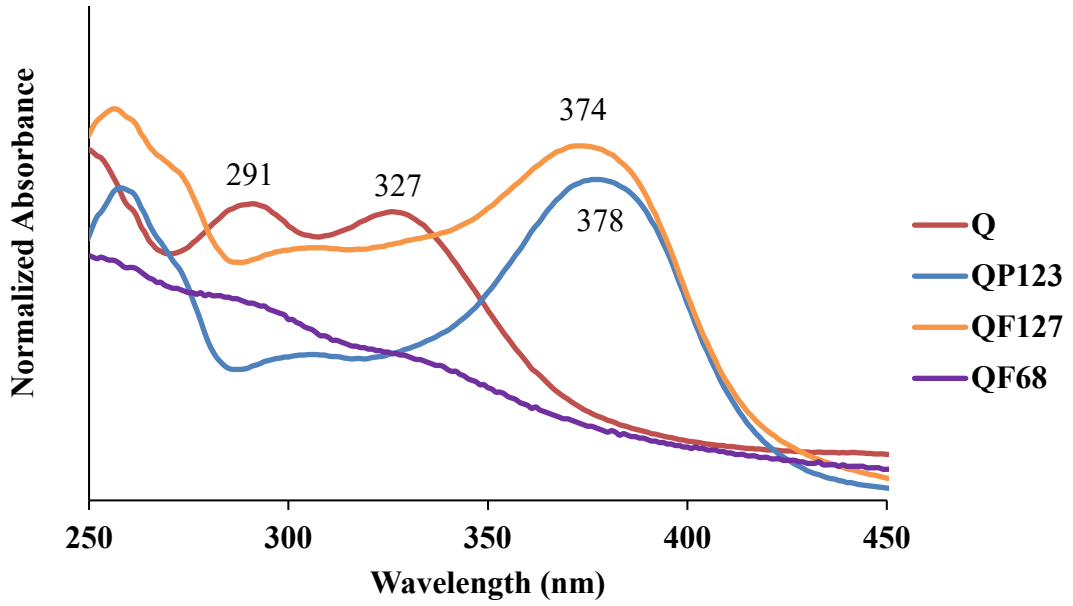

Appendix Figure 2. UV-visible spectroscopy of quercetin-Pluronic formulations at week eight reveal native peak conservation (374 – 378 nm) for QF127 and QP123, indicating oxidative protection. These peaks are missing for QF68 and free quercetin; instead, degradation products (291 nm, 327 nm) are visible.

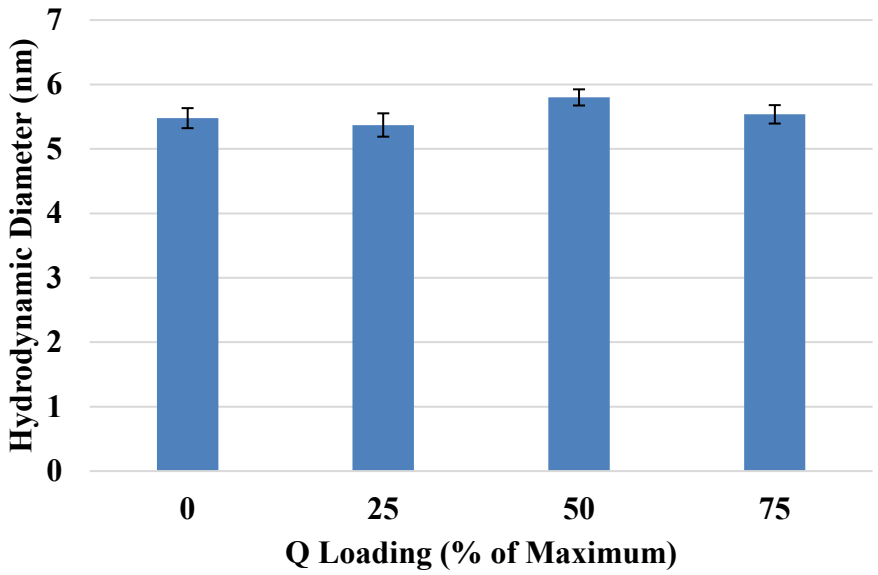

Appendix Figure 3. Hydrodynamic diameter of reduced quercetin loading in F68 DDS. In contrast to maximum quercetin loaded F68, discrete diameters were observed. DPBS was used as a solvent and measurements taken at 25 ºC. n = 3. Error bars = Standard deviation

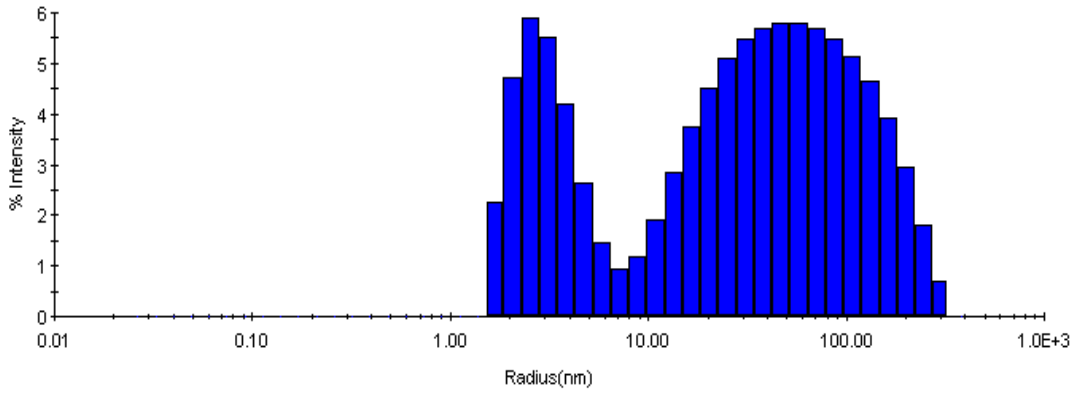

Appendix Figure 4. Representative histogram of maximum quercetin-loaded Pluronic F68 DLS data. Diameter results are multimodal.

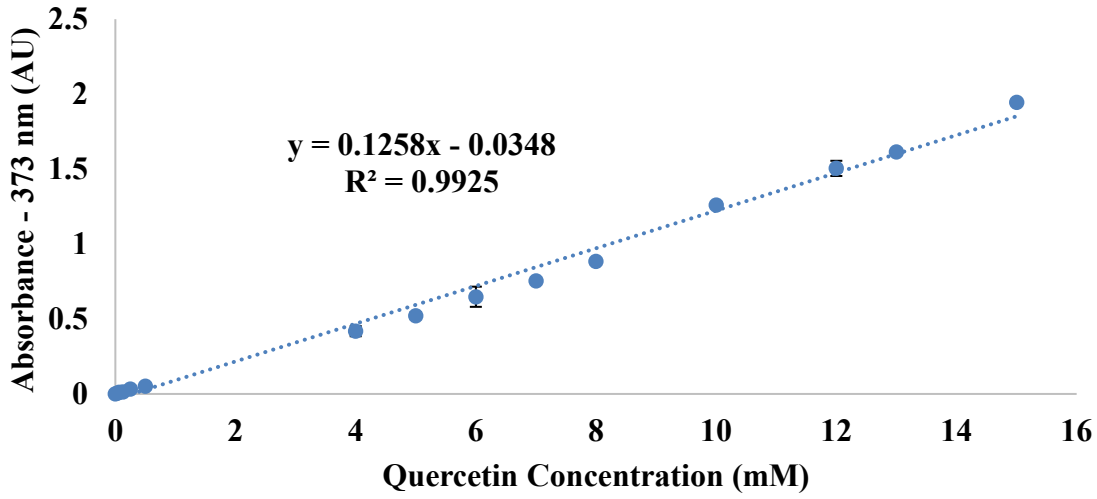

Appendix Figure 5. Quercetin absorbance at 373 nm at a range of quercetin concentrations in ethanol. Values were plotted for the standard curve, from which the concentration and total quercetin mass encapsulated was calculated.

A.

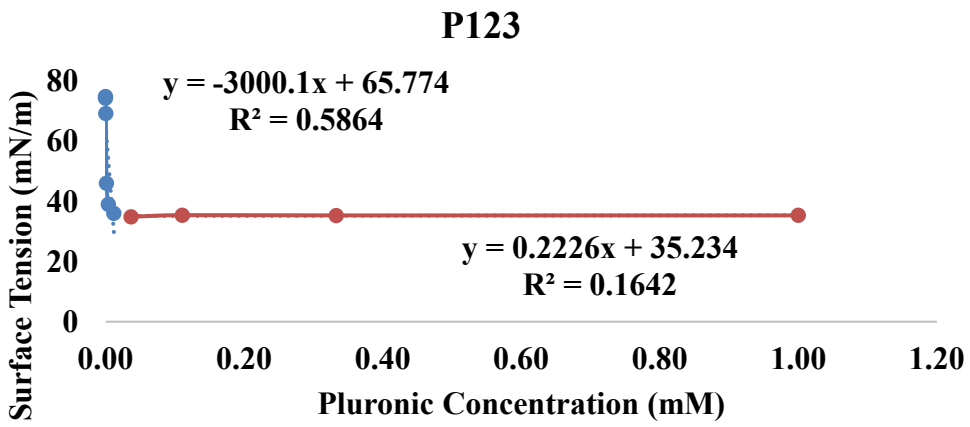

B.

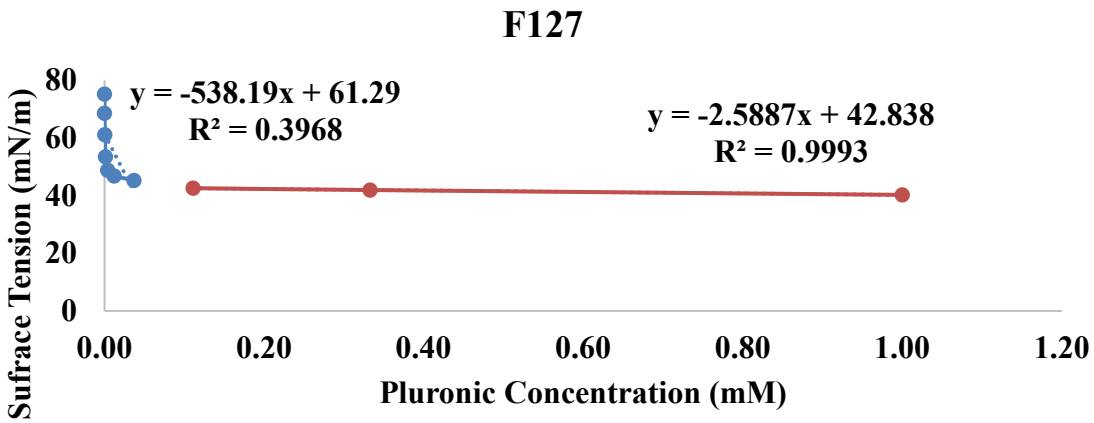

C.

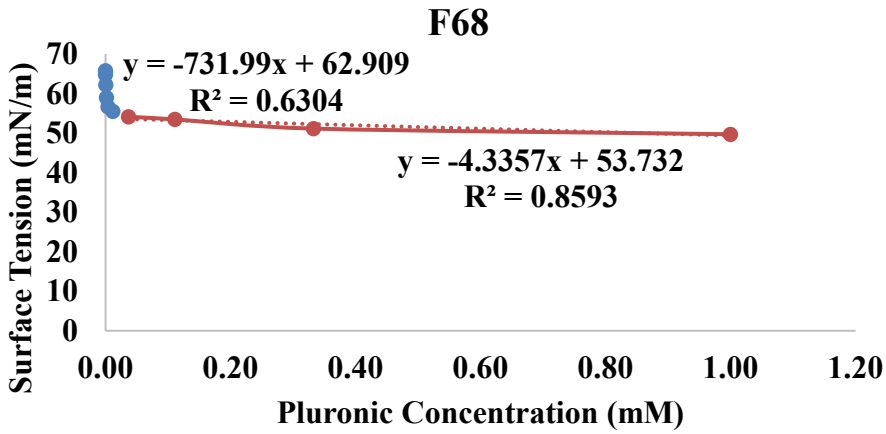

Appendix Figure 6. Example of blank P123 micelle raw tensiometer data **(A)**. Example of blank F127 micelle raw tensiometer data **(B)**. Example of blank F68 micelle raw tensiometer data **(C)**. The equations from the 2 curves of best fit (blue and red) were used to estimate the point of inflection. All the data acquired to calculate all CMC values are not presented here because all charts were repeated in triplicate for both blank and maximum quercetin-loaded micelles for all 3 Pluronic micelles tested, totaling 12 charts. These sample data generally represent what was observed in the other trials and experimentation.

A.

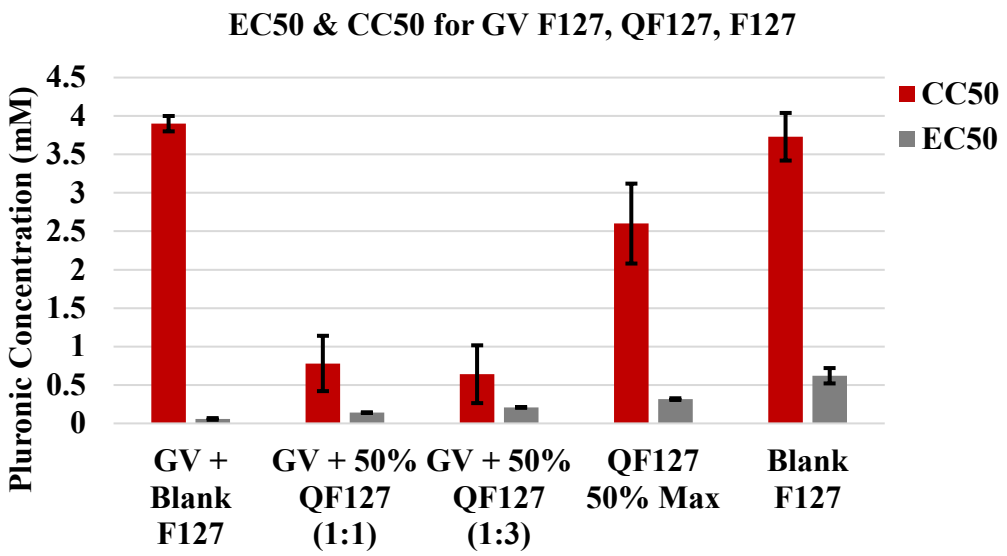

B.

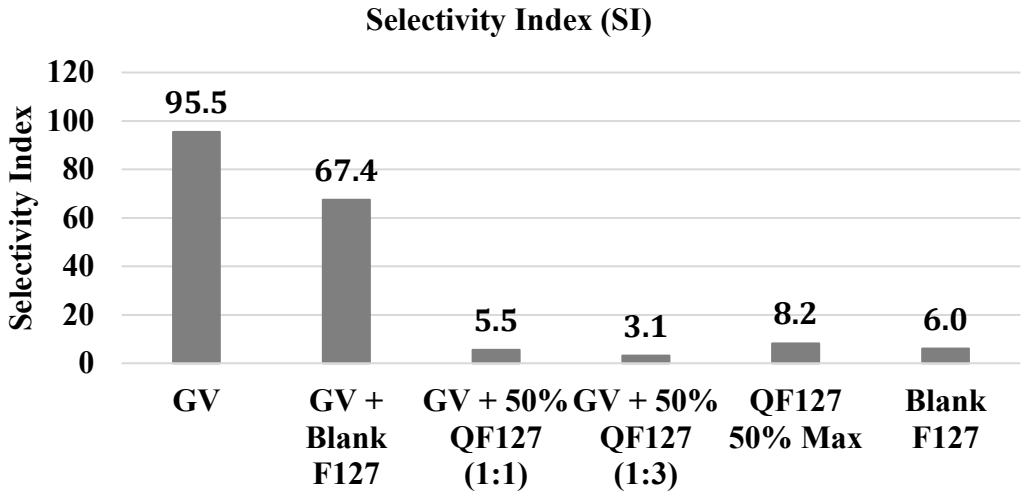

Appendix Figure 7. Summary of the CC50/EC50 assay results of 50% quercetin-loaded F127 DDS + ganciclovir (GV) **(A)**. The addition of the quercetin-loaded system resulted in increased toxicity. The selectivity indices (SIs) for the synergy results **(B)**. Addition of quercetin-loaded and blank F127 DDS to ganciclovir decreased the SI.

A.

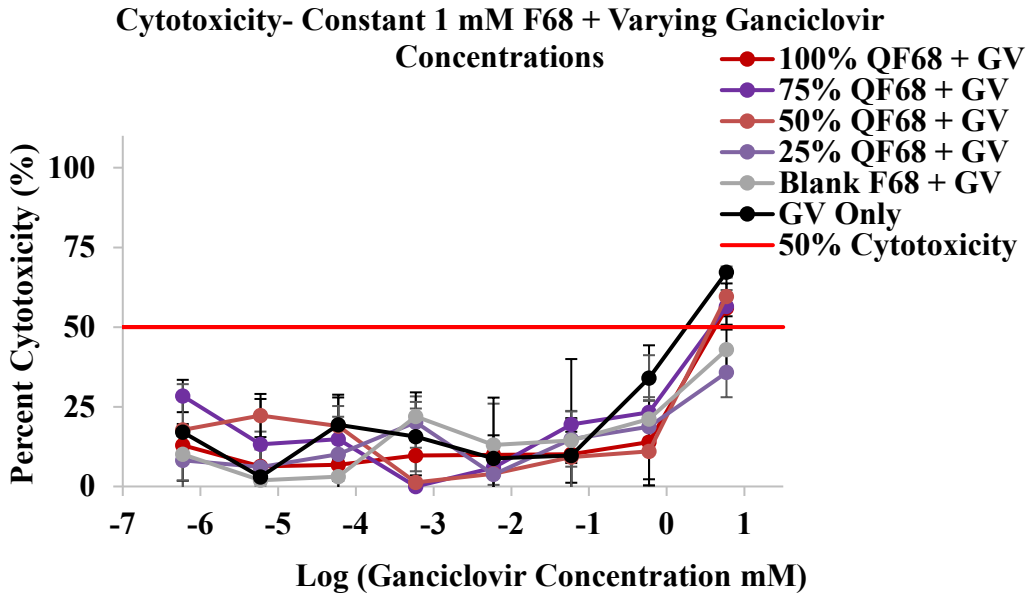

B.

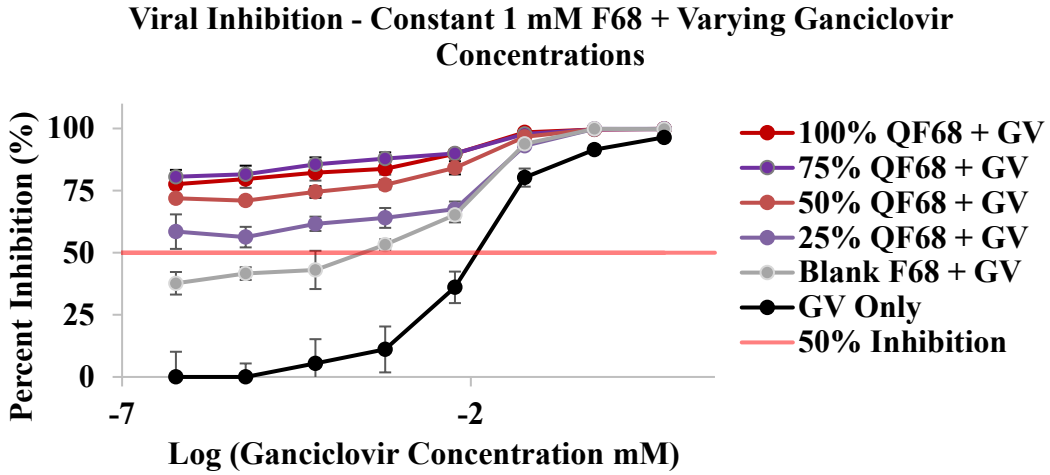

Appendix Figure 8. Synergy cytotoxicity results including 75% quercetin-loaded F68 DDS**(A)**. Synergy CMV inhibition results including 75% quercetin-loaded F68 DDS **(B)**.

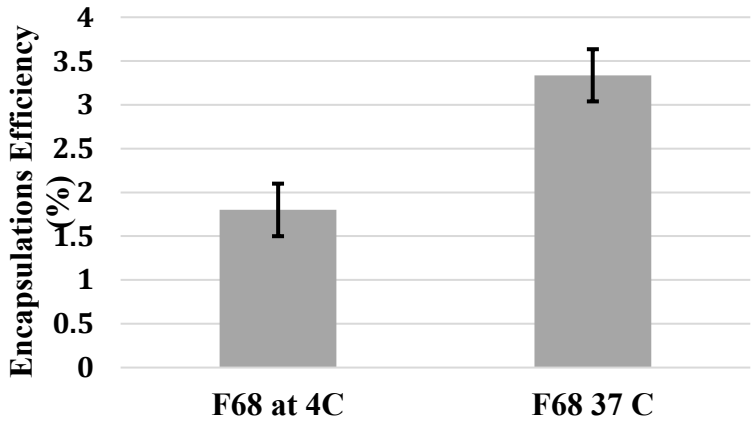

Appendix Figure 9. F68 loading efficiencies at 4 °C and 37 °C. Higher temperature results in a higher loading efficiency.

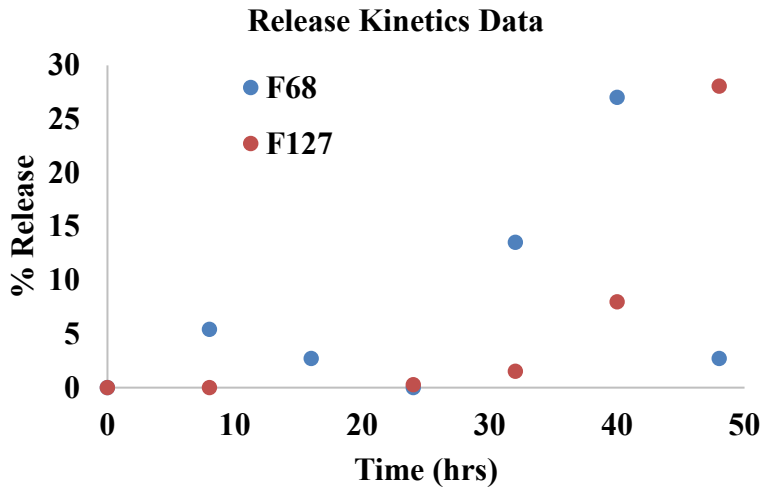

Appendix Figure 10. Results from maximum quercetin-loaded F127 and F68 release kinetic modeling. Due to high variability, they are inconclusive.

APPENDIX – DEVELOPED CLASS LAB MODULES

A requirement for the completion of my Master of Science degree was the development of a lab module for two USU Biological Engineering courses, Advanced Biomaterials (BENG-5850/6850) and Tissue Engineering (BENG-5890/6890).

The **Advanced Biomaterials (5850/6850) lab module** was developed to introduce students to basic drug delivery concepts. Two Pluronic nanocarrier (micelle) drug delivery systems were fabricated by the thin-film hydration method, characterized for carrying capacity and release, and compared. Quercetin was used as the hydrophobic drug delivered. The module was designed to be completed in 2-3 weeks, with two 1-hour lab sections per week. In addition to the lab module itself, a lab-write up with conceptual questions was developed. The module and write-up follow.

BENG 5850/6850 Nano-Drug Delivery Lab

Thin-film hydration lab:

Use the thin-film hydration method to fabricate quercetin-loaded F68, F127, and F68/F127 micelles as nano-drug-delivery vesicles. In Lab-1 you prepared LCST gels from F68 and F127. In this lab, you will employ these two Pluronics for encapsulating a sparingly soluble flavonoid, quercetin, which exhibits antiviral, antibacterial, and antioxidant properties. The two Pluronics exhibit distinct hydrophobic (PPO) to hydrophilic (PEO) ratios (see Lab 1, and below) and may thus be expected to have different loading efficiencies and release behavior. Mixtures of F68 and F127 will also be explored to determine if mixed-micelles exhibit distinct drug loading and release behavior from the two parent compounds.

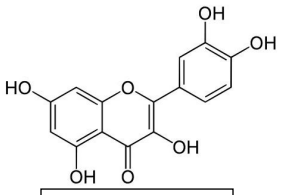

Quercetin

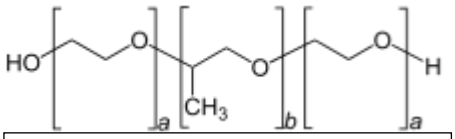

Pluronic PEO-PPO-PEO

F-68 has an approximate block length of a = 80 and b = 30 with molecular weight of ~8,400 Daltons

F-127 has an approximate block length of a = 106 and b = 70 with a molecular weight of ~12,500 Daltons.

Thin-film hydration

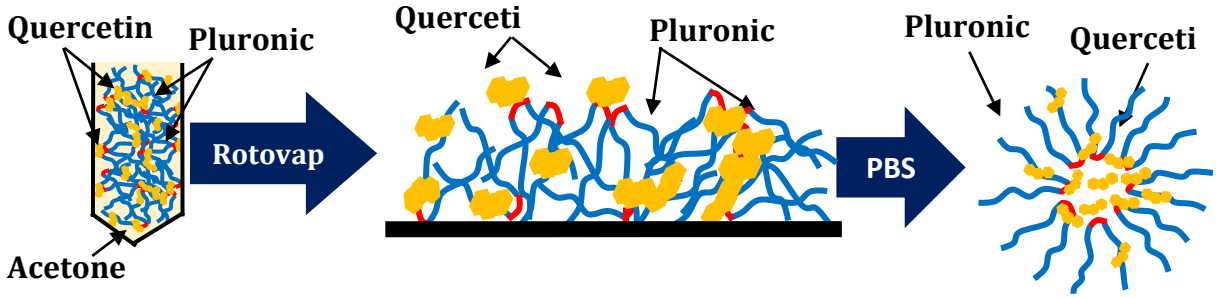

Schematic of the steps involved in the thin-film hydration method for loaded-micelle fabrication.

TA – prepare quercetin/acetone stock
Students – 10 groups of 3
Two groups per preparation (each group prepares their own, so we will have duplicates):

1. F68
2. F68:F127 (5:1)
3. F68:F127 (1:1)
4. F68:F127 (1:5)
5. F127

Ratios are mol F68:mol F127. Final Pluronic concentration of 10 mM in 10 mL of phosphate buffered saline (PBS) will be prepared.

Note! The Pluronic powders will first be dissolved in an acetone / quercetin solution that will be dried in a rotorary evaporator to form a thin film of Pluronic and quercetin. This thin film will later be resuspended in PBS, yielding quercetin-loaded micelles (and excess quercetin)

Protocols:

Before Lab (in class 11/8/19)

1. Calculate mass of Pluronic (or Pluronics) to achieve a 10 mM final concentration in 10 mL of PBS
2. Measure out mass of Pluronic/Pluronics in 15 mL centrifuge tube

Preparation

2. Add volume of quercetin/acetone stock for 8% w/w ratio
3. Bring final volume to 15 mL with acetone
4. Vortex for ~5 min or until optically clear

Evaporation

5. Transfer into round bottom flask
6. Rotovap for 20 min, 100 rpm, 40C
7. Remove flask – place in laminar flow hood overnight

Resuspension

8. Add 10 mL of PBS to flask – swirl vigorously
9. Place flask in fridge (4C) until resuspended

Filtration

10. To remove free quercetin – pass suspension through hydrophobic PVDF syringe filter (quercetin will adsorb to membrane surface)

Encapsulation efficiency lab:

Use absorbance peak of quercetin to quantify quercetin concentration and calculate encapsulation efficiency.

Protocols:

1. Sample of 10 uL from the resuspension
2. Dilute 10 uL into 1000 uL of EtOH – To disrupt micelles and release quercetin
3. Add 200 uL of dilution to plate and run absorbance at 373 nm
4. Compare absorbance against standard curve
5. Calculate encapsulation efficiency

Drug release lab:

Produce a drug release profile from quercetin-loaded micelles using a 3500 Dalton molecular weight cut off (MWCO) membrane.

Protocols:

1. Prepare dialysate by making 30% EtOH with PBS
2. Add 44.5 mL of dialysate to 50 mL centrifuge tube (TBD)
3. Take 100 uL sample of dialysate for time=0
4. Add 2 mL of quercetin-loaded micelles to slide-a-lyzer membrane
5. Place membrane in 50 mL centrifuge tube with dialysate
6. Take 100 uL samples from dialysate every 8 hrs for every 48 hrs
7. Put samples in well-labeled flip cap vials
8. After run is complete – add samples to well plate
9. Run absorbance of plate at 373 nm
10. Calculate concentration and fit release model

BENG 5850/6850 Nano-Drug Delivery Lab Write-Up

Name: _____

Group # and Lab Partner Names: _____

Please work individually to answer the questions in this final lab report. You may work with your lab team on preparing the graphs. Please submit your individual report via Canvas by the posted due date.

1. Plot a standard curve relating the known quercetin concentrations to measured absorbance values that can be used for encapsulation and drug loading efficiency calculations. Include a curve fit. For the plot make sure to label axes and include units. In the Figure caption for the calibration curve indicate the solvent and why absorbance measured at 373 nm.
2. What is Beer's law? Is it linear for all absorbance values? Why are sample dilutions often necessary when measuring absorbance?
3. Produce a table of encapsulation and drug loading efficiencies for all 5 Pluronic micelle systems using the data you generated (See Excel file for the raw data for all groups).
4. Generate a curve of encapsulation efficiencies with respect to Pluronic composition (F68/F127). Calculate the *expected encapsulation efficiencies* of the three mixed-micelles based on the measured quercetin encapsulation efficiency values in the pure F68 and F127 micelles. Plot the expected encapsulation values on the same graph with the measured data. Does the theoretic loading of the mixed-micelles match the experimentally measured loading?
5. Considering F68 and F127, comment on what properties lead to the differences in encapsulation efficiency. Considering the general properties of Pluronics, why do they form micelles in water, but are disrupted in ethyl alcohol? The molecular weight cutoff (MWCO) of the dialysis membrane was 3000 Da—could F68 or F127 pass through this membrane?
6. Cytotoxicity resulting from high drug concentrations is a major consideration when designing a drug delivery system. Thus, high loading efficiency is not always desired, depending on the release kinetics. What theoretical ratio of F68/F127 micelles would be necessary to achieve an encapsulation efficiency of 10% (assume maximum loading)?
7. Plot standard curve used for quercetin release calculations. Include curve fit. Label axes and provide a descriptive Figure caption.
8. Produce a % release vs. time curve for F68 and F127 using the release data (see Excel file for raw data). Label axes and provide a descriptive Figure caption.
9. For this *in vitro* experiment, we have fixed volumes of the quercetin source (micelle solution within the dialysis membrane reservoir) and sink (30% EtOH dialysate in the centrifuge tube). Discuss how this compares to an *in vivo* system that involves injecting this drug delivery vehicle into the blood stream and subsequent processes in this complex organism.

10. Various models (e.g. Zero-order, First-order, Higuchi, and Power law) are used to describe drug release behavior. Apply each of these models to the F68 and F127 quercetin release data and assess which has the best fit.

11. Using each model, estimate the time necessary to deliver a target quercetin dose of 0.25 mg for the quercetin loaded F68 and F127 in the *in vitro* system. Discuss how the selection of the model influences the predicted time, and the significance this may have for predicting *in vivo* behavior.

(1) Zero-order kinetics

$$\frac{M_t}{M_\infty} = k_0 t$$

(2) First-order kinetics $\frac{M_t}{M_\infty} = 1 - \exp(-k_1 t)$

(3) Higuchi model [30]

$$\frac{M_t}{M_\infty} = k_H t^{1/2}$$

(4) Power law model [31]

$$\frac{M_t}{M_\infty} = k t^n$$

where M_t/M_∞ represents the fractional drug release at time t and k_0, k_1, k_H, and k represent zero-order release constant, first-order release constant, Higuchi constant, and Korsemeyer–Peppas constant, respectively. In the power law model n is an exponent that characterizes the diffusional release kinetic mechanism. The data were analyzed

The **Tissue Engineering (5890/6890) lab module** was developed to introduce students to basic *in vitro* antiviral compound analysis. In the lab, the students use a simplified 96-well plate cell culture model to evaluate the anti-CMV drug ganciclovir. The cytotoxic concentration 50% (CC50) and effective concentration 50% (EC50) are determined and used to establish the therapeutic range. In this model, NIH/3T3 mouse embryonic fibroblasts and GRP-expressing murine CMV are used. The module was designed to be completed in 1 week with two 1.5-hour lab sections. The lab module follows.

BENG 5890/6890 Antiviral Compound Analysis Lab

Lab 8: Antiviral Compound Analysis

1. Introduction

When assessing a new potential antiviral compound, it is necessary to show both viral inhibition and low toxicity *in vitro* before moving to a more advanced animal model. *In vitro* assessment is used before more representative animal models because it less expensive, more controlled, and can act a preliminary screening test to select the most promising compounds.

In prescreening assessment, it is important to show that the compound can inhibit viral replication without leading to toxicity. Inhibition is differentiated from toxicity by defining the therapeutic range with two limiting values. The upper limit is conventionally defined by the cytotoxic concentration 50% (CC50), which is the antiviral concentration (mM) resulting in a 50% reduction in cell viability compared to a non-treated and non-infected cell control. The lower limit is the effective concentration 50% (EC50). The EC50 is defined as the antiviral concentration (mM) that results in 50% viral inhibition compared to a non-treated virally infected control, referred to as the viral control. A wide therapeutic range (high CC50 and low EC50) is representative of a compound that has targeted antiviral activity without leading to toxicity.

Assessment by defining the therapeutic range is a common practice in tissue engineering and drug design. In this lab, you will be assessing the common antiviral drug, ganciclovir, against cytomegalovirus (CMV) by defining the therapeutic range in an NIH/3T3 mouse fibroblast cell culture model. A green fluorescent protein (GFP) -expressing mouse CMV strain will be used to identify the degree of viral replication. GFP will be produced when the virus is replicating. This lab will require 2 lab sections.

2. Objectives

- Assess cytotoxicity of ganciclovir on NIH/3T3 mouse fibroblasts – define CC50
- Test ganciclovir antiviral activity against mouse cytomegalovirus (mCMV) – define EC50

3. References

- American Type Culture Collection (www.atcc.org)
- Faulds, D.; Heel, R. C. Ganciclovir. A Review of Its Antiviral Activity, Pharmacokinetic Properties and Therapeutic Efficacy in Cytomegalovirus Infections. Drugs **1990**, 39 (4), 597–638. https://doi.org/10.2165/00003495-199039040-00008.
- McGavin, J. K.; Goa, K. L. Ganciclovir: An Update of Its Use in the Prevention of Cytomegalovirus Infection and Disease in Transplant Recipients. Drugs **2001**, 61 (8), 1153–1183. https://doi.org/10.2165/00003495-200161080-00016.

4. Reagents, Supplies and Equipment

Students should come to lab prepared with the following:
1. Lab notebook

4.1 Reagents

1. Media
2. GFP-expressing mouse CMV (mCMV) stock in media ($2.8x10^6$ pfu/mL)
3. Ganciclovir stock solution in media (6 mM)
4. DPBS

4.2 Supplies

1. 96-well plate
2. 1.2 mL microtube strip rack (96-well)
3. Media basins
4. Centrifuge tubes

4.3 Equipment

1. Multichannel pipette
2. Fluorometer plate reader

5. Protocol

5.1 Preparing for mCMV inoculation

1. Three columns (1, 2, 3) of a 96 well plate have been seeded with 3T3 fibroblasts ($3x10^4$ cell/cm^2) previously
2. Column #1 = ganciclovir cytotoxicity assessment (non-infected)
3. Column #2 = viral inhibition by ganciclovir (infected)
4. Column #3 = cell (non-infected) and viral (infected) controls
5. Prepare 3 mL of GFP-expressing mCMV inoculation media at $3x10^2$ pfu/mL by diluting the mCMV stock in media in a centrifuge tube – mix well
6. Transfer the warm mCMV inoculation media to media basin – label the basin
7. Transfer 3 mL of warm normal media to a media basin – label the basin

5.2 Inoculating the NIH/3T3 fibroblasts with mCMV

1. Using a multichannel pipette, aspirate and discard spent media from the 3 columns of the 96-well plate
2. Using the multichannel pipette, add 100 µL of normal media from basin to all wells in column #1
3. Add 100 µL of normal media from basin to bottom 3 wells (A, B, C) in column #3 (for cell control)
4. Add 100 µL of mCMV inoculation from basin to all wells in column #2
5. Add 100 µL of mCMV inoculation from basin to top 3 wells (F, G, H) in column #3 (for viral control)
6. Let plate incubate for 15 minutes to allow viral attachment

5.3 Preparing ganciclovir treatments for infected and non-infected fibroblasts

1. Prepare ganciclovir treatment dilutions in 1.2 mL microtube strip rack
2. In first 2 columns of the strip rack, prepare ganciclovir dilution – 150 µL in each tube
3. Dilute ganciclovir stock into media at $\log_{10}$ dilutions from 6 mM to $6x10^{-7}$ mM (8 dilutions total) – use a dilution calculator if necessary
4. In column #3 of the strip rack, add 150 µL of media to every tube (for controls)
5. Warm the dilutions in the tube rack in the incubator

5.4 Treating infected and non-infected fibroblasts

1. Remove plate and tube rack (ganciclovir dilutions) from the incubator
2. Using a multichannel pipette, gently add 100 µL of treatment from tube rack column #1 to 96-well plate column #1
3. Using a multichannel pipette, gently add 100 µL of treatment from tube rack column #2 to 96-well plate column #2
4. Using a multichannel pipette, gently add 100 µL of treatment from tube rack column #3 to 96-well plate column #3
5. Return the plate to the incubator
6. Incubate for 3 days
7. Analysis will be performed the next lab section (in 3 days)

5.5 Preparing for analysis

1. Transfer 4-5 mL of warm DPBS into a media basin
2. Remove plate from incubator
3. Using a multichannel pipette, gently aspirate and discard the spent media/treatment from all wells of the plate (all 3 columns)
4. Add 200 µL of DPBS into every well (all 3 columns)

5.6 Ganciclovir cytotoxicity analysis

1. Capture a representative image of all wells in column #1 and non-infected cell controls in column #3 (A, B, C)
2. Count the cell density (cell/cm^2) in all wells using ImageJ
3. Average the cell density of the control wells in column #3
4. Calculate % cytotoxicity for each test well compared to the cell control using following formula:

$$\text{Cytotoxicity \%} = \left[1 - \frac{\text{test well density (cell/cm2)}}{\text{control well density (cell/cm2)}}\right] * 100\%$$

5. Cell control = 0% cytotoxicity
6. Graph % cytotoxicity vs. ganciclovir concentration
7. Using linear interpolation, calculate the ganciclovir concentration that results in 50% cytotoxicity
8. That concentration = CC50 (upper limit to the therapeutic range)

5.7 Ganciclovir antiviral activity analysis

1. After capturing images, perform the antiviral activity analysis
2. Carefully take plate to spectroscopy analysis lab in EL basement
3. Using the BioTek plate reader, read the fluorescence of all wells in column #2 and the viral control wells (F, G, H) in column #3
4. The plate reader is programmed to read fluorescence at 488/520 nm by performing an area scan and producing a single relative fluorescence value for each well
5. Export the fluorescence data as an excel file
5. Calculate % inhibition for each test well compared to the viral control using following formula:

$$\text{Inhibition \%} = \left[1 - \frac{\text{test well fluorescence (RFU)}}{\text{control well fluorescence (RFU)}}\right] * 100\%$$

6. Viral control = 0% inhibition
7. Graph % inhibition vs. ganciclovir concentration
8. Using linear interpolation, calculate the ganciclovir concentration that results in 50% inhibition
9. That concentration = EC50 (lower limit to the therapeutic range)

6. Results and Discussion

- What are the ganciclovir CC50 and EC50 values that define the therapeutic range?

7. Homework

Perform the linear interpolation to calculate CC50 and EC50 values.
Graph the CC50 and EC50 values on a bar chart to visualize the width of the therapeutic range.